International
WOCE
Newsletter

Number 22 April 1996

IN THIS ISSUE

Published by WOCE International Project Office at Southampton Oceanography Centre, UK

WOCE is More Than Observations and Modelling

W. John Gould

The WOCE Synthesis and Modelling Working Group under its co-chairs, Andrew Bennett and Lynne Talley has held its first meeting and will meet again in the UK in late April. The challenge facing the SMWG (in fact facing WOCE as a whole) is quite formidable – to guide the analysis and interpretation of WOCE as a truly global experiment.

WOCE will by the end of its observational phase have doubled the number of high quality deep ocean stations, it will be able to give some guarantee of the quality of the observations, it will have a comprehensive suite of tracer measurements and will be complemented by direct measurements of circulation from floats, drifters and moorings. Above all, TOPEX/POSEIDON and ERS-1 and 2 are delivering data of unprecedented precision and extent.

WOCE researchers are busy analysing their data sets and publishing numerous papers – the rapidly increasing size of the WOCE bibliography now standing at 1580 entries is testament to this. There are now a number of groups worldwide running eddy-permitting global models of various sorts and comparisons of model results and observations are steadily leading to recognition of the increasing realism of OGCMs.

So WOCE is a success – yes certainly in the sense of a return on the investment that countries have made in WOCE as an oceanographic programme. However if you start to ask questions about how will WOCE define the "State of the Ocean in the 1990s", or "What constraints do WOCE measurements have on the global heat and fresh water fluxes?" you start to realise that there is another layer of complexity beyond our first definition of success.

The merger of the WOCE (and other) data setswith models presents a substantial challenge that will be addressed by SMWG. Our plan is that the comprehensive nature of the WOCE data set will act as a catalyst to stimulate ocean data assimilation which for oceanographers is still in its infancy.

Workshops will be an important element of the synthesis phase and Lynne Talley who is organising the first one, the Pacific Workshop in California in August this year, says there has been a good response. We hope that it will be a stimulating meeting and that the community of Pacific scientists will start to identify and address the basin-wide issues.

WOCE displays now available

In March the IPO had a stand at Oceanology International '96 in Brighton, UK. We updated our displays from the ones we produced two years ago and we received many compliments on how professional it looked. The whole exercise was made possible by financial support from commercial companies involved in producing equipment for WOCE: Aanderaa Instruments, Chelsea Instruments, Clearwater Instrumentation, Guildline Instruments, Sea-Bird Electronics, Sippican Inc., SIS, Technocean Associates, TSK, Webb Research and R.M. Young. We are very grateful for these contributions.

We plan to have the display on show at the European Geophysical Society and The Oceanography Society meetings later this year. The displays are available for use at other events so please let the IPO know if you'd like to borrow them or need more information.

Newsletter

This issue of the International WOCE Newsletter, with a number of articles on XBT issues, marks our first venture into colour. A four page centre section will from now on be a regular feature and should enable us to better represent the output of WOCE research. This issue is also the first to be produced entirely electronically and should result in higher quality images. (We hope we have now left the era of paste and scissors.) The transition has not been entirely painless and I'd like to thank our Newsletter Editor Andrea Frische for a job well done and Stephen Peach of SOC who has helped us through a minefield of image formats.

Deadlines

The next two newsletters will concentrate on Tracers (deadline for copy 15 May) and Oceanic fluxes (deadline 15 August).

WOCE Status 1996

With this issue we are also mailing a document which summarises the status of the project. It replaces the annual Resource Assessment that used to be published each year to highlight the shortfall in commitments to WOCE observational components. We think that the tone of the new document better represents the issues that are of importance as WOCE approaches the end of its observational phase. The document, and comprehensive information on WOCE data sources are available on the World Wide Web (http://www.soc.soton.ac.uk/OTHERS/woceipo/ipo.html).

Classifying Surface Mixed Layers in the Pacific Ocean

Janet Sprintall and Dean Roemmich, Scripps Institution of Oceanography/UCSD, La Jolla, CA 92093, USA

The adequate simulation of climate behaviour, for the purposes of coupling the global circulation of atmosphere and oceans in climate prediction models, is crucially dependent on the ability to correctly parameterise the nature of the surface layer. The vertical structure of the surface layer can assume many different forms. It may consist of well-mixed layers, weakly restratified layers; it can contain inversions; fossil or remnant layers; and salinity-stratified barrier layers. It has a memory of months to years, illustrating the history of wind-forcing events and contributions from heat and freshwater fluxes. In some regions the structure may be complicated by horizontal advection. In this note we will investigate how the surface layer can best be statistically categorized for dynamically different regimes of the large-scale circulation in the Pacific Ocean. Plausible scenarios of causality are presented for the different surface layer structures, and how they relate to surface forcing conditions.

The high resolution XBT/XCTD data

High-resolution XBT/XCTD data (to 800 m depth) have been collected along a number of routes spanning the Pacific Ocean (Fig. 1). The network is designed to study upper ocean circulation, and mass and heat transport. However, the nature of the sampling programme also makes it ideal for a statistical study investigating the surface layer structure and variability. Generally four surveys are conducted per year along each transect, with an eddy-resolving station spacing of 30–40 km along track, and 10 km near boundaries, at the equator, and in topographically varying regions.

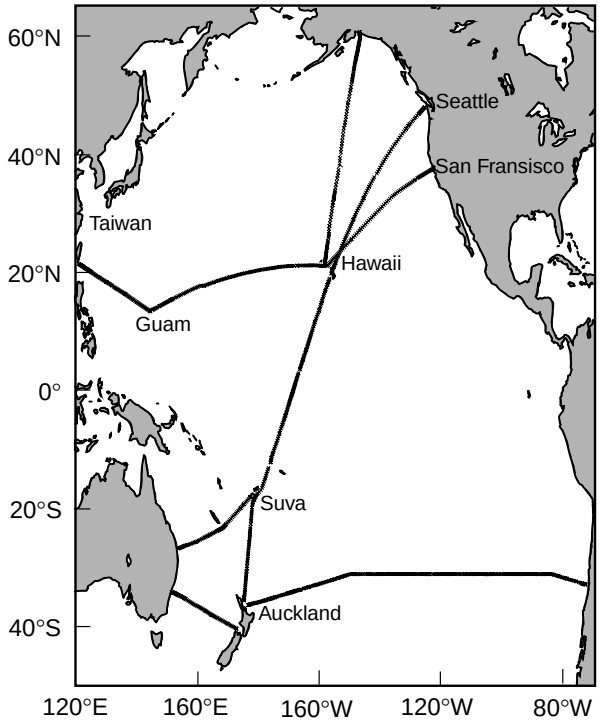

Figure 1. The high resolution XBT/XCTD transects of the Pacific Ocean.

We focus on two lines in the Pacific network. The line between Auckland and Suva was initiated in 1986 (40 cruise realisations), extended northward to Hawaii in 1987, and in 1993, sampling was continued all the way to Seattle. A March 1995 temperature section from the surface to 300 m between Auckland and Seattle is shown in Fig. 2a (page 21). Warmer temperatures are associated with the southern hemisphere summer. The spreading of isotherms at the equator indicates the Equatorial Undercurrent (EUC). Sampling along the San Francisco–Taiwan transect began in 1991, and there are 14 realizations. Rapid changes in temperature are commonly observed between San Francisco and Honolulu, indicative of both the transition across the California Current system, and the south-west orientation of the track itself. The western boundary northward flowing Kuroshio Current, and associated narrow regions of southward circulation just offshore are crossed on this transect.

Definition of the surface layer and the mixed layer depths

There are numerous ways to define the limiting depth of the surface layer. Obviously it is the depth somewhere in the main thermocline that has at some time come under the influence of atmospheric forcing. For this study, we determine the coldest sea surface temperature (SST) that ever existed in the data at 0.1° spatial intervals along a particular transect. For each cruise, we determine where this coldest sea surface isotherm is located in the water column. The depth of this isotherm defines the surface layer depth at that particular location and time. The surface layer definition is analogous to a local "ventilation" depth, as this is the depth to which atmospheric influence can be accounted for by local wind or heat fluxes.

The depth of the coldest isotherm that defines the surface layer on the Auckland-Seattle temperature section is shown in Fig. 2a, and on the section's temperature derivative with depth (dT/dz) in Fig. 2b. The surface layer definition is represented by the solid line in Fig. 2 and compared to the depth of the (SST-1°C) isotherm (crosses), a more familiar surface layer definition used in the literature. In the summer southern hemisphere between Auckland and Suva, the surface layer can extend to depths over 100 m, with the thermal signature of the North Cape Eddy, near New Zealand, evident. The summer seasonal thermocline

is present as illustrated by the high dT/dz region near the surface. It is this region that the (SST-1°C) criterion picks out. In the winter northern hemisphere between Honolulu and Seattle active ventilation is occurring. In the tropical regions, the surface layer and the (SST-1°C) criterion are coincident, both picking out the top of the thermocline, as illustrated in the lower panel by the increase in dT/dz occurring below the weak stratification in the upper layer. Note the stronger thermocline (high dT/dz) of the equatorial band, and the low stratification associated with the EUC core north of the equator centred at 140 m.

Within the surface layer we distinguish the mixed layer within the surface layer, as the depth to which active mixing is taking place at a particular time and location. The best criterion that describes the mixed layer in the majority of XBT profiles is the depth of the isotherm within 0.1°C of a "reference" temperature at 10 m. Once this "top" mixed layer has been determined the temperature at the bottom of the mixed layer becomes the "reference" level temperature and the search for isothermal fossil layers is continued down in the profile until the limiting depth of the surface layer is reached. Fossil layers are determined using the same 0.1° temperature change criterion.

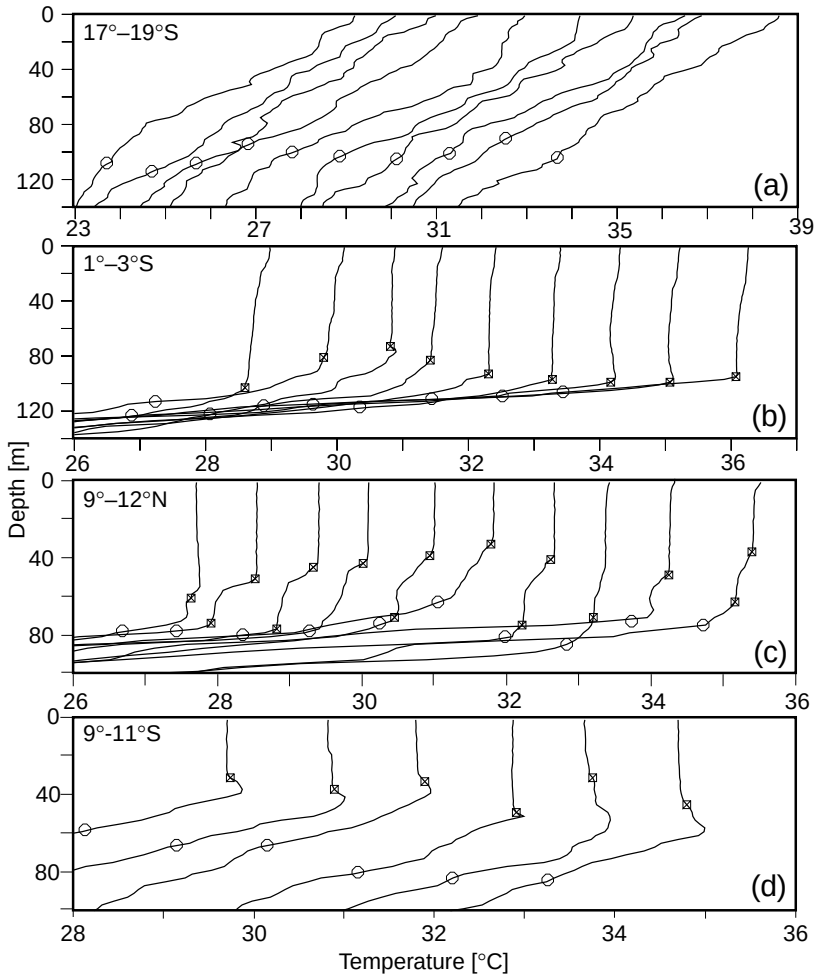

Figure 3. Surface layers (circles) and mixed layers (squares) observed along the Auckland–Seattle transect during March 1995 for the regions (a) 17–19°S; (b) 1–3°S; (c) 9–12°N and (d) 9–11°S.

Fig. 3 illustrates four different types of surface layers observed in the March 1995 transect between Auckland and Seattle. The mixed layer depth is indicated by the black square, and the surface layer depth by the circle. In Fig. 3a, successive XBT profiles (offset by 1°C) between 17–19°S exhibit a strongly stratified surface layer, where no mixed layer is evident. Whereas the successive XBT profiles at 1–3°S in Fig. 3b, strongly isothermal mixed layers, as defined by the 0.1°C temperature change, extend to 80–100 m depth. Fig. 3c shows an example of many casts containing a fossil layer occurring below the mixed layer. The top mixed layer and the underlying fossil layer are separated by a shallow thermocline between 40–50 m depth, occurring above the main thermocline. Fig. 3d displays temperature inversions of between 0.1–0.3°C strength, occurring at the base of a well-mixed layer. The six successive profiles shown here are each separated in space by about 40 km, and in time by about 1 hour.

Statistics of the surface layer structure

One of the benefits of the high-resolution XBT transects is that the quarterly surveys are exactly repeating, and hence we can represent the statistics of the structure of the surface layer both spatially and temporally. Along a particular transect, we calculate the percentage of casts for each 5° spatial band that contain fossil layers and inversions as defined in the above section.

San Francisco–Taiwan

For the 14 cruises between San Francisco and Taiwan (Fig. 4) most fossil layers and inversions occur between 130°W and 140°W. In this region off the Californian coast, the high percentage of casts that contain inversions show no seasonal preference although inversions have a tendency to occur near shore in the latitude band 130°W–135°W during boreal winter (NDJ) and spring (FMA), and further offshore in the latitude band 135°W–140°W during boreal summer (MJJ) and fall (ASO).

In spring, 33% of casts between 130°W–140°W contain fossil layers. Fossil layers are isothermal mixed layers that occur below a more recently formed upper mixed layer. The diffusion of heat in the upper mixed layer formed through periodic spring heating events, is slower than the response of the stronger winter wind-mixing events that formed the deeper mixed layers.

The area where fossil layers and inversions are predominant in the XBT casts corresponds to the California Current transition region, where salinity variability is known to influence the dynamics of the

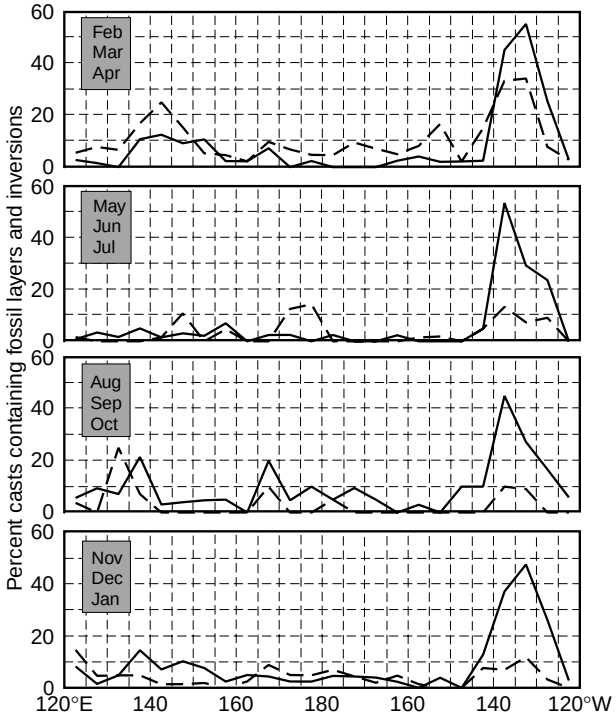

Figure 4. Percentage of XBT casts containing fossil layers (dashed) and inversions (solid) for the 14 cruises along the San Francisco–Taiwan transect, 1991–1995.

surface layer. The transition zone is a region of complex salinity structure, that is primarily associated with the interleaving of various water masses. A southeastward continuation of the Subarctic Frontal Zone separates the low salinity and temperature Pacific Subarctic water, formed further north under conditions of high precipitation and large heat loss, from the warmer, saltier eastern North Pacific water entering from the west (Lynn, 1986). Mesoscale eddies and energetic meanders complicate the transition zone (Lynn and Simpson, 1987). Such eddies and meanders would contribute to the strong variability exhibited in the vertical salinity and temperature profiles observed in the XCTD measurements, and result in the high incidence of inversions and fossil layers noted in the XBT observations that transverse the region.

Auckland–Seattle

Along the Auckland–Seattle track, over 30% of casts are found to contain fossil layers during winter (MJJ) and spring (ASO) near New Zealand, between 35°S–30°S (Fig. 5). The mean thickness of the fossil layers is 35 m, and they generally lie at about 80 m depth. This region corresponds to the formation area of the Subtropical Mode Water (STMW: Roemmich and Cornuelle, 1992). Generally, STMW forms in response to cooler winter sea surface and air temperatures, with large fluctuations on interannual and seasonal time scales. Fig. 5 shows that the occurrence of fossil layers during winter and spring may also be indicative of STMW formation.

Inversions are likely to occur in the high shear zones between the South Equatorial Current and the South Equatorial Countercurrent (15°S–10°S), and between the North Equatorial Countercurrent and the North Equatorial Current (5°N–10°N). In the southern hemisphere inversions occur during austral fall (FMA) and winter (MJJ). While in the northern hemisphere there is a slight preference for the presence of inversions during boreal summer (MJJ) and fall (ASO, however in this case, the zone is much more equatorward, and hence the seasonal signal less pronounced. Horizontal advection is a likely candidate for cause of inversions in these high shear zones.

Over 20% of casts in the equatorial band (5°S–5°N) contain fossil layers most of the year. XCTD measurements indicate that in the equatorial region, since the onset of the 1991–93 ENSO event, the surface layer salinity has been much lower than average, whereas below this it is saltier. The extensive freshening of the surface layer in early 1992 was the subject of a study by Roemmich *et al.* (1994). They observed salinity stratified, isothermal barrier layers in the equatorial bands, suggesting that they were created as fresher surface water from the west flows eastward over the saltier central Pacific water in an equatorial surface jet. In the equatorial central Pacific, it seems that the anomalous eastward freshwater jet is a necessary requirement for barrier layer formation, as barrier layers have not been observed in XCTD measurements during the prolonged

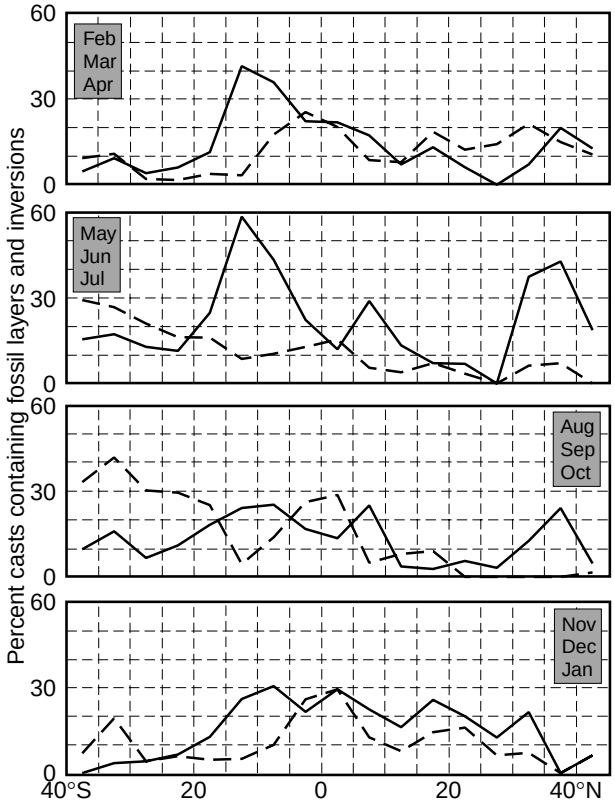

Figure 5. Percentage of XBT casts containing fossil layers (dashed) and inversions (solid) for the 40 cruises between the Auckland–Hawaii (1986–1995), and the 8 cruises between Hawaii–Seattle (1991–1995).

1991–93 El Niño other than when the 1992 eastward jet was present.

Conclusions

The main objective of this work has been to investigate how the surface layer can best be categorized for dynamically different regimes of the large-scale circulation in the Pacific Ocean. We have examined how the mixed layer structure and the statistics correlate with the wind history and the seasonal heating cycle in forming fossil layers and inversions. Features such as fossil layers and inversions were demonstrated to be ubiquitous in regions of the Pacific Ocean, and consistently appear in the XBT data during certain periods of the year.

References

Lynn, R.L., 1986: The subarctic and northern tropical fronts in the eastern North Pacific in spring. J. Phys. Oceanogr., 16, 209–222.

Lynn, R.L., and J.J. Simpson, 1987: The California Current system: The seasonal variability of its physical characteristics. J. Geophys. Res., 92, 12947–12966.

Roemmich, D., and B. Cornuelle, 1992: The Subtropical Mode Waters of the South Pacific Ocean. J. Phys. Oceanogr., 22:10, 1178–1187.

Roemmich, D.R., M.Y. Morris, W.R. Young, and J.R. Donguy, 1994: Fresh equatorial jets. J. Phys. Oceanogr., 24:3, 540–558.

Geostrophic Transports of the Major Current Systems in the Tropical Indian and Pacific Oceans

G. Meyers, J-R. Donguy+, and R. Bailey**
**CSIRO Division of Oceanography, GPO Box 1538, Hobart, Tasmania 7001, Australia*
+Centre ORSTOM de Brest, BP 70, 29280 Plouzané, France.

Due to their large size, the variation of the general circulations of both the Pacific and Indian Oceans have rarely been described in their totality using hydrographic data. However, the development of the expendable bathythermograph (XBT) programme, particularly since the mid 1980s as a result of the Tropical Ocean Global Atmosphere (TOGA) Programme and the World Ocean Circulation Experiment (WOCE), has provided the basinwide observations of the thermal structure required to describe the major current systems. This paper summarises some recent work (Donguy and Meyers, 1995 and 1996; Meyers *et al*., 1995; Meyers, 1996) which uses this widely dispersed sampling to document the variability of the major, tropical currents throughout the Indian and Pacific Ocean basins. The studies are based on frequently repeated XBT lines which were, if fully implemented, monitored at least 18 times per year with an XBT drop every 60 nmiles.

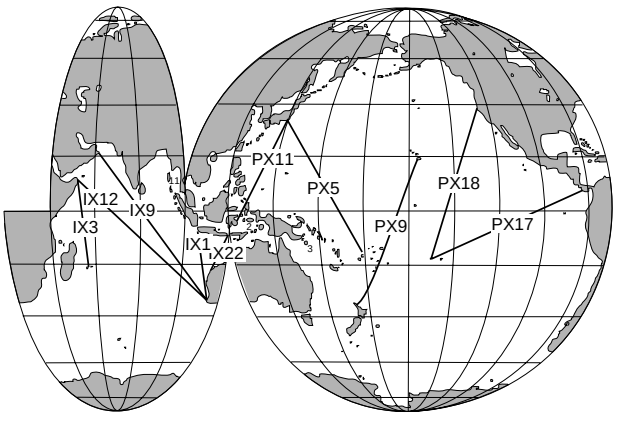

Figure 1. Location of XBT lines.

The method

XBT data and the climatological temperature/salinity relationship were used to calculate the mean annual and seasonal cycles of dynamic height and geostrophic transport of major currents relative to 400 db along 9 shipping tracks (Fig. 1) covering a large part of the tropical Indian and Pacific Oceans. The data were selected in bands centred on the most frequently repeated XBT tracklines for the period 1967 to 1988 for the Pacific Ocean, and for the period 1983 to 1994 for the Indian Ocean. The data were in general processed by the procedures described by Bailey *et al*., 1995. Longterm bimonthly mean temperature was calculated in 1° latitude bins along the tracks, except near coastal boundaries where bins were adjusted to have one in shallow water (<500 m) when possible. The transport function (vertically integrated dynamic height) was then calculated using the mean temperature/salinity relationship. The stochastic errors in bimonthly mean transports were 1 to 2 Sverdrups on the most sampled tracks.

Tropical Pacific Ocean

The mean annual cycle of transport of the North Equatorial Current (NEC), the North Equatorial Countercurrent (NECC) and the South Equatorial Current (SEC) (south of 2.5°S) were determined between the ridges and troughs of the transport function (Donguy and Meyers, 1996). Mean transports of the NEC and NECC increase regularly with longitude from east to west, as discussed in detail in the paper. The NECC has a large annual cycle with a transport-maximum during northern fall and winter. Seasonal variations of the NEC are small. Seasonal variations

of the SEC are slightly smaller than variations of the NECC, and they have considerably different phase from track to track (Fig. 2a, page 21). The SEC is described in more detail here because it was covered by several lines in both oceans.

Tropical Indian Ocean

In the northern hemisphere, low dynamic heights prevail during the NE monsoon and high dynamic heights during the SW monsoon inducing an alternating Somali Current (Donguy and Meyers, 1995). In the southern hemisphere, at 7°–8°S a trough of low dynamic height occurs during the whole year. Empirical orthogonal function (EOF) analysis was used to document the variation of these features. The geostrophic transports calculated on the XBT routes show spatially coherent patterns with strong seasonal variations, particularly in the Arabian Sea and along the equator. The mean transport of the South Equatorial Current (Fig. 2b) increases regularly with longitude from east to west in all months. It has small annual variations and the phase of the annual maximum progresses consistently westward, something which is not evident in the SEC in the Pacific (Fig. 2a). As expected, the SEC in the Indian Ocean is much weaker compared to the SEC in the Pacific Ocean.

Variability of the Indonesian throughflow

The XBT line Fremantle–Sunda Strait transects the eastern Indian Ocean between northwestern Australia and Java. It was established in 1983 with low-density sampling and upgraded to a frequently repeated line (>18 times per year) in 1987 to monitor currents. Variation of the thermal structure during 1983 to 1994 shows a rich mixture of annual, semiannual, and interannual timescales (Meyers *et al*., 1995; and Meyers, 1996). EOF analysis of anomalies of sea surface temperature (SST), dynamic height, and depth of the 2°C isotherm D20 identifies two distinctive signals (see Fig. 3). The Variation of Indonesian throughflow and the El Niño Southern Oscillation (ENSO) signal (EOF 1) appears throughout the region and is strongest off the coast of Australia. A modulation of the annual signal (EOF 2) appears off the coast of Java. EOF 2 has a shorter timescale than the ENSO signal, and its temporal coefficients are correlated to zonal winds over the equatorial Indian Ocean. For both EOFs, anomalously low SST and dynamic height occur at the same time as anomalously shallow D20 and *vice versa* for opposite anomalies. The XBT data, used with a climatological temperature-salinity relationship, gives the net, relative (0/400 dbar) geostrophic transports T through the section. For long timescales, T is representative of Indonesian throughflow. The variations associated with ENSO show a maximum during the La Niña of 1988–1989 and minima during the El Niños of 1986–1987 and 1991–1994. The peak-to-trough amplitude of the ENSO signal is 5 Sv. For the shorter timescales, T is representative of currents from the Indian Ocean flowing in and out of the region between northwestern Australia and Indonesia, changing the volume of upper layer water stored there. Associated with EOF 2, a sharp peak in westward transport developed during May to October 1994. When the XBT data is combined with available hydrographic data to investigate the deeper currents and the total throughflow, the maximum net, relative transport toward the west between Australia and Indonesia is 12 Sv in August/September (Meyers *et al*., 1995).

Conclusions

XBTs have provided a cost-effective way of providing widescale sampling of the upper ocean thermal structure for geostrophic transport as well as heat storage studies. The challenge for the future is to combine such subsurface information with widescale surface topography data provided by the latest satellite missions such as TOPEX/ POSEIDON and ERS-1&2.

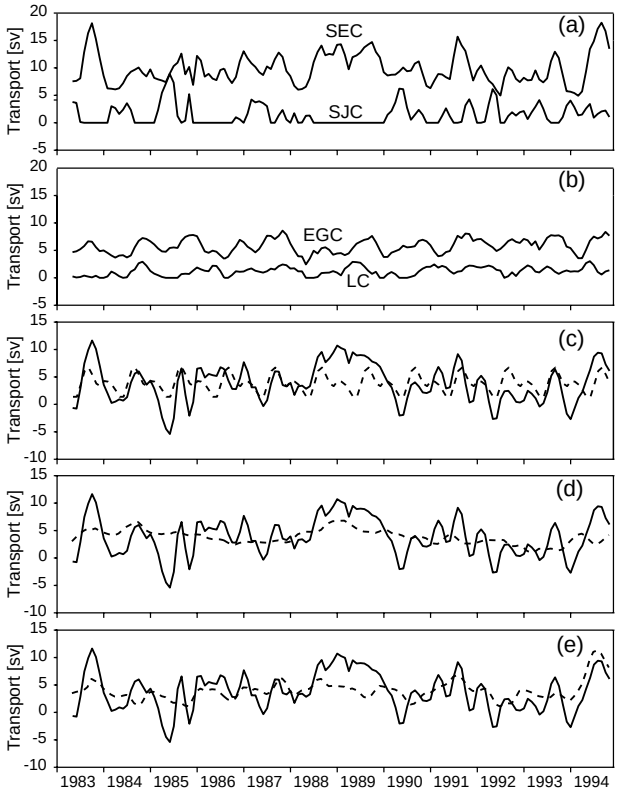

Figure 3. Geostrophic transport (0/400 dbar) in Sverdrups (10^6 m^3/s) : (a) South Equatorial Current SEC and South Java Current SJC and (b) Leeuwin Current LC and Eastern Gyral Current EGC. Positive values indicate westward flow for the SEC, eastward for the SJC and EGC, and southward for the LC. (c) Net geostrophic transport (0/400 dbar) through IX1 from Shark Bay to Sunda Strait (solid line) and mean annual cycle for the period 1983–1994 (dashed). (d) Same as (c), but with the ENSO signal in throughflow estimated by regression analysis with joint EOF1 (dashed), (e) Same as (c), but with the flow through line IX1 estimated by regression analysis with joint EOF2 (dashed).

Acknowledgements

The authors would like to acknowledge all the organisations and people contributing to the TOGA/WOCE XBT network, especially all those involved in the CSIRO, ORSTOM, SIO, and NOAA XBT programmes. A special word of thanks goes to the many hundreds of volunteer observers onboard the merchant vessels who helped to collect the data.

References

Bailey, R., A. Gronell, H. Phillips, G. Meyers, and E. Tanner, 1994: Cookbook for quality control of expendable bathythermograph (XBT) data. CSIRO Marine Laboratories Report No. 221, 75pp.

Donguy, J-R., and G. Meyers, 1995: Observations of geostrophic transport variability in the western tropical Indian Ocean. Deep-Sea Res., Part I, 42, 1007–1028.

Donguy, J-R., and G. Meyers, 1996: Mean annual variation of transport of major currents in the Tropical Pacific Ocean. Deep-Sea Res. (in press).

Meyers, G., 1996: Variation of Indonesian throughflow and ENSO. J. Geophys. Res. (in press).

Meyers, G., H. Phillips, and J. Sprintall, 1991: Space and time scales for optimal interpolation of temperature: Tropical Pacific Ocean. Progr. Oceanogr., 28, 189–218.

Meyers, G., R.J. Bailey, and A.P. Worby, 1995: Geostrophic transport of Indonesian throughflow. Deep-Sea Res., Part I, 42, 1163–1174.

Meyers, G., J. Sprintall, H. Phillips, J. Peterson, and T. Fonesca, 1989: Design of an ocean temperature observing network in the seas north of Australia. Part I, Tropical Pacific Ocean: Statistics. CSIRO Marine Laboratories Report No. 204.

Phillips, H., R.J. Bailey, and G. Meyers, 1990: Design of an ocean temperature observing network in the seas north of Australia. Part II, Tropical Indian Ocean: Statistics. CSIRO Marine Laboratories Report No. 211.

Intensive Measurements of Sea Surface Temperature and Salinity in the Western Pacific

C. Hénin, Surtropac Group, Center ORSTOM de Noumea, BP A5, Noumea, New Caledonia

Temperature and salinity play a critical role in oceanic circulation, and therefore in the distribution of water masses. For this reason, the description and analysis of sea surface salinity (SSS), sea surface temperature (SST) distributions and of their seasonal and inter-annual variations are essential for understanding the influence of oceans on global climate. The inter-tropical western Pacific happens to be the oceanic area of the planet where rainfall is most abundant, which results in a marked lowering of surface salinity (Lukas and Lindstrom, 1991), and it is also the place where the warmest waters in the upper layers are found, acting as the planet's heat reserve, and usually referred to as the 'Warm Pool'.

While global surface ocean temperatures have been fairly well documented through satellite remote measurements, available data of salinity are scarce.

In 1969 ORSTOM Centre in Noumea developed a network of commercial vessels operating between New Caledonia and Japan. By regrouping surface temperature and salinity measurements from meteorological buckets, taken along the shipping routes, Donguy and Hénin (1978) and Delcroix and Hénin (1989) were able to correlate salinity distribution, rainfall and the movements of the Convergence Zones of the Wind. The bucket technique by volunteer crews allows only 4–6 measurements per day. Furthermore the accuracy is estimated to be only 0.2 to 0.3°C in temperature and 0.2 in salinity respectively.

The annual number of measurements taken by the vessels within the ORSTOM Pacific network has varied, reaching as much as 10,000 observations/year between 1977–83. Unfortunately, this figure is gradually decreasing, due to difficulties encountered. During 1994 less than 2,000 observations were made.

Development of the automated TSG network

We have just pointed out the need to introduce automation in the measurement of surface temperature and salinity, *i.e.* the need for better accuracy, for simplicity of method and for a much greater number of observations. We selected the SBE21 thermosalinograph (TSG) manufactured by SeaBird Electronics Inc. The conductivity cell incorporate tributyl tin coatings to reduce biological fouling. TSGs installed on commercial ships in tropical regions the biological fouling process may be crucial. It has to be set as close as possible to the engine water intake mainly to reduce increase of temperature. Depending on the ship this was generally possible.

Median values of temperature and salinity over 20 measurements are recorded every 5 minutes. For the geographical positioning we were able to interface our equipment with an inexpensive separate satellite positioning system. A complete description of the system can be found in Grelet *et al.* (1992). The new automated technique constitutes a notable improvement in the accuracy of both surface temperature and salinity over the old bucket sampling technique. From comparisons with CTD surface observations during four oceanographic cruises in the western equatorial Pacific differences of 0.00 to 0.03 in salinity were observed while the temperature measured by TSG was 0.1 to 0.3°C greater than CTD surface temperature. In order to improve sea surface temperature measurements we actually compare temperature from separate sensors at the entrance of water intake and fixed to the hull to *in situ* observations. Tests are in progress at ORSTOM Centre.

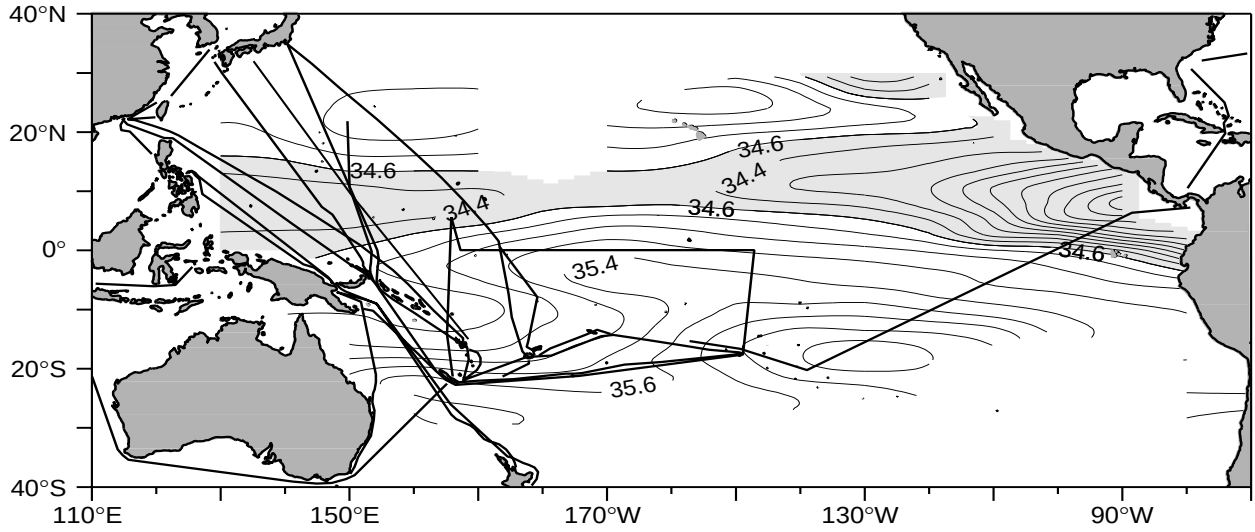

Figure 1. TSG network in the Pacific Ocean during 1994 and mean sea surface salinity for the 1974–1989 period.

The TSGs were regularly calibrated at the SeaBird factory. From basic data (frequencies) and pre- and post-calibration coefficients for 4 different SBE21 systems during the 1993–95 period operating on commercial vessels we observed that salinity drift was never more than 0.001 per month which is comparatively very small (Bitterman and Millard, 1994). A calibration every year or every two years may give the guarantee that the change in salinity is of the order of 0.01–0.02. The associated change in temperature is less than 0.005°C.

Since late 1990, six commercial vessels and three Research Vessels were selected to refine and perfect the automated surface water measurement system. The monitoring effort was focused on the western and central Pacific where the salinity distribution is well contrasted with high salinity waters of more than 36.2 near French Polynesia and low salinity waters (less than 34.8) under the convergence zones (Intertropical Convergence Zone [ITCZ] and South Pacific Convergence Zone [SPCZ]). The area of observation extends from Japan to New Zealand, and from Southeast-Asia and Australia to French Polynesia (Fig. 1).

Variability of SSS and SST observed with TSG network

From the recent intensive automated observations of SSS and SST by TSG we may present some results:

The temperature diurnal cycle

In the western equatorial Pacific during the intensive observation period (IOP) of the COARE programme (Coupled Ocean Atmosphere Response Experiment) we had the opportunity to observe the diurnal cycle with our TSG system. During a three month period (December 1992 to February 1993), RV Le Noroit cruised along 18 cross-equatorial tracks, experiencing varying cloud cover and wind strength. These affected the amplitude of the diurnal temperature cycle, and disturbed the description of temperature distribution along the 5°S–5°N runs (each one lasting approximately three days). During the 20–23 January 1993 section (Fig. 2) while the wind was very weak during three days the diurnal heating is well observed on the SST records with an amplitude of about 0.7°C and a maximum occurring at approximately 1400 to 1500 local time.

Effect of rainfall

Local rainfall affects both temperature and salinity. The effect on temperature is small (a 0.1– 0.3°C temperature drop has been frequently observed during a rain squall), but much greater on surface salinity. Depending on the intensity and duration of rainfall, this latter may vary by as much 1.0 (observed from RV Le Noroit between 3°N and 4°N in January 1993). The rainfall lowers the sea surface salinity and the sea surface temperature. This effect and the diurnal heating are seen in T-S diagram on Fig. 3.

This temperature diurnal variability, coupled with the effect of localized rainfall in tropical areas, could lead one to question the validity of surface temperature and salinity measurements taken by the traditional network of

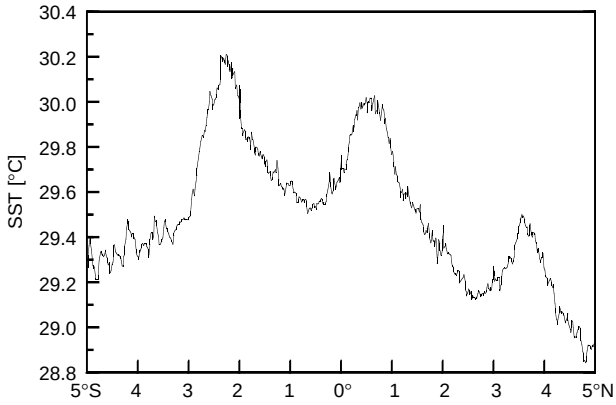

Figure 2. Sea surface temperature (°C) along 156°E between 5°N–5°S during a light wind period (20–23.1. 1993)

commercial vessels, and even those gathered by research vessels. Studies are being carried out on the diurnal temperature cycle and on the effect of freshwater impact on the surface layer of oceans. The automated TSG bring new observations for these studies.

Surface Salinity fronts

Along the Equator, a very large zonal surface salinity front was observed in October 1994 during the Flupac cruise with a sharp gradient near 172°W (33.8–34.5 west of 175°W and 35.2–35.3 east of 170°W). These observations reflect the El Niño event with the eastward extension of low salinity waters of the Warm Pool and the strong zonal salinity gradient on its eastern edge.

SSS structures along the quasi meridional merchant ship routes were already described by Delcroix and Hénin (1991). From traditional bucket observations they described the seasonal and the interannual variations. The new thermosalinographs records now allow to observe fine sea surface structures along the shipping lines. Fig. 4 presents the SSS distribution during the 1992–1995 period along the Japan–Tarawa–Fiji line crossing the equator near 174°E (every two months since June 1992 and every month since August 1995). Low salinity waters are observed under the ITCZ near 7°N and SPCZ near 9°S. During this El Niño period very large SSS variability is detected on the equator (from less than 33.6 in August 1993, more than 35.2 in March 1994 and since April 1995). This induces very pronounced meridional salinity fronts (more than 1.0 over a few miles respectively near 4°N and 4–8°S) between high salinity equatorial surface waters and low salinity waters associated with ITCZ and SPCZ. These fronts would not be so well described with bucket sampling. Recent work using drifters and SSS TSG data suggests that in addition to evaporation and rainfall zonal currents and equatorial upwelling may explain such equatorial SSS distribution (Hénin *et al*, 1995).

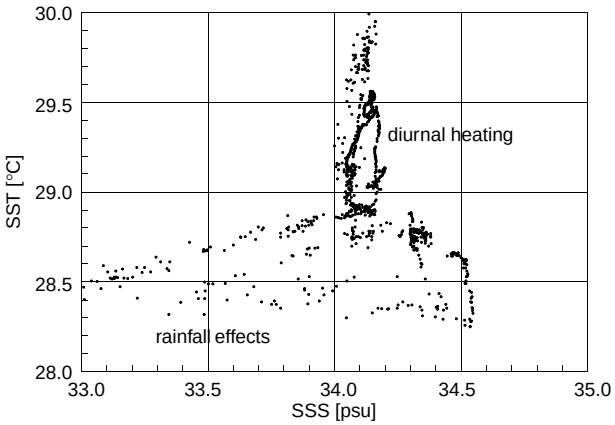

Figure 3. Temperature/Salinity diagram observed along 156°E on the 5°S–5°N section showing rainfall and diurnal heating effects (3–6 January 1993).

Conclusion

The study of the variability of tropical SST and SSS distribution using first three years of intensive observations by TSG on commercial vessels has proved to be somewhat difficult to carry out due to the high frequency variations introduced by the diurnal cycle (in the case of temperature) and by rainfall (in the case of salinity). By developing intensive automatic observation systems and using smoothing and filtering techniques we may eliminate these local effects.

During the experimental period, and using a limited number of ships, we were thus able to demonstrate that intensive automated surface water monitoring was indeed possible, and that it improved the accuracy of the data and the density of coverage along the tracks followed.

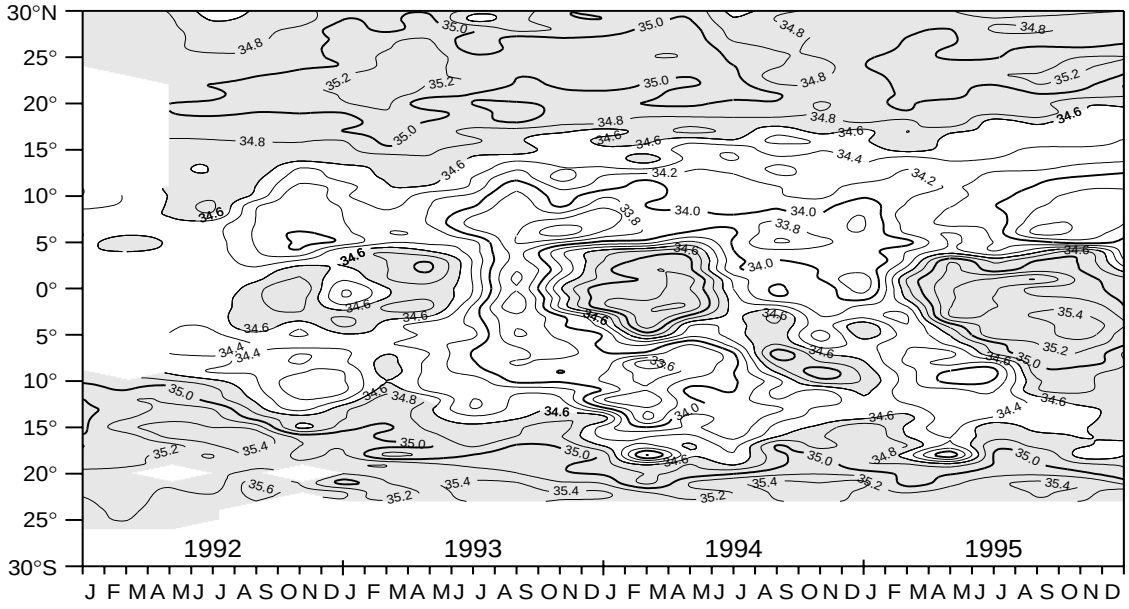

Figure 4. Sea Surface Salinity distribution along the Japan–Tarawa–Fiji line for the 1992–95 period.

References

Bitterman, D.S., and R.C. Millard, 1994: Shipboard thermosalinograph intercomparison test results from the NOAA RV Malcolm Baldrige. NOAA Technical Memorandum ERL AOML-82.

Delcroix, T, and C. Hénin, 1989: Mechanisms of subsurface thermal structure and sea surface thermohaline variabilities in the southwestern tropical Pacific during 1979-85. J. Mar. Res., 47, 777–812.

Delcroix, T., and C. Hénin, 1991: Seasonal and interannual variations of sea-surface salinity in the tropical Pacific Ocean. J. Geophys. Res., 96, 22135-22150.

Donguy et Hénin, 1978: Hydroclimatic anomalies in the South Pacific. Oceanologica Acta Vol. 1, 1, 25–30.

Grelet, J., B. Buisson et C. Hénin, 1992: Installation et utilisation d'un thermosalinographe à bord d'un navire marchand. Notes Techniques, Sciences de la mer, Oceanographie physique, 7, Centre ORSTOM de Noumea, Nouvelle Caledonie, 99pp.

Lukas, R., and E. Lindstrom, 1991: The mixed layer of the western equatorial Pacific Ocean. J. Geophys. Res., 96, Suppl., 3343–3357.

Summary of Field Tests of the Improved XCTD/MK-12 System

Alexander Sy, Bundesamt für Seeschiffahrt und Hydrographie, Postfach 30 12 20, 20305 Hamburg, Germany

An XCTD field evaluation on Meteor cruise No. 30/3 (WHP Section A1) in the eastern North Atlantic in December 1994 and measurements under realistic ship-of-opportunity conditions in September/October 1995 have completed a series of field trials started in 1992. The first at-sea tests revealed significant deficiencies in the system's performance (Sy, 1993). The urgent need to improve the reliability and accuracy of XCTD measurements led to the development of various modified devices by the system's manufacturer, Sippican, Inc. The combined modifications result in a new configuration of the MK-12 hardware, firmware and software, and include changes of the XCTD probe. After several field and laboratory tests carried out by the manufacturer (Elgin, 1994), the results demonstrated significant improvements in the overall system performance. The purpose of the two field trials reported here was to check the manufacturer's specification independently, *i.e.* from the customer's point of view. The system's accuracy for XCTD measurements is claimed by the manufacturer to be ±0.03°C for temperature, ±0.03 mS/cm for conductivity, and ±5 m or 2% for depth (Sippican, 1992; 1994).

Operational details of the XCTD versus CTD intercomparison

12 XCTD probes were calibrated by Sippican, Inc. in September 1994 and made available for the planned at-sea test. The XCTD test sites are located west of the British Isles in an area from 52°N to 53°N and 15°W to 23°W. This ocean area provides favourable conditions due to its well developed hydrographic stratification in both temperature and salinity.

Severe weather conditions forced a premature end of our regular research programme before we had the opportunity to carry out the XCTD test. Therefore, it was decided to use a combination of T-5 XBT and XCTD probes *en route* home as a poor makeshift substitute to complete our hydrographic section in a rough-and-ready way (test A, 9–10 December 1994). After successful and problem-free launching of 6 XCTDs and 12 XBTs at a ship's speed of about 6 knots, we were surprised by a sudden unpredicted favourable change of the weather situation. We returned to the break-off point of the hydrographic section to resume our field work including the originally planned XCTD versus CTD intercomparison (test B, 13–14 December 1994).

Field test B was carried out with XCTD drops at stations #542 at 52°20'N, 18°52'W and #546 at 52°20'N, 15°47'W side by side with the down-profiling of a well calibrated NBIS MK-IIIB CTD. The CTD data were processed according to WOCE standards. XCTD data processing included the editing of spikes and noise by 5-point-moving-median filtering of temperature and conductivity (Sy, 1985), editing of start-up and profile end transients, and compaction to 2 dbar intervals. The accuracy of the reference CTD data was estimated as ΔT ±2 mK for temperature, ΔS ±0.002 for salinity and Δp ±2 dbar for pressure. The temporal stability of all parameters was extremely good.

Test results

All 12 probes launched gave traces from the sea surface to below 1000 m depth. No completely erroneous profile or calibration failures were detectable. The peak-to-peak noise was found to be in the range of the resolution of the MK-12 (±0.01°C, ±0.01 mS/cm) and no increasing noise with depth appeared. Also, the system grounding problem and the data offset at 900 m were obviously solved. The XCTD temperature section of test A corresponds well to the XBT section as well as to the CTD section, which was carried out 3 days later. In contrast to the 6 drops of test A, which were carried out without any difficulties at all, 3 drops (50%) of test B encountered problems. One drop failed, although good data were acquired, due to a software breakdown and data loss. One profile became very noisy below 730 m depth with unusable data, which may have indicated a signal wire problem. During one drop a wire jam was detected, which fortunately could be removed in time to prevent a premature wire break.

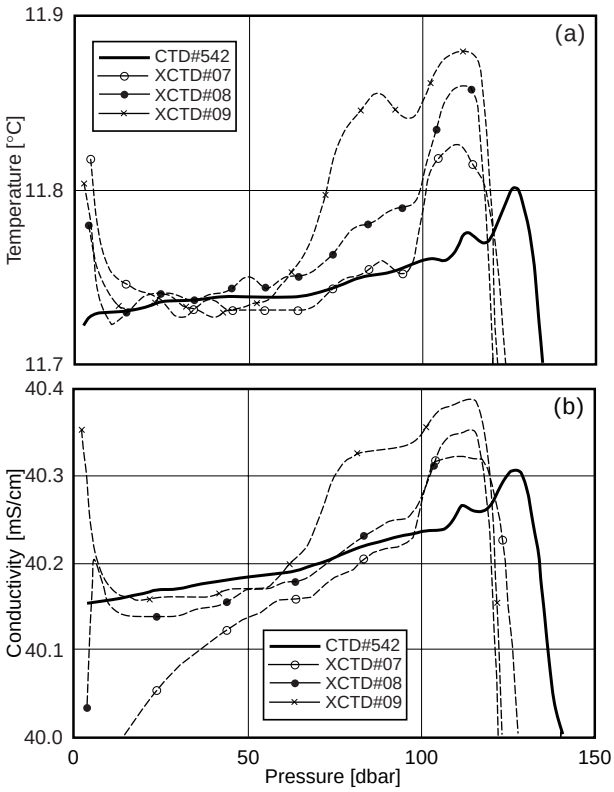

Figure 1. CTD and XCTD profiles of the upper 150 dbar at stat. #542 (a) temperature, (b) conductivity.

For test B the comparison of data from the homogeneous mixed layer provides a good estimate of the parameter accuracy and the start-up transients. The range of temperature differences between XCTD and CTD traces does not exceed the ±0.03°C limit below 10 m depth (Fig. 1a). However, the conductivity differences of some profiles exceed the ±0.03 mS/cm limit significantly (Fig. 1b). Generally, the XCTD conductivity is low with respect to the reference CTD. A greater discrepancy between XCTD and CTD conductivity is revealed for the upper 50 m of two drops (one in each test) caused by a slow start of the conductivity measurement (see drop #7 in Fig. 1b) Elgin (1994) provides the plausible explanation that air bubbles remaining in the conductivity cell cause too low a conductivity measurement until they eventually collapse by increasing pressure. The reduced overall accuracy and the start-up problem demonstrate the difficulty of controlling the conductivity parameter and consequently the computed salinity. Increasing differences of some traces below 60 m are probably caused by temporal variability of the field (Fig. l).

The temperature accuracy found in the mixed layer of the upper ocean remains stable also for the deeper ocean (Fig. 2a). The conductivity difference becomes smaller with increasing probe depth and eventually falls inside the ±0.03 mS/cm limit in the lower half of the traces (Fig. 2b). This indicates that the data quality is influenced by increasing pressure, i.e. the bubble formation in the conductivity cell on launching is probably a more general problem. Ordinary air bubbles seem to be responsible for the slow start effect and micro bubbles for the reduced conductivity accuracy at the profile's upper part. Elgin (1994) reported on different resolution across the range of conductivity, with the poorest resolution at the high end. The measurements at the test sites, however, do not show these high conductivity values. As for conductivity, the salinity difference is also significantly reduced with greater depth. It should also be noted that the 42.921 mS/cm value previously used as standard conductivity was changed to the commonly recommended 42.914 mS/cm value (R. Elgin, pers. comm.).

The hydrographic stratification allows an easy evaluation of the depth formula. As for XBT probes (Hanawa *et al*., l995), the XCTDs fall faster than specified. The fall rate variability is small. The depth error is estimated to be about -30 m at 900 m depth (or 3.3%). That corresponds to previous findings (Sy, 1993) and shows that probably no change of the hydrodynamically effective underwater body design was made. Thus, for a more accurate re-calculation of the depth fall rate formula, all old and new XCTD versus CTD intercomparison data can be used.

Measurements along a transoceanic section onboard a merchant vessel

A suitable opportunity to extend the test results by experiences obtained under realistic ship-of-opportunity conditions was presented by CMS Köln Express from 29 September to 2 October 1995, when a complete section from the English Channel to the Grand Banks (Line AX3) was carried out. All probes were launched by a scientist

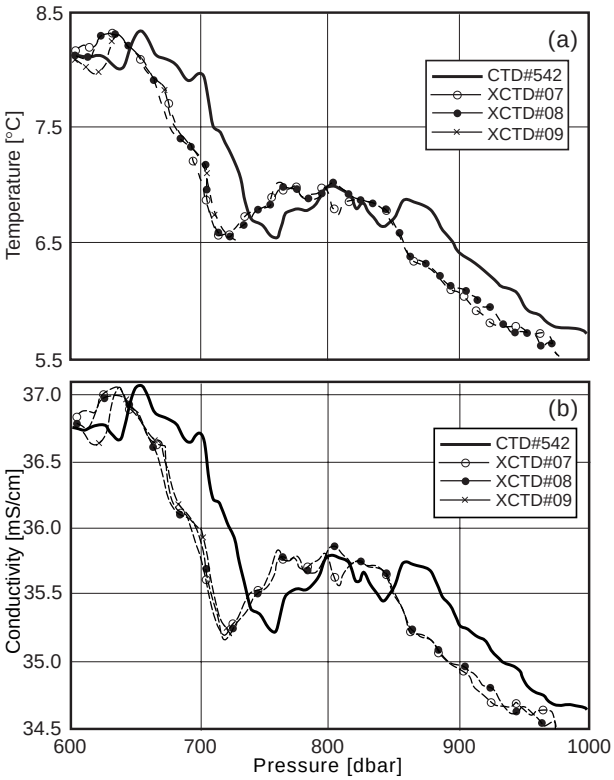

Figure 2. CTD and XCTD profiles of deeper layers at stat. #542 (a) temperature, (b) conductivity.

from the vessel's stern (launch height: 10 m). For data acquisition the same equipment was used as 9 months before, except software rev. 3.03. From 60 probes, calibrated by Sippican, Inc. in August 1995, 4 probes failed due to probe malfunctioning and another 4 probes failed due to fatal software problems. 35% of all conductivity profiles are affected by the conductivity start-up problem (defined as slow start conductivity transient effects below 10 m depth).

The measurements were carried out under severe weather conditions. The ship's speed of 12–19 knots and the strong head wind added up to relative windspeeds of up to 60 knots. XCTD probes are designed to cover the upper 1000 m at a maximum ship's speed of 10 knots. The depth range of XCTD profiles was found between 460 m and 764 m with a mean depth range of 606 m. For many ship-of-opportunity programmes this reduced depth range will not meet their requirements. No relationship between windspeed and depth range or windspeed and probe malfunctioning could be deduced. The probe malfunctions occurred at high and at low windspeeds and are thus more likely a manufacturing problem. One should expect to find a strong dependence of the depth range from both ship's speed and windspeed. In this case, however, both effects are superimposed (Fig. 3). The visible influence of windspeed on the depth range appears in terms of an increasing maximum depth variability, but without a decreasing mean maximum depth.

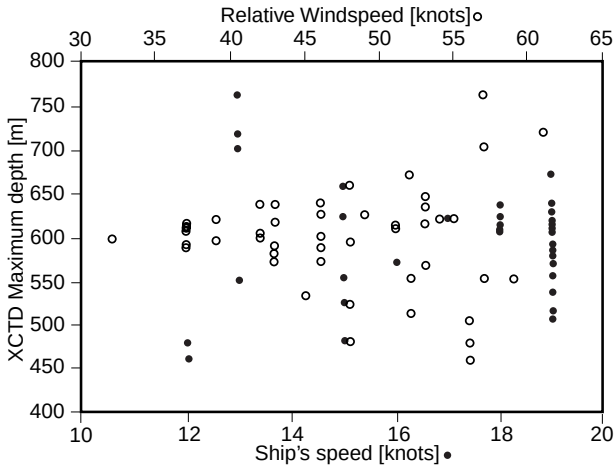

Figure 3. XCTD depth range versus relative windspeed and versus ship's speed.

Conclusion

The results of the field evaluation of December 1994 and of the transoceanic section 9 months later conclusively reveal that modification efforts of the manufacturer during the last years have resulted in a significant XCTD/MK-12 system performance improvement. Obviously most performance difficulties encountered at previous sea trials have been successfully solved. The system is close to the point of meeting the claimed specification. Unsolved deficiencies are the conductivity start-up problem, the reduced conductivity accuracy at low pressure, and the inaccurate depth formula. Also the MK-12 software, although easy to use, needs a careful revision. To review the XCTD depth fall rate will be the next action to be taken by the IGOSS Task Team on Quality Control of Automated Systems (TTQCAS).

References

Elgin, R.H., 1994: An evaluation of XCTD performance with design improvements. Sippican, Inc., Marion, Mass., USA, unpublished manuscript, 6 pp.

Hanawa, K., P. Rual, R. Bailey, A. Sy, and M. Szabados, 1995: A new depth-time equation for Sippican or TSK T-7, T-6 and T4 expendable bathythermographs (XBT). Deep-Sea Res., 42, p. 1423–1451.

Sippican, Inc., 1992: MK-12 Oceanographic data acquisition system, User's Manual. Sippican, Inc. Marion, Mass.

Sippican, Inc., 1994: XCTD: Expendable conductivity, temperature, depth profiling system. Document presented at Oceanology International '94, Brighton, 8–11 March 1994.

Sy, A., 1985: An alternative editing technique for oceanographic data. Deep-Sea Res., 32, p. 1591–1599.

Sy, A., 1993: Field evaluation of XCTD performance. WOCE Newsletter, No. 14, p. 33–37.

Ship-of-Opportunity (SOOP) Co-ordination Plan

R. Bailey, P. Dexter[+], V. Detemmerman[†], and R. Keeley[‡]*

**CSIRO Division of Oceanography, PO Box 1538, Hobart, Tasmania 7001, Australia*

[+]WWW Department, World Meteorological Organisation, PO Box 2300, CH-1211 Geneva 2, Switzerland

[†]WCRP, World Meteorological Organisation, PO Box 2300, CH-1211 Geneva 2, Switzerland

[‡]Marine Environmental Data Service, 1202-200 Kent Street, Ottawa, Ontario, Canada K1A 0E6

Introduction

A co-ordination plan to fulfil upper ocean data requirements which have been established for GOOS and GCOS, based on the results of programmes of the World Climate Research Programme (WCRP), and which can be met at present by measurements from ships of opportunity (SOO), has been established under the Integrated Global Services System (IGOSS). With the cessation of the TOGA and WOCE research programmes of WCRP, the operation

and funding of the data collection networks developed for these programmes will cease unless some mechanism is established (under IGOSS, GOOS, or CLIVAR) to continue the management, funding and coordination of the activities. The plan will make maximum use of existing operational mechanisms of IOC and WMO, most notably those of IGOSS and the International Oceanographic Data and Information Exchange (IODE) in the transition of the programme from research to operations. Specifically, these mechanisms are the co-ordination of operations of the IGOSS Ship-of-Opportunity Programme (SOOP) managers; the IGOSS Group of Experts on Communications and Products (GE/CP); the IODE Group of Experts on Technical Aspects of Data Exchange (GE/TADE); and the Global Temperature Salinity Programme (GTSP) Steering Group.

Justification

The initial upper ocean thermal data requirements to be met by the plan are those which were developed by the TOGA and WOCE programmes for the low density XBT (expendable bathythermograph) network, and endorsed by the WCRP Ocean Observing System Development Panel (OOSDP). The final report of the OOSDP has emphasised the value of long-term monitoring of upper ocean heat content using XBTs from ships of opportunity (SOO) for climate prediction. It recommended the operational maintenance of the existing TOGA and WOCE network. This represents an agreed base network, to be maintained operationally and on which research programmes can build as required. The XBT network is recognised at present as being one of the major means of obtaining upper ocean thermal data at the required spatial and temporal scales. The newly-formed GOOS/GCOS/WCRP Ocean Observation Panel for Climate (OOPC) will be charged to continuously assess these requirements for operations and research, taking into account new technological developments and scientific advances, in particular the work of the CLIVAR Upper Ocean Panel (UOP). The Intergovernmental Committee for GOOS has agreed that IGOSS should be responsible for the continued operational maintenance of the SOO programme, based initially on the continuation of the former TOGA/WOCE XBT network.

The implementation plan is therefore directed initially towards the continued operational maintenance and co-ordination of the low-density ship-of-opportunity network. This network in itself supports many other operational needs (such as for fisheries, shipping, defence, etc.) through the provision of upper ocean data for data assimilation in models and for various other ocean analysis schemes. The continuing challenge is to optimally combine upper ocean thermal data collected by XBTs from the SOO with data collected from other sources such as the TAO array and satellites (*e.g.* AVHRR, altimeter, etc.).

It is recognised that there are observations other than upper ocean temperatures (such as salinities) which can be collected under the SOO programme. The report of the OOSDP identifies these as of importance to monitor climate related ocean changes. Likewise there are other programmes, such as those conducted by fisheries agencies or navies, which can augment the data collected through the SOO. The proposal has been designed to be flexible enough to accommodate these other measurements and programmes as the opportunities, technological capability and operational needs arise. However, initially it is considered most important to have the proposal focused on supporting climate prediction in order to ensure the continued operation of the present network. The use of the network to support climate prediction has already been clearly identified as a priority. The network may be later extended to incorporate other observations and requirements as appropriate.

SOO programme organization and responsibilities

The plan calls for the establishment of an *ad hoc* Ship-of-Opportunity Management Committee (SMC), co-sponsored by IGOSS, GOOS, GCOS and the WCRP, charged with the responsibility of managing the resources made available by contributing nations to meet the scientific requirements provided to it from GOOS, GCOS and the WCRP. The plan also calls for the formalisation of a SOOP Implementation Panel (SOOPIP) within IGOSS. This panel will have as one of its terms of reference, the requirement to support the SMC in implementing the scientific programme with the allocated resources.

Summary

The plan has been derived from the input of individuals involved in the operation of the present and past WOCE, IGOSS, and TOGA XBT networks. Accordingly, it has been widely discussed, modified and generally accepted by these programmes and GOOS. The true success of the transfer of the SOOP from a research to an operational activity now lies in the hands of those organisations who will be active participants in GOOS.

Data are coming in!

The Current Meter DAC (Oregon) has recently acquired data from the Kuroshio Extension Regional Experiment (WOCE designation PCM7). The dataset consists of 12 year-long (1993–1994) records from 4 moorings (at instrument depths of 500–5000 m) on a linear array near 36°N and 143°E. The measurements were obtained by Dr Zack Hallock of the Stennis Space Center (Mississippi). These records join other Pacific data from PCM9 (52 records on 19 moorings at 32.5°S and 179–170°W) and from PCM11 (Samoa Passage, 26 records on 5 moorings near 10°S and 170°W). All of this data will hopefully be available at the WOCE Pacific Workshop 19–23 August this year in Newport Beach, California.

For more information on the status of the current meter programme and data go to:http://tethys.oce.orst.edu/cmdac.html

Joint Environmental Data Analysis Center Contributions to WOCE

Stephen Diggs, Norman Hall and Warren White, Scripps Institution of Oceanography, 0230, La Jolla, CA 92093-0230, USA

The Joint Environmental Data Analysis (JEDA) Center is a collaboration between Scripps Institution of Oceanography (SIO) and the National Oceanographic Data Center (NODC). One objective is to quality control upper ocean temperature profiles over the Pacific Ocean. These profiles are collected in both real-time and delayed-mode from a variety of national and international sources. Another objective is to construct products (*e.g.*, maps of temperature anomalies at standard depths) from these quality controlled profiles in order to examine seasonal-to-interannual changes in upper ocean temperature over the global ocean. These products are disseminated through cooperative agreements with a number of government and academic institutions, and through their publication on our JEDA Center Web Page over the Internet.

Quality control

The JEDA Center receives both real-time and delayed-mode temperature profiles from NODC at regular intervals. These profiles have already been checked by NODC and the Marine Environmental Data Service (MEDS) for location errors, duplication, and outliers when compared to the Levitus global mean and standard deviation of upper ocean temperature. They arrive in Global Temperature and Salinity Pilot Project (GTSPP) file format, which is designed to carry meta-data and error flags on each temperature-depth pair in the profile. At the JEDA Center, each temperature profile is then inspected visually by a skilled operator utilizing an interactive software system. The set of quality control procedures and the definition of flag codes have been agreed upon over a series of meetings conducted by an international group of interested scientists over the past 5 years under the auspices of the World Ocean Circulation Experiment (WOCE) International Project Office (IPO). These procedures and codes are published in a manual; *i.e.,* WOCE IPO Report No. 133/95.

A typical interactive quality control (QC) session begins with plotting positions of monthly temperature profiles to the global map window on the screen (Fig. 1). Next, the operator selects a region of interest (*i.e.*, with the rubber-band box in this figure) to begin checking a regional group of profiles. These selected profiles are displayed in a regional map window on the screen, where individual stations can be readily seen. Upon request, the interactive system begins automatically selecting 10 nearest neighbour profiles for display in a "waterfall" plot (Fig. 2 top). If any one of the selected profiles deviates significantly from the others, the user may then select that profile for visual inspection compared with a 3-s envelope of Levitus historical variability (Fig. 2 right). If appropriate, the operator can then flag temperature-depth pairs in that profile. Upon completion of the flagging operation, the operator then returns to the waterfall plot for examination of other suspicious profiles. When all profiles have been visually inspected in this manner, the next batch of 10 observations in the regional subset are examined in the waterfall plot. This process of selection and QC is repeated until all profiles in the regional group (and ultimately in the Pacific and global groups) have been inspected.

As a final check on the efficacy of these WOCE QC procedures, we produce monthly maps of upper ocean temperature and heat storage anomalies over the global ocean. These maps allow additional outliers (*i.e.*, those anomalies which stand above the surrounding values) to be detected, leading to the identification of additional erroneous profiles, which are then flagged as such. These flags, together with those from the WOCE QC procedures, are

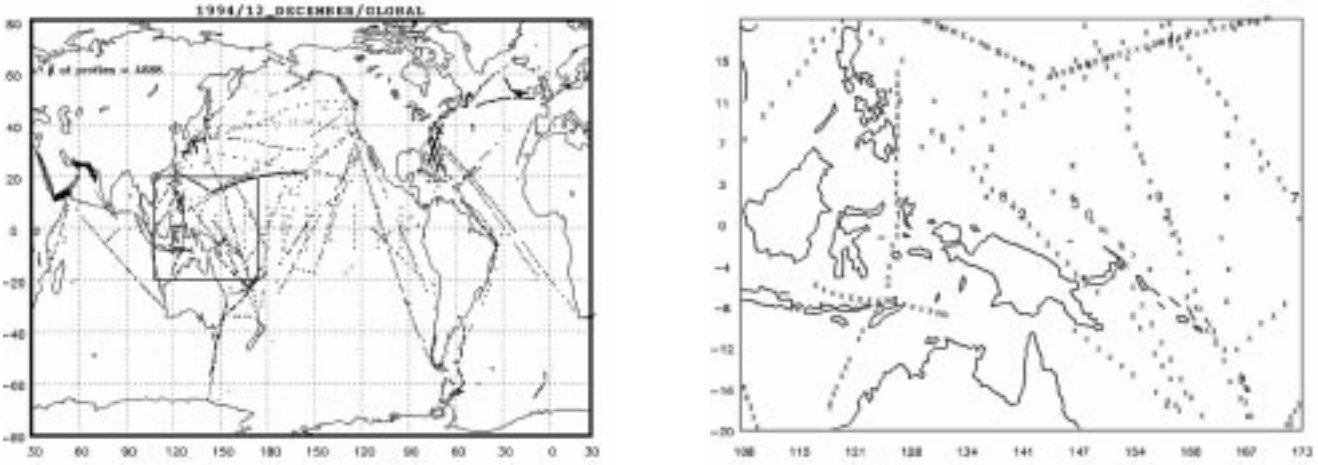

Figure 1. Global (left) and selected regional (right) screen maps from the interactive QC software system.

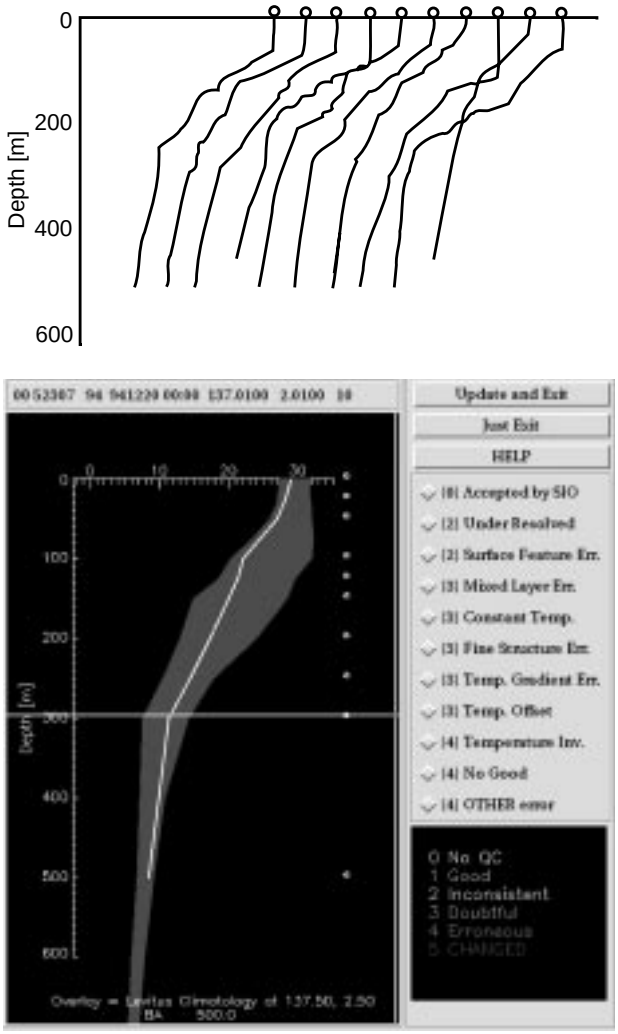

Figure 2. Waterfall plot of nearest neighbour profiles (top) and single profile selection window from the interactive QC software system (bottom).

then transmitted to NODC for incorporation into their database. Presently, the JEDA Center has conducted WOCE QC procedures on 1990, 1991, and 1992 temperature profiles in the Pacific Ocean. Similar WOCE standards have been applied to temperature profiles in the Indian and Atlantic Oceans for this same period by the Commonwealth Scientific, Industrial, and Research Organisation (CSIRO) in Hobart and the Atlantic Oceanographic and Meteorological Laboratory (AOML) in Miami, respectively.

Recently, we have completed software development in Practical Extraction and Report Language (PERL), which will allow this interactive software system (*i.e.*, incorporating WOCE QC procedures) to become available to the public.

Scientific analyses

Temperature profiles gathered by WOCE, Tropical Ocean Global Atmosphere (TOGA), and Climate Variability and Predictability (CLIVAR) field programs are analyzed at the JEDA Center to produce bimonthly global maps of upper ocean temperature and heat storage anomalies from 1955 to the present. This allows for the study of climate change on ENSO (El Niño-Southern Oscillation) and Decadal time scales.

From this 40-year time sequence of global anomaly maps, we can construct characteristic animations of dominant ENSO variability, like those displayed in Fig. 3 (page 22), for sea surface temperature and upper ocean heat storage. These animations, with each frame separated by 3 months, display the evolution of ENSO over the 2 years prior to the mature phase of El Niño in the eastern equatorial Pacific Ocean, the latter characterized by warm sea surface temperature and heat storage anomalies there. Upon inspection of these animations, ENSO-scale anomalies in both variables can be seen propagating eastward from the eastern Indian Ocean to the eastern Pacific Ocean. These findings are consistent with those observed earlier by Gill and Rasmusson (1983) for the equatorial Pacific Ocean, and by Tourre and White (1996) for the tropical Indo-Pacific Ocean. In these animations, eastward propagation of the ENSO signal continues from the eastern Pacific Ocean into the Atlantic Ocean in sea surface temperature but not in heat storage. Similar animations (not shown) have been constructed for ENSO-scale sea level pressure and wind anomalies, which are responsible for the ENSO signals being able to propagate eastward from one ocean basin to the other. We surmise that this comes about from some ocean-atmosphere coupling mechanism that has yet to be understood.

Products

The JEDA Center publishes products and data through a variety of means. We regularly contribute real-time global maps of heat storage anomalies to the Climate Diagnostics Bulletin (CDB) of National Centers for Environmental Prediction (NCEP) and the Products Bulletin of the Integrated Global Ocean Services System (IGOSS). We were one of the first Data Assembly Centres to create a presence on the World Wide Web (WWW). Our Web site has recently been expanded to make available a greater variety of products to the community. Recent changes have also made navigation within our site more intuitive for students.

Fig. 4 shows the image map of the JEDA Center Web Page, with the selected products and information given as follows:

Temperature Profiles: containing a link to NODC and all GTSPP datasets.

Data Distributions: containing basin and global distributions of historical temperature-salinity profiles in 5-year segments from 1900 to 1990.

Temperature Climatology: containing climatological upper ocean temperature (*i.e.*, annual and monthly) at standard depths over as much of the global ocean as possible (*i.e.*, from approximately 30°S–60°N), constructed for the 10-year reference period 1980–1989.

Real-Time Analysis: containing images of our most recent bimonthly maps of sea surface temperature and heat storage

anomalies. This is a hypertext version of bimonthly analyses published in the Climate Diagnostics Bulletin.

New Animations: containing Quicktime and MPEG movies of our most recent mapping exercises, showing the evolution of ENSO-scale anomalies of upper ocean temperature. This is done in conjunction with Yves Tourre at Lamont-Doherty Earth Observatory (LDEO).

Historical Analyses: containing compressed ASCII versions of gridded fields used in creating global and basin maps of upper ocean temperature anomalies. Anomalies from individual observations have been interpolated onto a 2° by 5° latitude-longitude grid for each bimonth from 1955 to the present. Detailed procedures are given in read-me files.

Images of Ocean Temperature Anomalies: images in this section include global distributions of observations, heat storage anomalies, and surface temperature anomalies for each bimonth from 1980–1996. We expect to extend this back to 1955 by the end of the year.

Scientific Lectures: recent lectures by JEDA scientific associates are located here. Topics include "Global Temperature Change and Solar Signals" and "Antarctic Circumpolar Waves", with others forthcoming.

In addition to our standard Web Page, we have recently constructed a comprehensive "Global Ocean Observation Database". GOODbase is a fully relational and object oriented database holding all historical physical and chemical profiles submitted to NODC through 1994. Fig. 5 shows results from a typical GOODbase query. The user has selected XBT data from the month of October 1977 and the distribution of the observations is presented along with downloading and formatting options.

The Uniform Resource Locator (URL) for the JEDA Center Web Page is:

http://cyberia.ucsd.edu/jeda.html

Figure 4. JEDA Center Web Page.

For more information on GOODbase, please point your Web browser to:

http://cyberia.ucsd.edu/goodbase/goodbase.html

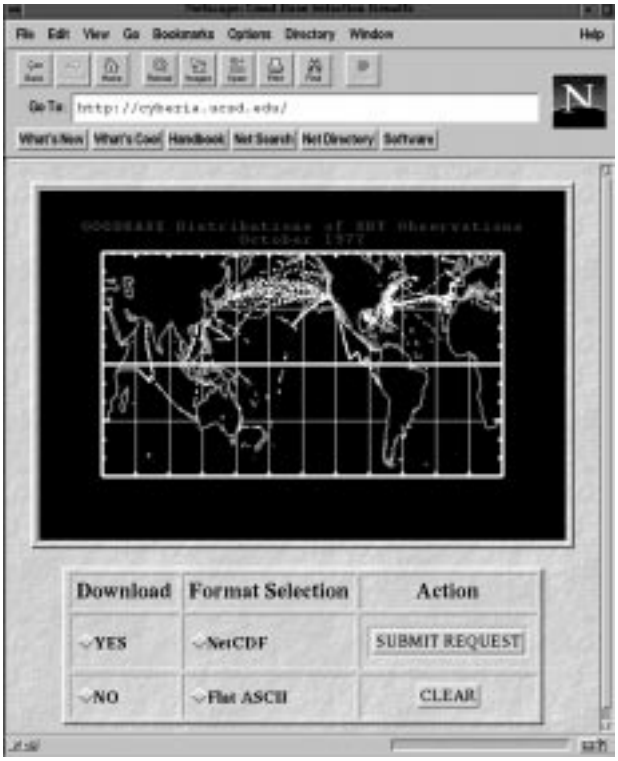

Figure 5. GOODbase query result with downloading and formatting options.

Future directions

The JEDA Center is committed to serving the international scientific community by making oceanographic data and analyses available in variety of ways. Our Web Page is being continually being enhanced to include more interactivity and flexibility when choosing animations, images and gridded fields. The GOODbase Web Page is currently being re-fitted with a graphical user interface for fast and efficient data browsing, selection, and downloading.

References

Gill, A.E., and E. Rasmusson, 1983: The 1982-83 climate anomaly in the equatorial Pacific. Nature, 306, 229–234.

Levitus, S., 1982: Climatological atlas of the world ocean. NOAA Prof. Paper 13. U.S. Government Printing Office. Washington, D.C., 173 pp.

Tourre, Y. and W.B. White, 1996: ENSO signals in upper ocean temperature over the Indian and Pacific Oceans. J. Phys. Oceanogr., 26, (in review)

Global Subsurface Data Centre (GSDC) for TOGA and WOCE

M-C. Fabri, A. Dessier[+], G. Maudire*, Y. Raguenes*, and J-P. Rebert[‡]; *IFREMER/SISMER, BP70, 29280 Plouzané, France, [+]ORSTOM, BP70, 29280 Plouzané, France, [‡]COI, 1 rue Miollis, 75732 Paris, France*

The Upper Ocean Thermal Data Assembly Centre (UOT-DAC) in Brest collects subsurface temperatures both in real time and in delayed mode. The centre collates the data, eliminating duplicates and provides a standardized quality-controlled data set to the World Data Centres A and B for Oceanography. Selected data sets are provided to scientists on a routine basis.

Data set

Most of the observations are made routinely by the VOS (Voluntary Observing Ships) XBT network sampling along regular shipping lines recommended by TOGA and WOCE. Additional observations come from research vessels, navies, fishing vessels and moorings. The largest dataset is the collection of eXpendable BathyThermograph (XBT) data (Fig. 1).

Setting up a VOS line includes the training of the crew and the management of the XBT probes and the collected data. France is contributing to this network by setting up 6 lines in the Atlantic Ocean, 3 lines in the Indian Ocean and 15 lines in the Pacific Ocean with XBTs provided by NOAA up to 1995 (support is not yet decided for 1996).

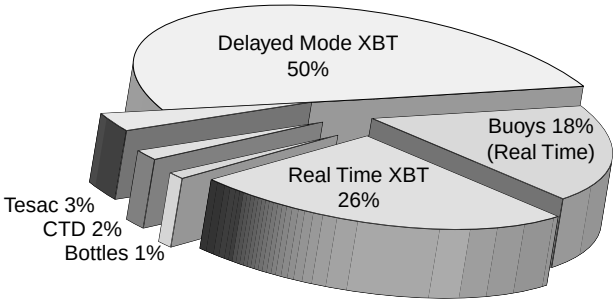

Figure 1. Composition of the data base per type of profile (February 1996).

Data flow

Real-time (RT) data (BATHY messages) are received electronically from the French IGOSS Centre, METEO FRANCE in Toulouse the first week of each month. They are replaced by the more complete delayed mode (DM) data when they are transferred to the data centre (see the time distribution on Fig. 2). The time lag between the receiving of RT data and the DM data is about three years due to the slowness of the data flow but also due to some technical problems like frequent changes in the exchange formats. Moreover about 24% of the RT profiles are never replaced by DM data.

Fig. 3 provides a comparison of the number of XBT data collected in each ocean for each year from 1985 onwards. The number of profiles available in each ocean seem to be linked to the ocean sizes. Sampling in the Indian Ocean seems to remain steady whereas it seems to decrease slightly from 1992 onwards in the other oceans.

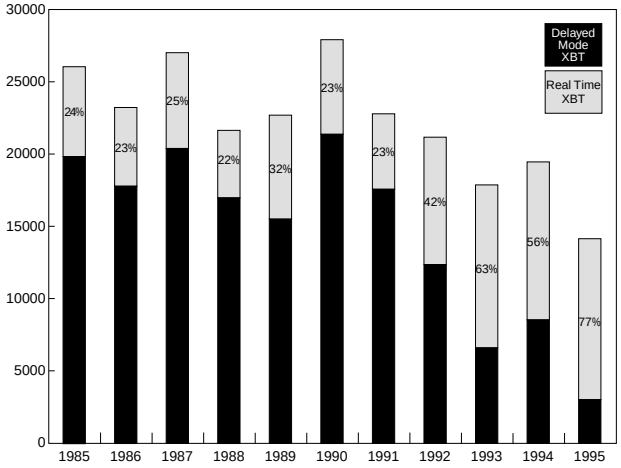

Figure 2. Composition of the data base in real time and delayed mode XBT (January 1996).

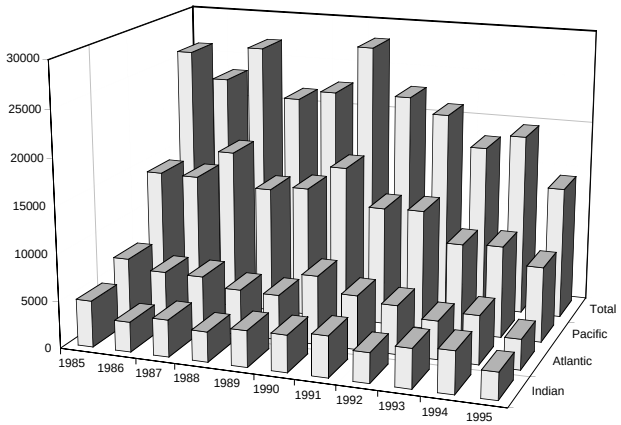

Figure 3. Data base per year and ocean (January 1996).

Quality control (QC)

The data base is continuously updated, using merging procedures to replace real-time data by the corresponding delayed-mode data. Emphasis is put on duplicate checks (automatic and visual). Every incoming set of profiles is examined objectively first (automatic checks) and then subjectively according to the IOC recommendations. Each profile is then visually checked on an interactive graphic display with the results of the automatic checks. Standard flags are applied to each temperature/depth pair as well as to header elements.

Data Quality flags are as follows:

0 : No Quality Control done
1 : Good data
2 : Probably good data
3 : Probably bad data
4 : Bad data
5 : Changed value

If data are already flagged by one of WOCE Regional Science Centres, the original flags are not modified and the profiles are archived in the data base in full resolution. For practical reasons the QC are performed in the following order:

- Automatic checks that follow international requirements (spikes, gradient tests, temperature inversions,...)
- Duplicate test: complex procedure checking for identical (irrespective of ship's name) and near-identical observations; best data is kept
- Data: consistency with neighbouring data
- Land test: visual inspection of dot plot for each data set (eliminate data on land)
- Speed test: if vessel exceeds 25 knots, position/date of observation reviewed
- Climatology: Temperature data quality control is based on data editing and visual comparison with the Levitus Climatology (*i.e.* five degree squares and seasonal climatology)

Access to data

The GDC provides data files in different formats and different kind of maps. All products can be generated on request with the following possible selection criteria: data type (XBT, CTD, Bathy,...); date of measurement; ocean (Atlantic, Pacific, Indian); geographical selection (latitude, longitude); vessel (radio code, name or NODC code); institution (name, NODC code).

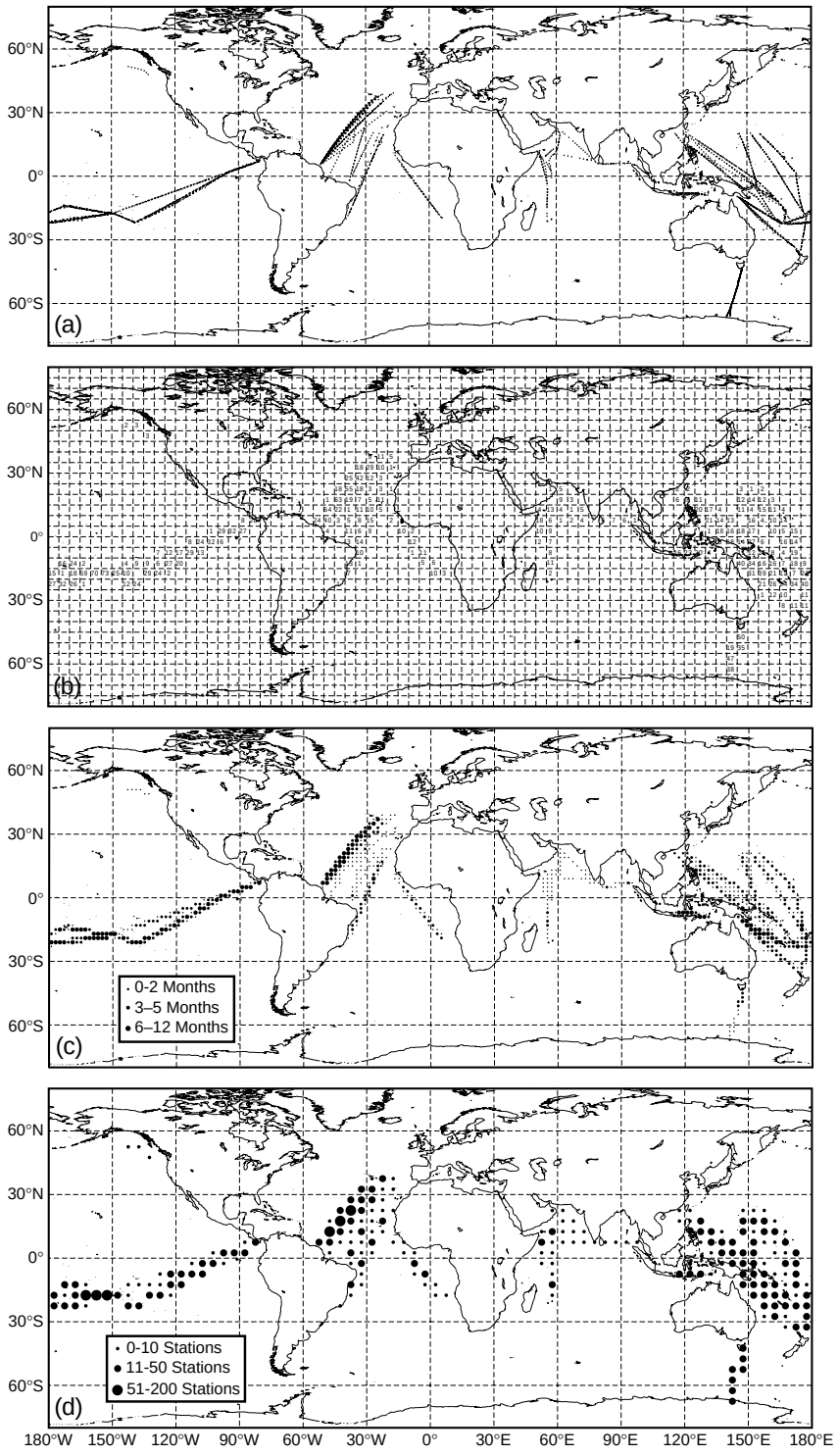

Figure 4. Maps available at GSDC: (a) Location of profiles; (b) Number of profiles by geographical squares; (c) Dots as a function of classes of profiles numbers by geographical squares; (d) Dots as a function of the number of months for which profiles were archived for each geographical square.

Data products

1. Data files are available in several ASCII output formats (TSDC, Hydro, GTSPP, Medatlas).
2. Four kinds of maps are available to show the space distribution of the profiles: Location of Profiles (Fig. 4a); Number of profiles by geographical squares (*e.g.*: 5° x 5°, Fig. 4b); Dots as a function of classes of profile numbers by geographical squares (Fig. 4c); Dots as a function of the number of months for which along the ship lines appear clearly on these maps).
3. Statistics are available such as: Number of stations; Distribution of stations according to data types and oceans; Distribution of stations according to vessels,

years, months and oceans; Distribution of stations according to institutions and years.

4. A detailed 6 monthly report (in French) of the centre's activities is also issued.

Some data products are already available on the WWW, such as maps of station location for each year from 1985 to 1995. Newly-archived data are available on line as well. As soon as data files are archived, users can find a new map of station location, the number of stations, data file volume and the data file. A description of the format is also available on line.

Conclusion and perspective

This data set begins in 1985, when it was initiated for the tropical (30°N–30°S) region, and was extended world-wide for the WOCE experiment in 1990. Accordingly the present data set is more substantial in the tropical area. It must be pointed out that one of the important objectives of the TOGA experiment was to set up an operational observing system of the upper ocean, associating the available i*n situ* observations with a realistic model. This has been done in the past, where monthly data sets from the Brest centre were assimilated in the LODYC numerical model in Paris (Morlière *et al*., 1990). As a result, both the numerical model and the quality control procedure of the data set were improved. Such kind of product could be prepared for the WOCE and also for the forthcoming programmes like CLIVAR and GOOS.

Reference

Morlière, A., Rebert J.P., Servain, J., and Merle, J., 1990: An operational 3-dimensional simulation of the Tropical Atlantic Ocean with assimilation of the *in situ* observations. International TOGA Scientific Proceedings, Honolulu, WCRP-43/WMO/TD-No. 379, pp 19–27.

Data requests can be sent to GSDC by e-mail or regular mail. Data products can be provided on different digitalized supports *e.g.*: diskettes, tapes, ftp or WWW.

For data shipment and more information contact:

Marie-Claire Fabri
IFREMER/SISMER
BP 70
29280 Plouzané, France
e-mail: Marie.Claire.Fabri@ifremer.fr
WWW: http://www.ifremer.fr/sismer/program/gsdc/
Tel: +33-(02)-98-22-42-00
Fax: +33-(02)-98-22-46-44

The Water Masses, Velocity Structure and Volume Transport of the Agulhas Current at 31°S

Lisa Beal, Southampton University Department of Oceanography, S.O.C., UK; and Harry Bryden, James Rennell Division, S.O.C., UK.

The Agulhas Current is an intense Western Boundary Current (WBC) and probably has the largest volume transport of any WBC in the world's oceans, after the Gulf Stream. An accurate determination of the transport of the Agulhas Current is an essential ingredient in determining the intensity of the circulation and convective overturning in the Indian Ocean. As part of UK WOCE, the Agulhas Current Experiment (ACE) aboard RRS Discovery crossed the Agulhas Current at 31°S, along WOCE hydrographic section I5W, during February–March 1995 (Fig. 1). Fifteen hydrographic stations were occupied along the section and three acoustic current profiling techniques were used to measure the current: a hull-mounted ADCP, a lowered ADCP (LADCP) and an Acoustic Correlation Current Profiler (ACCP). Six moorings comprising 26 current meters, two with upward looking ADCPs, were laid in the current, to be collected in April 1996. Here the combined CTD and LADCP data set is used to describe the water mass characteristics of the current and to estimate its volume transport.

This was the first use of an LADCP by UK scientists and all initial set up and processing methods were courtesy of Dr Eric Firing of the University of Hawaii. An ADCP in a pressure case is mounted on the CTD frame so that surface

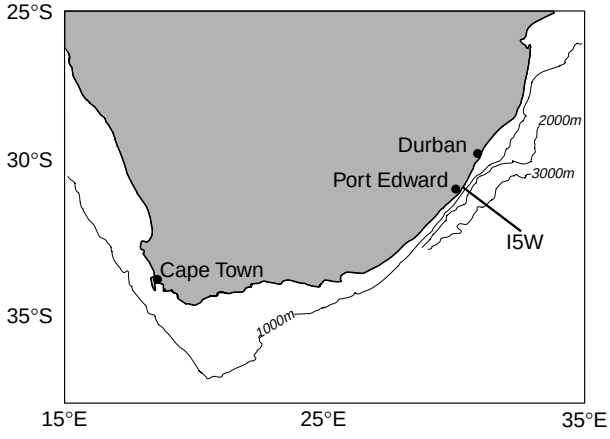

Figure 1. Location of I5W.

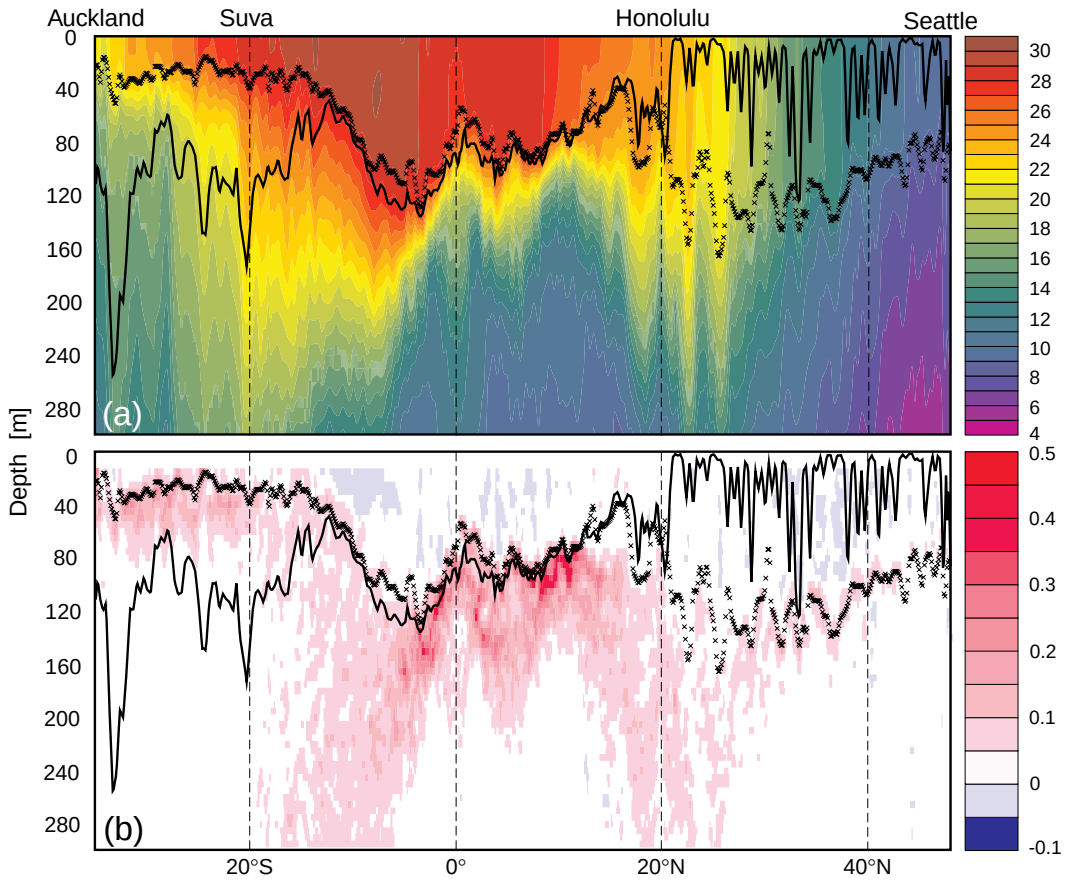

Sprintall and Roemmich, page 3 *Figure 2. Temperature (a) and it's derivative with depth (b) along Auckland–Seattle in March 1995. The solid line indicates the depth of the surface layer. The crosses indicate the depth of SST-1°C.*

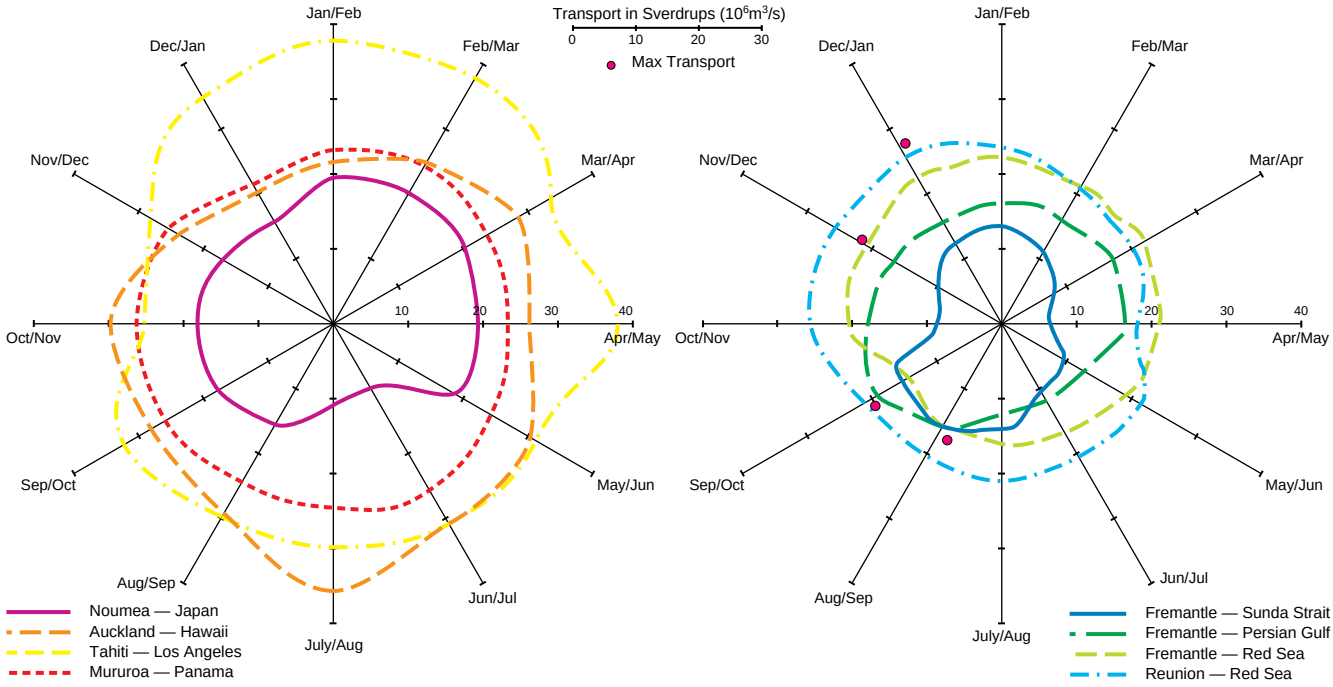

Meyers et al., page 7 *Figure 2. Annual cycle of the geostrophic transport of the South Equatorial Current in Pacific Ocean (left), and Indian Ocean (right), calculated from bimonthly mean temperatures using a mean temperature salinity relationship. The transports in Sverdrups are indicated by distance from the origin. The shipping track is indicated in the legend.*

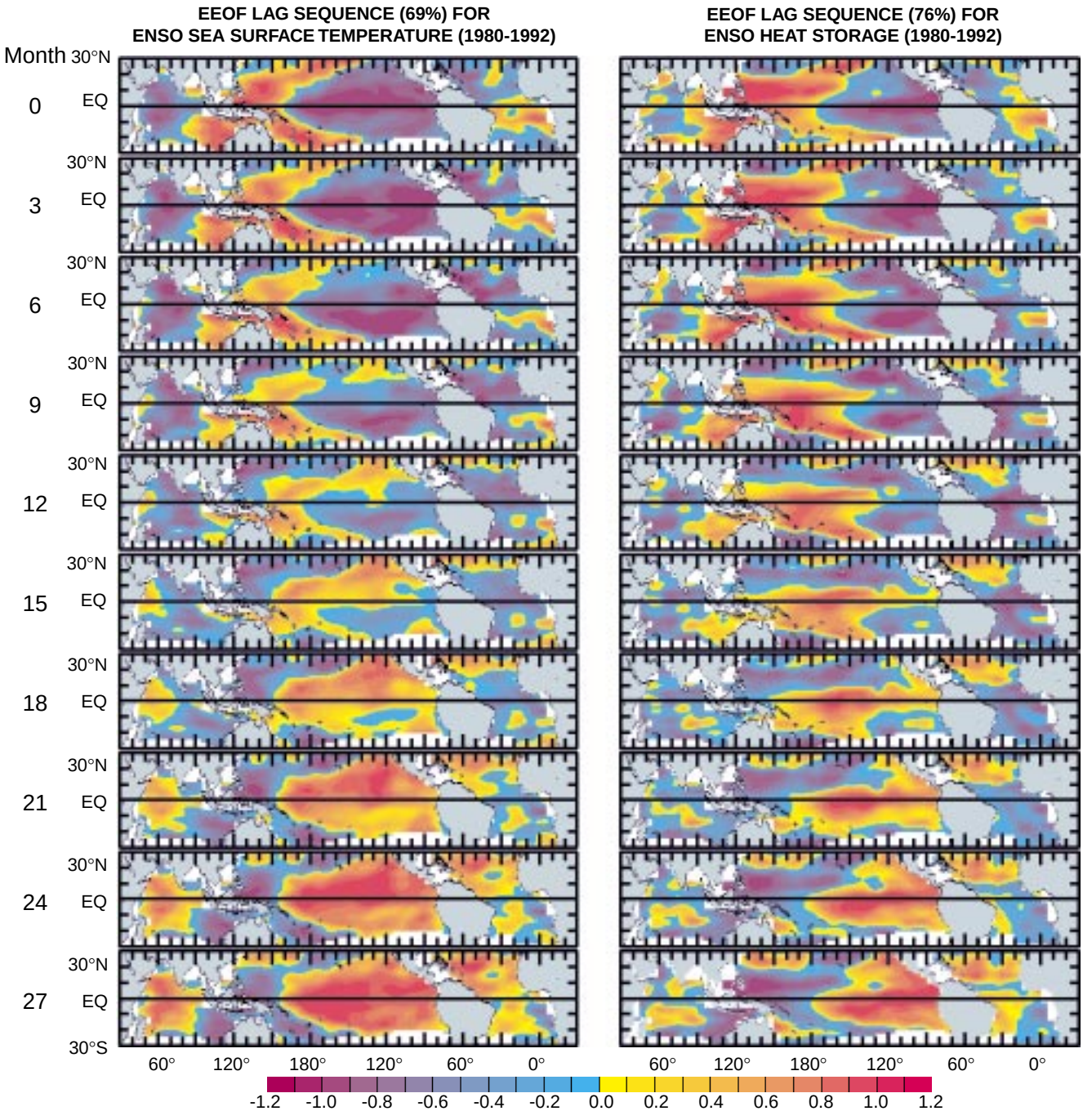

Diggs et al., page 16 *Figure 3. Dominant ENSO variablity characterised by animations for surface temperature and heat storage anomalies.*

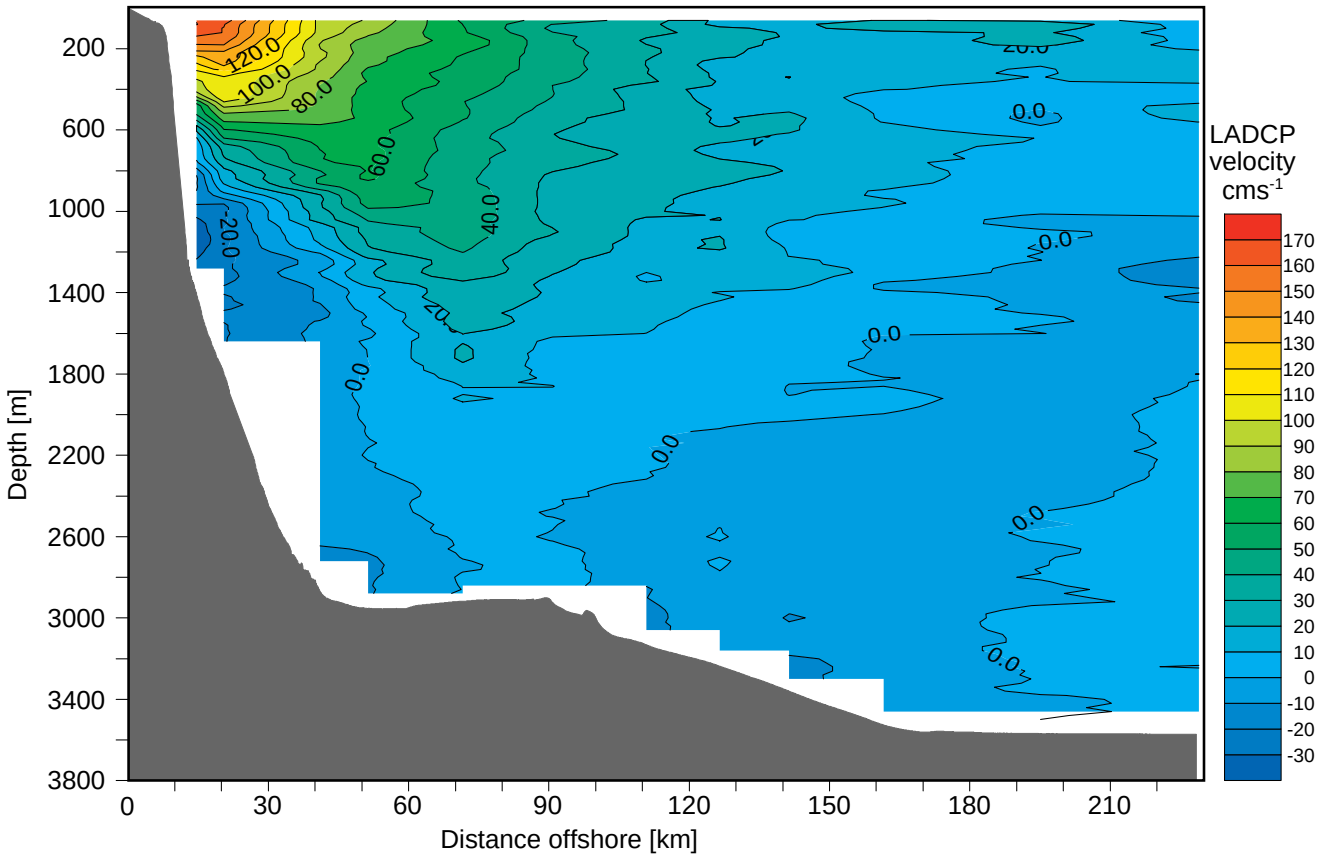

Beal and Bryden, page 25 *Figure 4.* Velocity on I5W measured with a lowered ADCP in February 1995.

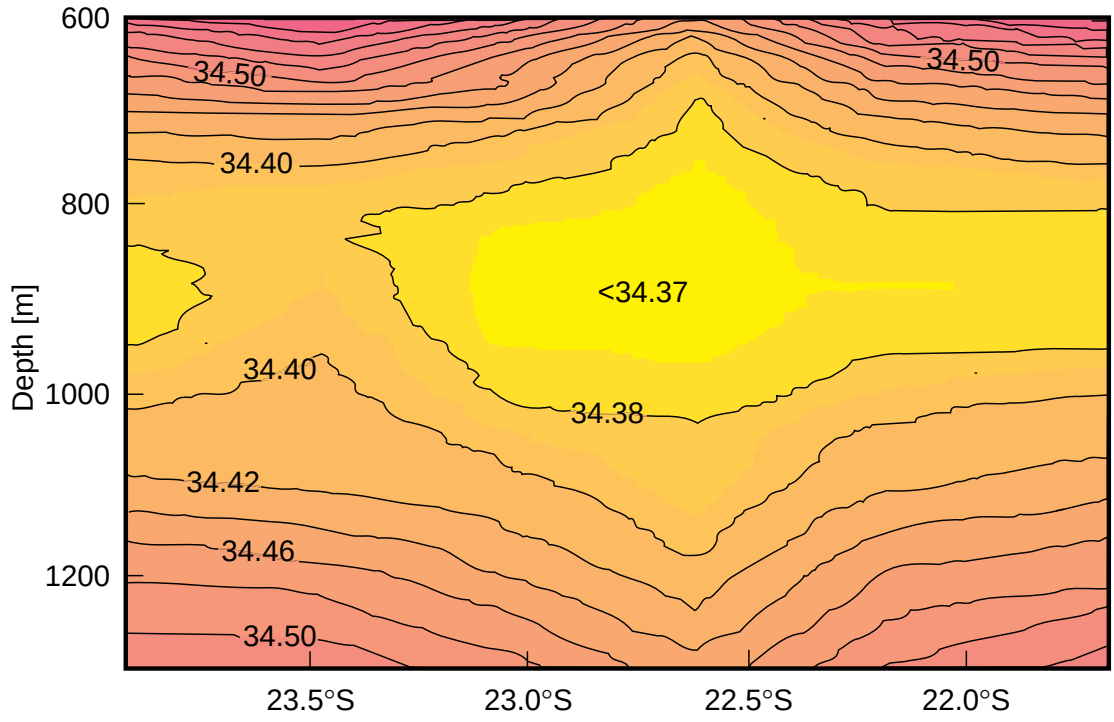

Tomczak and Andrew, page 28 *Figure 3. Enlargement of the salinity distribution for stations 31–36 and the depth range 600–1300m.*

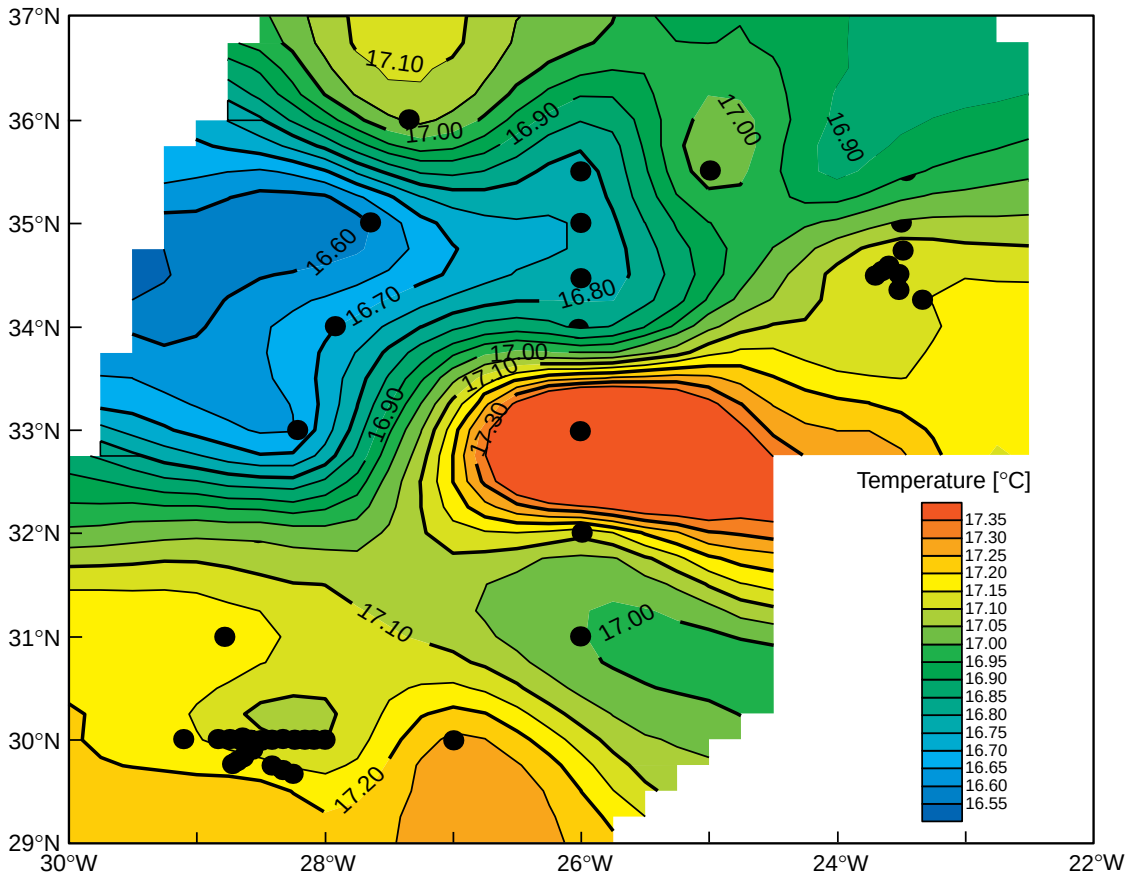

Cromwell et al., page 33 *Figure 3. Potential temperature on the isopycnic surface s_o = 26.55. Westward flow at 35°N is cooler than the main body of the Azores Current. CTD station locations are indicated by black circles.*

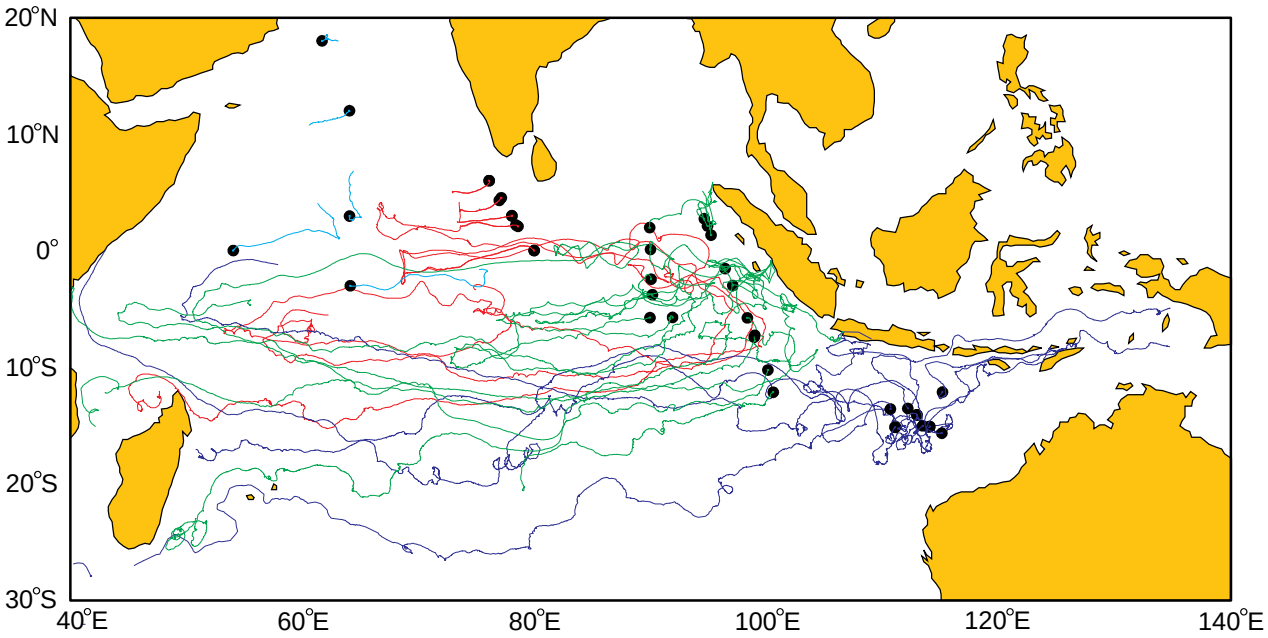

Michida and Yoritaka, page 38 *Figure 1. Trajectories of drifters released between 1990 and 1993.*

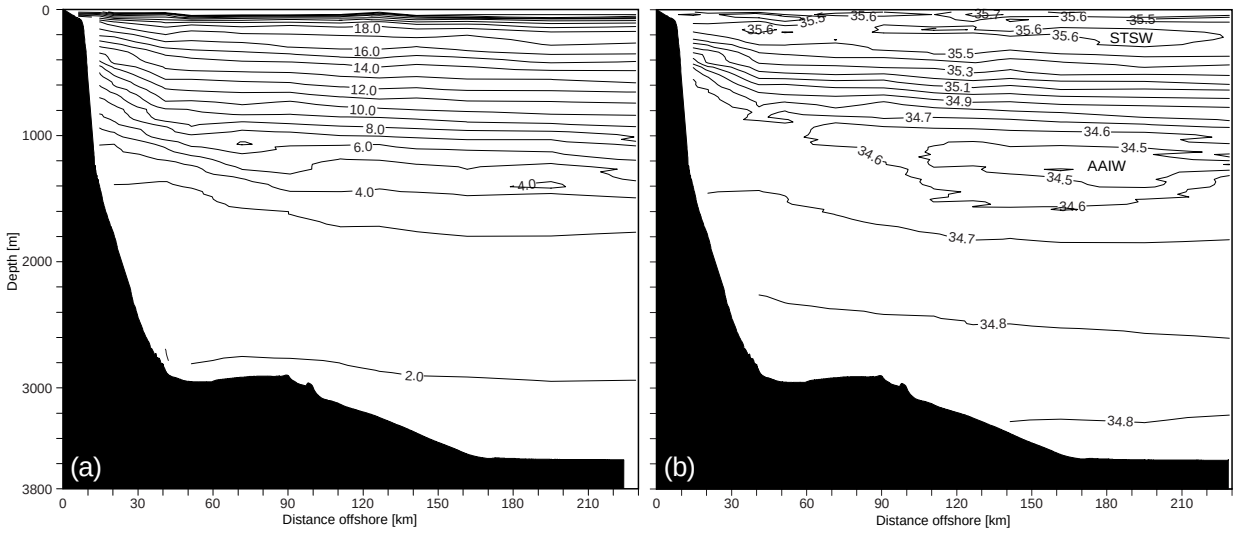

Figure 2. Vertical distribution of temperature (a) and salinity on IW5 in February/March 1995.

to seabed velocity measurements can be obtained from each hydrographic cast. Data quality from the LADCP was excellent throughout the experiment except on the shelf where station depths were less than 70 m, so that all data collected were within the bottom interference layer. To obtain the ocean current from the LADCP measured velocities, we need to remove the effect of instrument movement. This is achieved by differentiating the measured velocities to give vertical shears, but then the mean (or barotropic) current is also removed. If an uninterrupted LADCP record exists for the cast, this barotropic component can be restored by integrating the ship velocities, measured velocities and shear velocities over the entire duration of the cast. This universal component is added to the vertically integrated shear profile to give the absolute ocean current. This technique produces good results provided the data gap due to bottom interference is small.

The isotherms and isohalines shoal towards the shore, indicative of a poleward flowing WBC (Figs. 2a and b). At about 40 km offshore, coincident with the foot of the continental slope, the gradient of the isotherms increases 20 fold so that the 10°C isotherm rises by 1m in 100 m towards the slope. The mixed layer is less than 20 m deep across the section and the thermocline, defined by the depth of the 4°C isotherm, is 1500 m thick in the interior and rises to 1100 m underneath the core of the WBC. Similar hydrographic features were found by Toole and Warren (1993) in November 1987.

The salinity maximum in the Agulhas Current is subsurface, positioned at about 200 m depth. This salinity stratification is typical of more northerly waters where Subtropical Surface Water (STSW) made salty by evaporation, advects northward in the interior flow and is capped through surface warming and precipitation, by a warmer, fresher layer of Tropical Surface Water (TSW). The presence of TSW is an indication of the swift southward flow of the water. Below the STSW, making up most of the thermocline waters, is South Indian Central Water (SICW) which is formed at the subtropical front by the sinking of mixed subtropical and subantarctic surface water masses. Antarctic Intermediate Water (AAIW) appears below the SICW at a depth of 1200 m, indicated by a low salinity signature of 34.40. Further inshore, along the same σ_θ surface of 27.35 as AAIW, there is a pool of water with anomalously high salinity (34.70) and low oxygen, situated directly below the core of the current. Toole and Warren (1993) noticed such a feature in their crossing of the Current and attributed it to Red Sea Water (RSW), which has been reported around the south west Indian Ocean by a number of authors (Grundlingh, 1985; Gordon *et al*., 1987 and Valentine *et al*., 1993). Valentine *et al*. (1993) suggested that RSW mixes with AAIW at the same depth at about 20°S, so modifying the AAIW and giving it a larger range of salinities. It remains a mystery then, that in this section the two water masses appear spatially separated. RSW (or modified AAIW) lies within 50 km of the continental slope, whilst the AAIW is predominantly found more than 110 km offshore (Fig. 3). The water masses are similarly separated in the Toole and Warren (1993) data. At depths greater than 2500 m lies North Atlantic Deep Water (NADW) with characteristic high salinities and high oxygen concentration and a potential temperature of about 2°C.

To calculate geostrophic transport a zero velocity surface was chosen at 1500 m as the surface between nominally southward flowing AAIW and northward drifting NADW. Comparing the ACE geostrophic section to the RRS Charles Darwin section the dimensions and position of the current is similar, although peak surface velocities are almost $100\,\mathrm{cm\,s^{-1}}$ greater in the ACE data. The geostrophic transport is estimated as 50 Sv, compared to 43 Sv from the Toole and Warren (1993) data.

A full depth velocity field through the Agulhas Current taken from direct LADCP measurements is shown in Fig. 4 (page 23). The velocity component is rotated 40° from north, normal to the ship track and is positive to the southwest (220(T)), following the contour of the continental slope. The surface core of the current is about 20 km offshore, as in the geostrophic section, but the

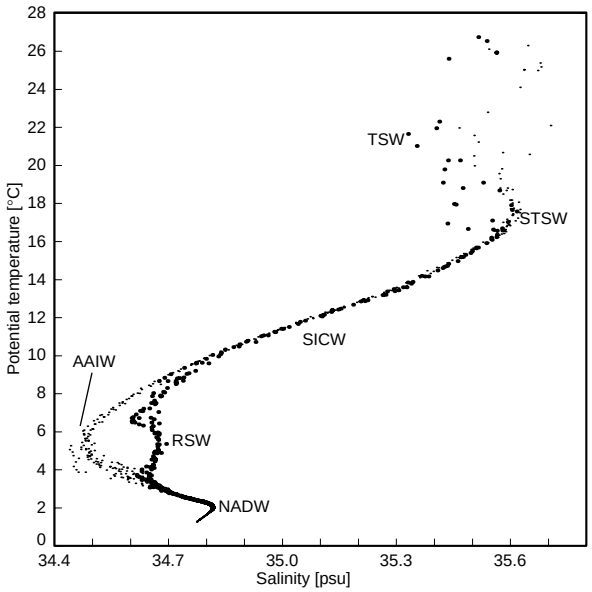

Figure 3. T-S diagram showing the water masses present in the Agulhas Current. Large dots are data from within 50 km of the coast, small dots are data further than 110 km offshore.

current is wider and penetrates to 2500 m, far deeper than the estimated 1500 m, and peak surface speeds in the current are just over $170\,\mathrm{cm\,s^{-1}}$, much less than the $260\,\mathrm{cm\,s^{-1}}$ estimated from geostrophic shear. Against the continental slope at a depth of about 1200 m there is evidence of a countercurrent, or recirculation cell, with north-eastward velocities reaching. This countercurrent is coincident with the patch of modified AAIW underneath the current core. Toole and Warren (1993) had evidence of a countercurrent, similarly positioned, when they used ADCP profiles to reference their geostrophic shears. However, they discounted the possibility that Red Sea Water was flowing northward and chose to disregard the ADCP data in favour of their chosen level of no motion, 500 m above the lowest common depth of each station pair. Perhaps the most striking feature of the LADCP data is that the zero velocity surface is clearly V-shaped and not horizontal (or following the sea bed) as assumed in past investigations (Duncan, 1970; Lutjeharms, 1972; Jacobs and Georgi, 1977; Toole and Warren, 1993). It is as shallow as 800 m next to the continental slope and plunges down almost to the sea bed some 80 km offshore, before rising again more gently on the offshore side of the current. The volume transport of the Agulhas Current from the LADCP data is 71 Sv. For comparison, the Sverdrup transport deduced by Hellerman and Rosenstein (1983) from wind stress curl was just 50 Sv and the volume transport deduced by Toole and Warren (1993) was 85 Sv.

The V-shaped zero velocity surface from LADCP results was used to recalculate absolute currents from the geostrophic shear in order to estimate a more accurate geostrophic transport and to compare the new geostrophic velocity field with that of the measured currents. The shape and features of the modified geostrophic current are very similar to those measured directly by the LADCP (Fig. 5). Most differences in the two sections occur within 100 m of the sea surface, particularly in the core of the current where geostrophic velocities are as much as $40\,\mathrm{cm\,s^{-1}}$ larger than the LADCP velocities. A lens of swiftly flowing surface water 135 km offshore is evident in the geostrophic section but not in the LADCP data. The volume transport of the Agulhas Current estimated from geostrophic shears using a reference level deduced from the LADCP data is 68 Sv, some 10% smaller than the LADCP estimate above.

Our estimate of the volume transport of the Agulhas Current is 71 Sv (as measured by LADCP), 14Sv smaller than that estimated by Toole and Warren (1993). However, Toole and Warren's data yielded a transport of 70 Sv when referenced to their underway ADCP profiles. The difference in the transports seems primarily due to the countercurrent at depth flowing northeast along the continental slope, which is clearly evident in the LADCP section.

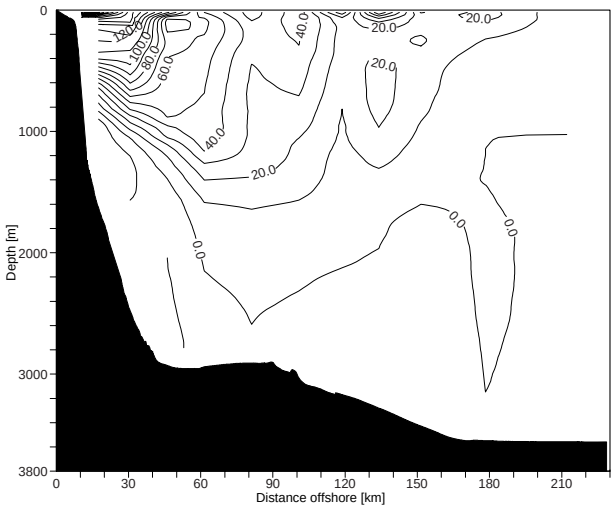

Figure 5. Geostrophic velocity field (cm/s).

Acknowledgments

We are very grateful to Nick Crisp for operating the LADCP aboard RRS Discovery and for his friendly help and advice throughout the cruise and post–processing of the data. We are grateful for the use of Eric Firing's software for the LADCP data processing and for his expert advice on all aspects of LADCP. Thanks to Robin Tokmakian for getting the software running during the cruise. Thanks also to Stuart Cunningham who collected and processed the CTD data and to Mike Griffiths who worked up the positioning data. Finally thanks to Steve Alderson for his pstar expertise.

References

Duncan, C.P., 1970: The Agulhas Current. PhD dissertation, University of Hawaii, 76pp.

Gordon, A.L., J.R.E. Lutjeharms and M.L. Grundlingh, 1987: Stratification and circulation at the Agulhas Retroflection. Deep-Sea Res., 34, 565–599.

Grundlingh, M.L., 1985: Occurrence of Red Sea Water in the southwestern Indian Ocean, 1981. J. Phys. Oceanogr., 15, 207–212.
Hellerman, S., and M. Rosenstein, 1983: Normal monthly wind stress over the world oceans with error estimates. J. Phys. Oceanogr., 32, 1093–1104.
Jacobs, S.S., and D.T. Georgi, 1977: Observations on the southwest Indian/Antarctic Ocean. In: A Voyage of Discovery, pp43–84. M. Angel, editor, Pergamon Press, Oxford.
Lutjeharms, J.R.E., 1972: A quantitive assessment of the year to year variability in water movement in the southwest Indian Ocean. Nature Physical Science, 239, (91), 59–60.
Toole, J.M., and B.A. Warren, 1993: A hydrographic section across the subtropical South Indian Ocean. Deep-Sea Res., I, 40, No. 10, 1973–2019.
Valentine, H.R., J.R.E. Lutjeharms, and G.B. Brundrit, 1993: The water masses and volumetry of the southern Agulhas Current region. Deep-Sea Res., I, 40, No. 6, 1285–1305.

Eddy Formation in the Antarctic Intermediate Water of the Subtropical South Pacific Ocean (Implications for XBT Analysis)

Matthias Tomczak and Colin Andrew, Flinders Institute for Atmospheric and Marine Sciences, Flinders University of South Australia, GPO Box 2100, Adelaide, SA 5001, Australia

A subsurface eddy located between 500 m and 1500 m depth was observed in the South Fiji Basin during WOCE section P14C. It was embedded in Antarctic Intermediate Water and had hydrographic properties identical to its surroundings. Evidence is presented that it may have formed through interaction of the South Equatorial Current with the Lau Ridge or the Kermadec/Tonga Ridge.

The presence of the eddy has strong repercussions for the calculation of geostrophic currents from XBT data, which use levels of no motion near 800 m. Such a reference level would cut through the strongest currents in the eddy; it would eliminate the geostrophic currents associated with the eddy and project them into the surface layer, leading to unrealistic surface currents.

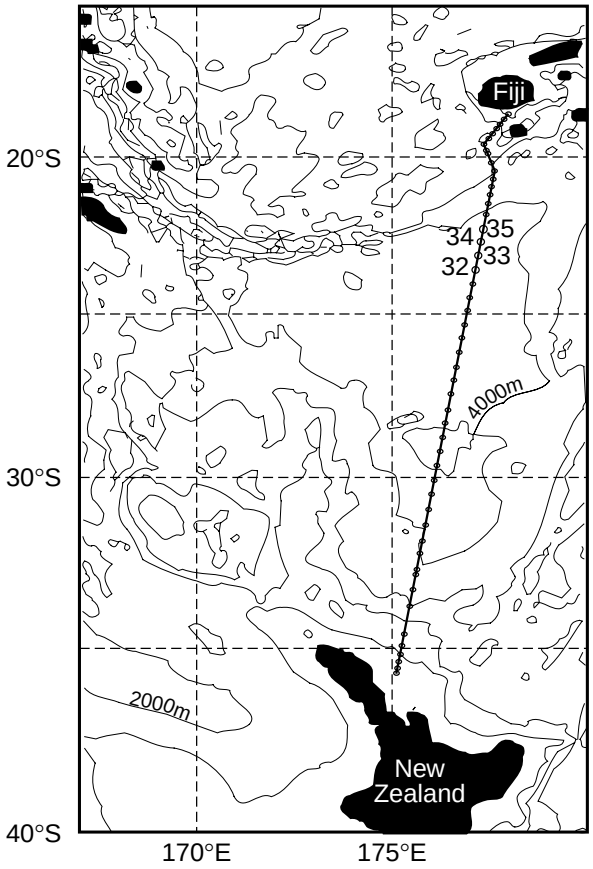

Figure 1. Topography of the western South Pacific, showing the South Fiji Basin between New Zealand and Fiji , and station positions for WOCE cruise P14C.

Introduction

Eddies are the most energetic elements of oceanic turbulence. Currents associated with eddies are usually stronger than the mean circulation, causing transient reversal episodes in the prevailing current. The discovery of rotating lenses of Mediterranean Water in the deeper layers of the Atlantic Ocean showed that the occurrence of eddies is not restricted to the surface circulation. We report here the observation of an eddy found at 1000 m depth in the western subtropical South Pacific Ocean. The eddy was embedded in the general movement of Antarctic Intermediate Water and had the same water mass properties as its surroundings. A more comprehensive report is given in Tomczak and Andrew (1996).

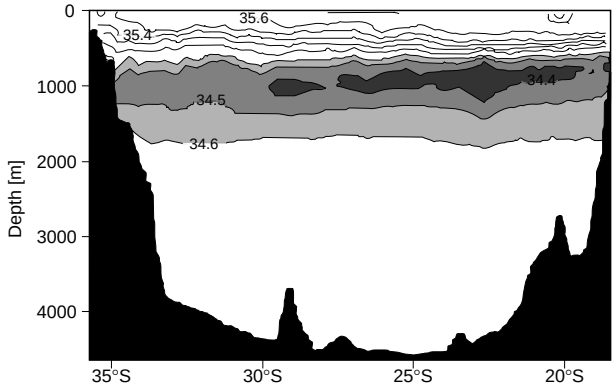

Figure 2. Salinity from New Zealand (left) to Fiji (right) across the South Fiji Basin (WOCE section P14C).

Observations

The eddy was found on WOCE section P14C. This section across the South Fiji Basin between New Zealand and Fiji (Fig. 1) was covered by RV Knorr during September 1992, using the Scripps conductivity/temperature/depth

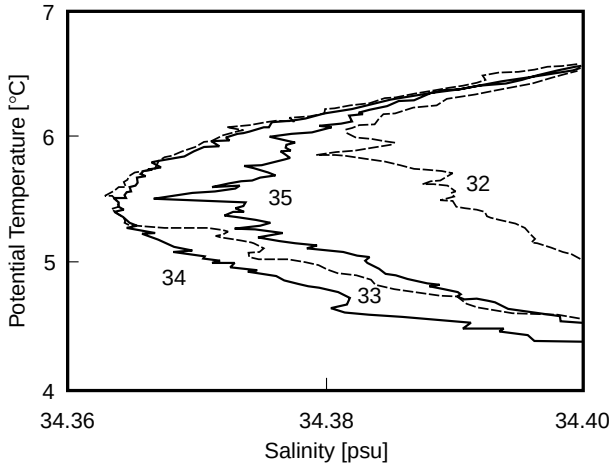

Figure 4. Potential temperature-salinity diagram for stations 32–35 over the depth range of Antarctic Intermediate Water.

(CTD) system with the WOCE 36 bottle rosette. The CTD data were processed to 1 m intervals. Fig. 2 shows the salinity along P14C. The Antarctic Intermediate Water is easily identified by the salinity minimum centred on 900 m. The eddy is seen as an expansion of the salinity minimum layer at stations 32–35. Fig. 3 (page 23) shows this feature in detail. Note that the eddy is identified by more than a single station and is therefore not a product of instrument malfunction or operator error at one station. Water mass properties in the eddy were very close to those found in its vicinity. Fig. 4 shows TS-diagrams for stations 32–35. Apart from much lower small scale variability and slightly lower salinity, the TS-diagrams for stations 33 and 34 correspond closely to that of station 35. Geostrophic currents in and near the eddy are shown in Fig. 5. The eddy is embedded in the westward movement of the South Equatorial Current. Anticyclonic rotation in the eddy enhances the westward motion on its northern side and the eastward motion on its southern side. Eddy velocities are comparable to those of surface currents in the subtropical gyre.

Discussion

Comparison of the hydrological properties inside the eddy with those found in its surroundings shows that the water contained in the eddy came from the same source. This is quite unlike the situation encountered with meddies, which carry a small volume of Mediterranean Water, kept together by the eddy's rotation, through a North Atlantic Deep Water environment. It also makes this type of eddy much more difficult to detect. McWilliams (1985) produced a survey of "submesoscale coherent vortices", eddies of slightly smaller horizontal scale than the well known mesoscale eddies and – more importantly in this context – characterised by a subsurface maximum of the associated velocity field. He states that such submerged eddies are "numerically abundant but usually well separated from each other" and that "at most locations their presence is a rarity". His census of submerged eddies, which produced ample evidence for their abundance, was based on comparison of TS-diagrams from individual stations with TS-diagrams typical of the oceanic structure in the vicinity and therefore identified only eddies with water mass properties different from their surroundings.

While the eddy observed during P14C fits McWilliams' description, it differs from his examples by having identical properties to the water outside. The obvious question raised by the observations is: What caused the eddy? Could it be generated as part of the process of winter convection in the AAIW formation region southwest of Chile (McCartney, 1977)? This appears unlikely, since it would have isolated the AAIW inside the eddy from the mixing processes in the South Equatorial Current to which

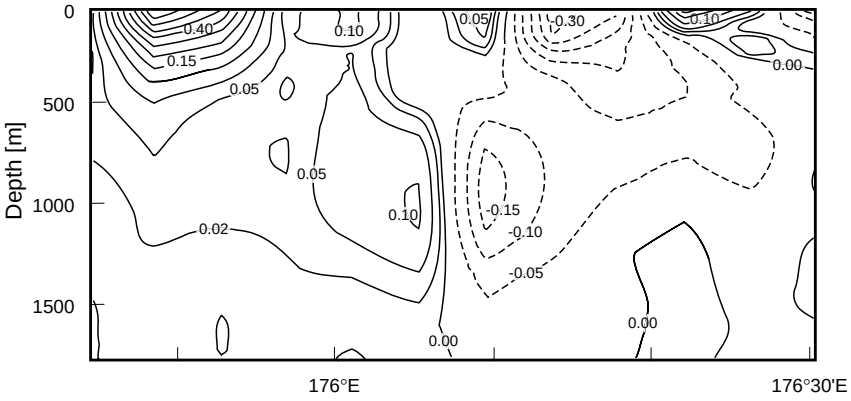

Figure 5. Geostrophic currents in the region of the eddy, referenced to 18000 kPa (circa 1800 m). Broken lines indicate westward flow, contouring interval is 5cm s^{-1}.

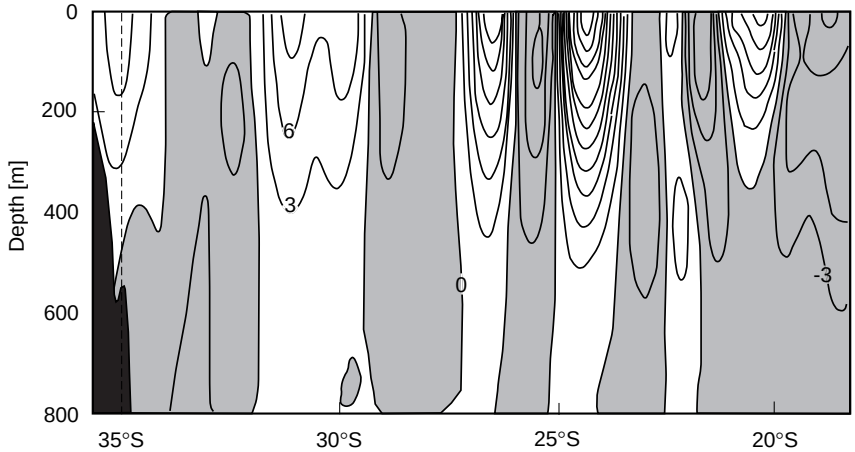

Figure 6. Geostrophic velocity across P14C relative to 800m, contouring interval is 3cm s^{-1}. Adapted from Roemmich et al. (1994).

AAIW is usually exposed, and which lead to a gradual rise of the salinity minimum from 34.2 to 34.4 (Tomczak and Godfrey, 1994). In other words, the minimum salinity inside the eddy should be much lower than the lowest salinity found outside if its origin were as far east as to the west of southern Chile. From Fig. 4 it can be seen that the difference in the salinity minimum between stations 3 and 34 inside the eddy and stations 32 and 35 on either side of the eddy is less than 0.02, which indicates that the eddy formation region cannot be far away.

While the arguments of the last paragraph rule out the eddy's generation in the region of AAIW formation, there is no reason to believe that the water found in the eddy did not originate in the vicinity of the observation area. Its T-S properties were identical to those of its surroundings, and its nutrient and oxygen values indicate that its water was of the same age as the water in which it drifted. The water contained in the eddy must therefore have been formed in the extreme south-east of the South Pacific Ocean, but it was enclosed in the eddy only in the not too distant past. Two ridges east of the South Fiji Basin rise to less than 1000 m depth. The Lau Ridge runs along 178°W, connecting the main islands of Fiji with North Island of New Zealand, and forms the eastern limit of the South Fiji Basin. North of 21°S it occasionally rises to 600 m depth and less. The Kermadec and Tonga Ridges connect North Island with Tonga further east, from 178°W near New Zealand in the south to 174°W north of Tonga. North of 22°S they exhibit a large continuous region with less than 600 m water depth. Both ridge systems are only some 1000 km to the east of the eddy. It appears that the eddy may have formed by interaction of the current at the depth of AAIW with the bottom topography east of the South Fiji Basin. The same generation mechanism was proposed for an eddy observed in the Circumpolar Deep Water (Gordon and Greengrove, 1986).

The existence of the eddy has important consequences for the analysis of geostrophic currents from XBT transects. A high density XBT section between New Zealand and Fiji has been operational for some time now as part of the WOCE XBT effort (Roemmich and Cornuelle, 1990). Calculation of geostrophic currents from XBT data assumes a well defined temperature-salinity relationship and a level of no motion of about 800 m (the maximum depth of the "deep blue" XBT probe). In most situations, currents at 800 m depth are weak and uniform in space, and the assumption of a level of no motion at 800 m gives quite realistic upper layer velocities. The same calculation applied to the data from P14C would place the level of no motion through the eddy, which would suppress the geostrophic circulation associated with the eddy and project it into the surface layer, giving an unrealistic eddy-like circulation at the surface. This is seen in Fig. 6, taken from Roemmich *et al.* (1994), which shows geostrophic currents for P14C referenced to 800 m depth. The strong surface currents indicated near 24–25°S are not supported by our Fig. 5, which indicates banded east-west structure near the surface but of quite moderate strength and stronger currents at the 1000 m level. It appears that careful analysis of isotherm variability at the bottom of XBT sections is necessary to identify and eliminate eddies before a level of no motion is defined.

References

Gordon, A.L., and C.L. Greengrove, 1986: Abyssal eddy in the southwest Atlantic. Deep-Sea Research, 33, 839–847.

McCartney, M.S., 1977: Subantarctic Mode Water. Deep-Sea Research, 24, suppl., 103–119.

McWilliams, J.C., 1985: Submesoscale, coherent vortices in the ocean. Review of Geophysics, 23, 165–182.

Roemmich, D., and B. Cornuelle, 1990: Observing the fluctuations of gyre-scale ocean circulation: a study of the subtropical South Pacific. Journal of Physical Oceanography, 20, 1919–1934.

Roemmich, D., M. Morris, and B. Cornuelle, 1994: XBT results on P14C - Auckland to Suva. US WOCE Report 1994 (US WOCE Implementation Report 6). US WOCE Office, College Station, TX, 12–14.

Tomczak, M., and J.S. Godfrey, 1994: Regional Oceanography: an Introduction. Pergamon Press, Oxford.

Tomczak, M., and C. Andrew, 1996: Eddy formation in the Antarctic Intermediate Water of the subtropical South Pacific Ocean. Journal of Marine and Atmospheric Science, Cochin University, India, in press.

Additions to the IPO Home Pages

Peter M. Saunders

Because transatlantic communications on the WWW are generally slow during normal working hours the Data Products Committee suggested the IPO mirror the DIU home pages, primarily for European use. We have not done that, but on a new page, have provided links to the most commonly sought after data types. (http://www.soc.soton.ac.uk/OTHERS/woceipo/data.html) Try it!

To assist modellers assess the performance of OGCMs we have also made available the current meter statistics prepared prior to WOCE by Bob Dickson and Ken Medler (Fisheries Laboratory, Lowestoft). 2728 records contain current variance (EKE) but not means. The data can be downloaded altogether (size 200k), or in depth intervals, and locations can be viewed either globally or by ocean. (http://www.soc.soton.ac.uk/OTHERS/woceipo/flowstats.html)

Recirculation of the Brazil Current South of 23°S

Merritt R. Stevenson, Inst. Nac. de Pesquisas Espaciais, São José dos Campos, SP 12201-970, Brazil

Brazilian participation in WOCE has been through project COROAS (Oceanic Circulation in the Region of the SW Atlantic). One component of COROAS is the study of the influence of eddies in the Brazil Current using Lagrangian drifters. This subproject represents Brazil's contribution to the SVP of WOCE. To date the drifter component has fabricated and launched 16 low cost drifters (LCDs), 15 of them off SE Brazil and one in the Polar Front of the SW Atlantic (Fig. 1.) Construction procedures for the drifters closely followed Sybrandy and Niiler (1991) and are considered to be representative of WOCE standard drifters. Average life expectancy of Brazilian LCDs is as yet poorly known, due to the small numbers of drifters thus far launched. The durations of the transmissions after LCD launch are summarized in Table 1. To reduce the overall service costs of using ARGOS, the PTTs were programmed to turn off after different time intervals. The LCDs were launched in groups of 5: the first group being programmed to turn off after 12 months, the second group after 9 months and the third group after 6 months. Drifter 3194, launched in the Polar Front, was programmed to transmit until its loss of battery power. This drifter (3194) is still transmitting some 19 months after its deployment. It is hoped that drifter longevity for Brazilian LCDs that transmit without externally programmed time duration limits will approximate the mean values of almost 300 days obtained by other participants in SVP (WOCE, 1995).

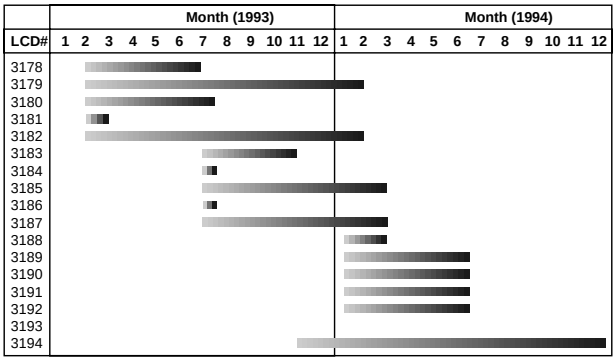

Table 1. Lifetime of the low-cost drifters.

Western Boundary Current Experiment

Five WOCE standard, LCDs with surface water temperature sensors were launched on 17 February 1993, as part of a western boundary current experiment in project COROAS. A thermosalinograph, aboard the University of São Paulo, RV Professor W. Besnard, was used to locate a thermohaline front, normally associated with the western boundary of the Brazil Current (BC), located in the northern part of the COROAS area, off SE Brazil. The LCDs were launched in a box pattern across this western boundary of the BC, with the fifth drifter being launched within the box.

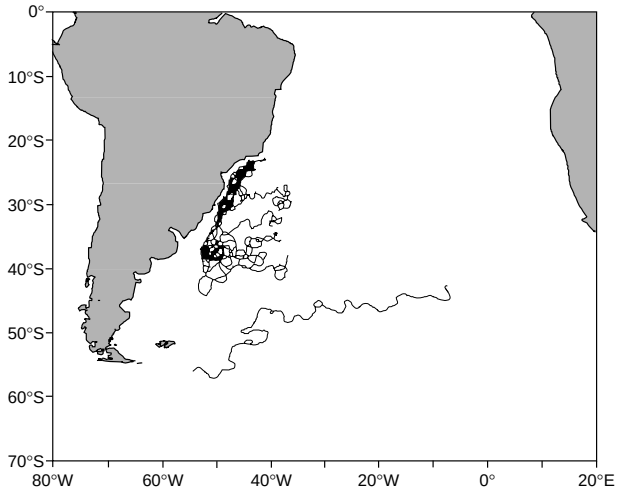

Figure 1. Tracks of Brazilian drifters released in the SW Atlantic.

Preliminary Results

All five drifters indicated the presence of eddies as they moved southwesterly within the BC. As the drifters approached the Brazil-Malvinas Confluence (BMC), one drifter moved offshore, apparently along the north side of the BMC. Upon reaching the BMC region, another drifter stopped transmitting for a period of several months. The remaining three drifters (Fig. 2) moved westward, onto the continental shelf: 3178 at 28.5°S, 3179 at 30.5°S and LCD 3180 at 33.4°S. Subsequently, the three LCDs assumed northeasterly tracks along the shelf until they approximated their original deployment positions, thereby almost closing their circulation patterns. The recirculation period for this part of the Brazil Current varied from 115 to 161 days (3178/3180) for the three drifters, depending on the drifter and its path. Detailed examination of these trajectories shows the onshore movements to occur when the drifters approximated the current shear of cyclonic eddies. The location of some of these eddies seems to be associated with regional topographic features; this resulted in drifter tracks from the subsequent two experiments describing similar trajectories (Fig. 1). Mean currents for the first experiment were to the SW (215–226°) at 15–18 cm/s (3178/3180); the mean return currents were to the NE (31–35°) at 5–17 cm/s (3178/3180). Mean surface water temperatures for the southbound flow were 24.8–25.8°C and 17.6–23.3°C for the northbound current on the shelf. Mean surface water temperature in the northerly coastal current was found to be several degrees lower than in the Brazil Current. This

would be expected if this coastal current consisted of a mixture of cool water from the Malvinas Current and warm water being recirculated from the Brazil Current.

Because of the importance of eddies in the Brazil Current, kinetic energies for the mean and residual flow fields were estimated. Mean kinetic energies per unit mass (MKE) for the southwesterly mean flow and residual displacement series containing eddies were found to be (3180/3179), and $1,332 - 4,207\,cm^2/s^2$ (3178/3180), and for the northeasterly flow were $12 - 145\,cm^2/s^2$ (3179/3180) and $2,384 - 4,661\,cm^2/s^2$ (3178/3179), respectively. While the mean velocity for the Brazil Current was found to be slightly greater than the equatorward coastal current, the eddy kinetic energy (EKE) in the returning flow appears to be equal or greater than that found in the Brazil Current. Overall, EKE energies accounted for 89.4–99.7% of the total kinetic energy.

While there is presently considerable interest in using specially designed drifters to obtain reliable estimates of ocean currents, previously published measurements of surface or surface layer currents in the region of the Brazil Current based on satellite-tracked drifters are very few. Olson et *al*. (1988) used a small number of surface drifters in the Brazil-Malvinas Confluence, together with satellite imagery to study the temporal and spatial variations in that region. Because their study area emphasized the Brazil-Malvinas Confluence, their drifters were all launched poleward of 35°S. These authors, however, comment on the complex structure with its eddies, filaments and meanders. They note that the Brazil Current reverses its southerly direction between 40° and 60°S and cite Reid *et al*. (1977).

Piola *et al*. (1987) used the international FGGE drifting buoy data base to determine the surface velocity field and kinetic energy due to the mean and eddy velocity fields. Due to their use of a 4° grid in the Brazil current region, the two mean velocities determined for the region were 24 cm/s toward 237° (centred at 26°S, 46°W) and 18 cm/s toward 210° (centred at 30°S, 50°W). Our mean velocity estimates for the Brazil Current are in general agreement with those of Piola et *al*. (1987). The higher spatial resolution of our data, however, permit the northerly extension of the Malvinas Current to be observed.

Their estimates for the kinetic energy per unit mass for the mean and eddy velocity fields in the Brazil Current were $200\,cm^2/s^2$ and $500\,cm^2/s^2$ respectively and for the Brazil-Malvinas Confluence region were $200\,cm^2/s^2$ and $1200\,cm^2/s^2$ respectively. Eddy kinetic energy accounted for about 71% of the total kinetic energy in the Brazil Current and 86% for the Brazil-Malvinas Confluence.

Intercomparison of the kinetic energy determinations shows the present estimates of the mean flow to be slightly smaller than those of Piola e*t al*. (1987), while the kinetic energy related to the eddy velocity field determined by the present study is at least double the values obtained from the FGGE data set for the same region. While eddy kinetic energy is dominant in both studies, its contribution is about 10–15% higher in the present study. In addition to the possibility of real interannual differences in the circulation, differing results might also be expected due to different drifter designs. The different spatial resolutions obtained by the present ARGOS system and the positioning system in use during the FGGE field work can also be expected to produce somewhat different results.

These preliminary results from our western boundary current experiment provide evidence that as the Brazil Current approaches the Brazil-Malvinas Confluence, some

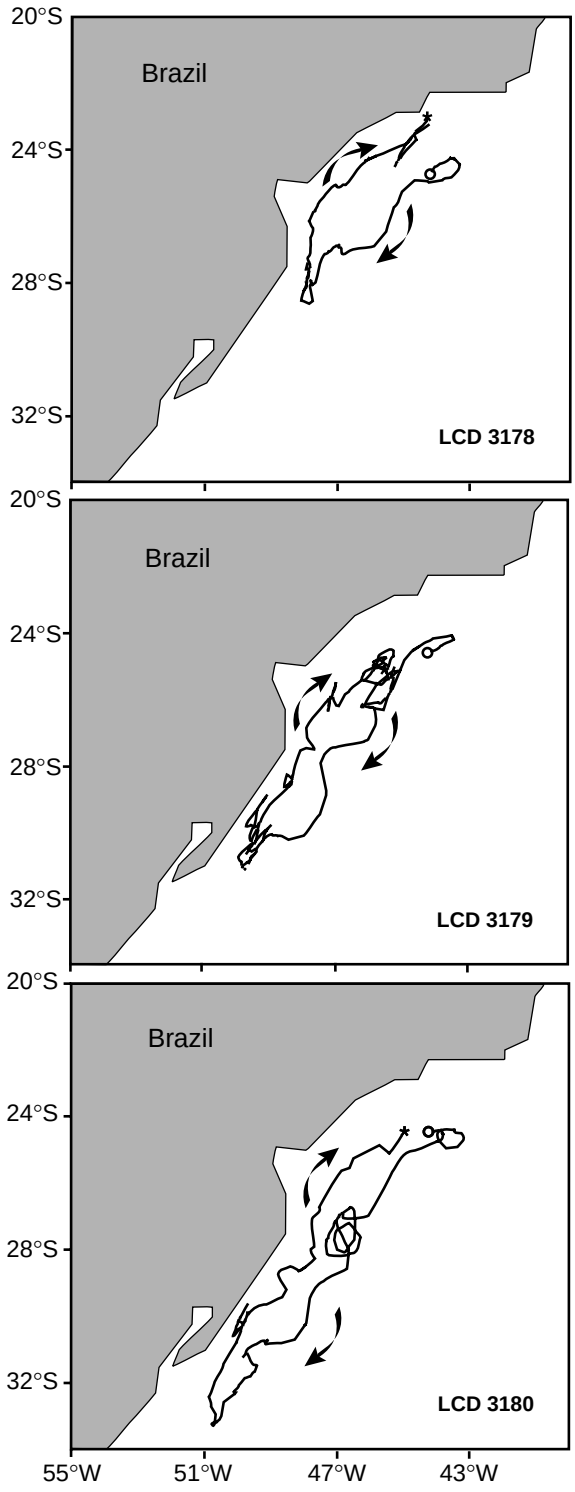

Figure 2. Tracks of three drifters released in the Brazil Current.

of the BC turns coastward at several locations and recirculates. This return flow becomes a part of the northeasterly coastal current between 33°S and 23°S.

Acknowledgements

This work was made possible by financial support from FAPESP (Contr. No. 91/0542-7) and CNPq (Contr. No. 403007/91-7). The Inter-Ministerial Commission for Sea Resources (CIRM) provided fuel for the RV Prof. Besnard, for this and several other COROAS cruises. The author wishes to thank Prof. Pearn P. Niiler for his encouragement in initiating this field work. Travel support was provided by WOCE-IPO to participate in three of the WOCE-SVP planning meetings.

References

Olson, D.B., G.P. Podesta, R.H. Evans, and O.B. Brown, 1988: Temporal variations in the separation of Brazil and Malvinas Currents. Deep-Sea Res. 35(12):1971-1990.

Piola, A.R., A.F. Horacio, and A.A. Bianchi, 1987: Some aspects of the surface circulation south of 20°S revealed by first GARP Global Experiment drifters. J. Geophys. Res. 92(C5):5101-5114.

Reid, J.L., W.D. Nowlin, Jr, and W.C. Patzert, 1977: On the characteristics and circulation of the Southwestern Atlantic Ocean. J. Phys. Oc., 7:62-91.

Sybrandy, A.L., and P.P. Niiler, 1991: The WOCE/TOGA Lagrangian Drifter Construction Manual. SIO Ref. 91/6, WOCE Rep. No. 63, 58 pp.

WOCE International Project Office, 1995: Report of the seventh meeting of the WOCE/TOGA Surface Velocity Programme Planning Committee (SV-7), Sea Lodge at La Jolla Shores, CA, USA, 2-4 November 1944. WOCE International Project Office, WOCE Report 129/95, 31pp.

Persistent Westward Flow in the Azores Current as Seen From Altimetry and Hydrography

David Cromwell, Peter Challenor and Adrian New, Southampton Oceanography Centre; and Robin Pingree, Plymouth Marine Laboratory.

The Azores Current is part of the eastern North Atlantic subtropical gyre and is generally considered to be an extension of the Gulf Stream. In this article, we investigate temporal and spatial variability of the eastward flowing, jet-like Azores Current by applying a new method (Challenor *et al.*, 1996) for combining altimetry data with hydrography along a coincident altimeter/cruise track. This enables one to produce time series of absolute (barotropic plus baroclinic) surface geostrophic currents.

Altimeter sea surface measurements contain information about both the geoid and the surface geostrophic ocean circulation. However, the geoid signal dominates and is generally not sufficiently well known at the small length scales required to identify the mesoscale ocean signal. In this study, we use hydrography to distinguish the mean ocean signal from the geoid along an ERS-1 satellite track south of the Azores, while in its 3-day repeat phases in early 1992 and early 1994, and thereby determine cross-stream absolute dynamic topography of the Azores Current at high temporal resolution. (A fuller version of our work has recently been accepted for publication (Cromwell *et al.*, 1996).)

In essence, our approach is as follows: since the altimeter can measure the variability of the current, if we can measure the absolute current at the time of one satellite pass, we can infer the absolute current at every pass. In our study, a conductivity-temperature-depth (CTD) section, with an assumed level of no motion at 2000 dbars, is used to determine a snapshot of absolute surface geostrophic flow of the Azores Current close to the time of overpass of the ERS-1 altimeter. We can then monitor the variability of the absolute surface geostrophic current for as long as the altimeter repeats the same track.

Fig. 1 shows the northeast Atlantic Canary Basin and Azores Current region. The ground track pattern of ERS-1 in its 3-day repeat configuration is indicated. Since ERS-1 (and the recently-launched ERS-2) has a high orbital inclination, the repeat tracks are near-meridional and so well-suited for examination of zonal geostrophic flows, such as the Azores Current. The highlighted track was surveyed between 37˚N and 31˚N on RRS Charles Darwin cruise 66 from 5 March to 7 March 1992. Hydrographic data (CTD profiles) collected at 1˚ latitude intervals along this section are combined with appropriately smoothed ERS-1 altimeter data from the 3-day repeat phases of January–March 1992 (Phase B) and January–early April 1994 (Phase D). This allows one to construct time series of 3-day repeat profiles of absolute surface geostrophic velocity perpendicular to the altimeter/cruise track (not shown here).

Fig. 2 shows the mean, and the mean ± standard deviation current profiles. Note that the standard deviation comprises both inherent variability of the Azores Current at any given along-track location, as well as random noise in the derived velocity estimates. The standard deviation is typically around $6 - 7\ \mathrm{cm\ s^{-1}}$ and is approximately constant with latitude. The main core of the Azores Current is seen near 32.5˚N. Surprisingly, perhaps, there appears to be no correlation between variability and strength of the mean flow. The mean profiles highlight the persistence of the flow structure, in particular a westward flowing component near 35˚N. There is a hint of a secondary westward, or even stationary, flow centred around 33.5˚N. There is also westward flow across the south of the section (south of 31.5˚N).

Comparing the mean profiles from phases B and D,

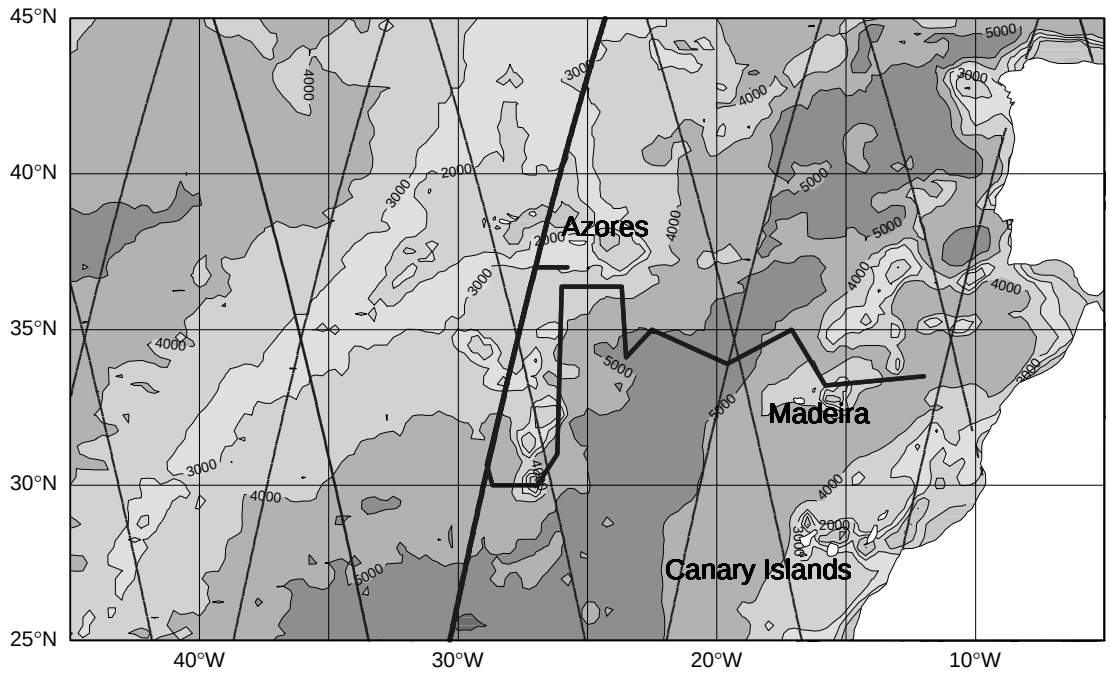

Figure 1. North East Atlantic Canary Basin and Azores Current region. The ground track pattern of ERS-1 in its 3-day repeat phases (Phases B and D) is indicated. The descending satellite pass on 7 March 1992 is shown as a heavy dotted line. The cruise track sailed by RRS Charles Darwin (Cruise 66) is depicted as a heavy solid line. The plot also shows the bathymetry with a contour interval of 1000 m. Part of the Mid-Atlantic Ridge can be seen extending from southwest to northeast in the western half of the map.

there is some evidence of interannual variability. In 1994,the two major lobes (centred near 32.5˚N and 35˚N) appear slightly stronger in magnitude, and the secondary westward lobe at 33.5˚N weaker, than in 1992. The existence of the westward flow near 35˚N was first identified by Pingree (1996) based on CTD and ADCP (acoustic Doppler current profiler) data collected during RRS Charles Darwin cruise 66. By combining the CTD section with altimetry we have established the persistence of this phenomenon in the early months of 1992 and 1994.

An isopycnal analysis was performed which revealed that the westward flow around 35˚N is cooler and fresher than the main body of the Azores Current. Fig. 3 (page 24) shows the potential temperature plotted on an appropriate isopycnic surface, $\sigma_o = 56.55$. If we regard the isotherms as proxies for streamlines, to a first approximation, then we see that warmer (~17.0°C) Azores Current water flows from west to east, while cooler (~16.5°C) recirculated water turns west near 35˚N, 28˚W. Examination of salinity distribution (not shown here) on the same isopycnic surface reveals that the westward flow is fresher than the eastward Azores Current.

The combined altimetry/hydrography analysis is restricted to the ERS-1 3-day repeat phases. Attempts to extend the time series of absolute profiles by incorporating 35-day altimeter data for the period April 1992 – December 1993 (ERS-1 Phase C) have been unsuccessful. This is because the along-track geoid slopes differ significantly over the 25 km separating the 3-day repeat track and the nearest 35-day repeat track. However, it is hoped to capitalise on a recent cruise (PML, October 1995) which occupied a

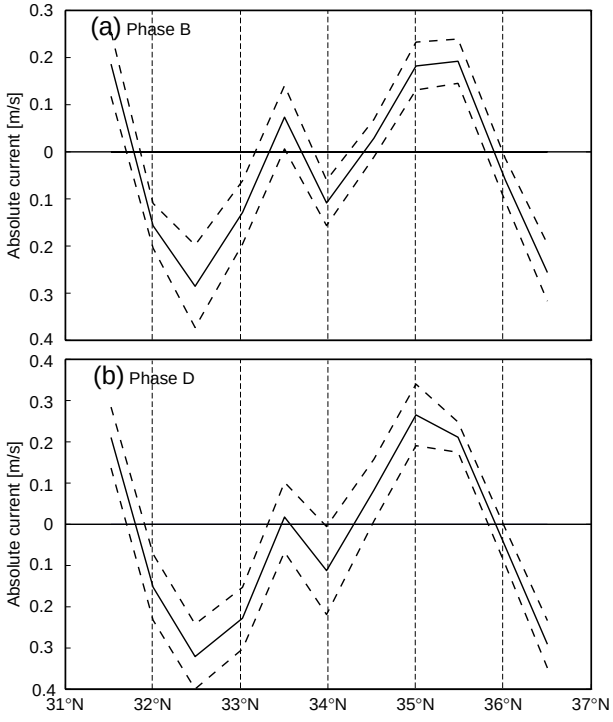

Figure 2. Mean Azores Current surface geostrophic velocity profile (solid line) and mean ± standard deviation profiles (dashed lines) for (a) ERS-1 Phase B (27 December 1991 to 30 March 1992) and for (b) Phase D (23 December 1993 to 10 April 1994). Positive current values indicate westward flow.

CTD/ADCP section along a 35-day repeat track. This would allow monitoring of the Azores Current for as long as ERS-1 or ERS-2 continues in orbit.

In this study, we have estimated absolute geostrophic velocities by assuming a level of no motion at 2000 dbar. This is probably accurate to a few $cm\,s^{-1}$. An alternative method for calculating absolute surface geostrophic velocities, if sufficiently accurate ADCP and navigation data is available, is to match ADCP and geostrophic shear profiles below the wind-driven surface layer and extrapolate back to the surface (as was performed in the Drake Passage by Challenor *et al*., 1996). This approach has the added benefit that it is not necessary to assume an arbitrary level of no motion. However, due to the sparseness of the CTD sampling and absence of 3D GPS which gives accurate ship's heading (*e.g.* King and Cooper, 1993), this approach was unsuccessful in the present study. It is also hoped to use differential GPS techniques in the future to enhance the accuracy of underway ADCP velocities to less than 1 $cm\ s^{-1}$ for 10-minute average velocities King *et al.,* (1996). However, removal of tidal and inertial oscillation from ADCP data will likely remain problematic.

The driving mechanism for the westward flow is not clear. We speculate that sea bottom topography could play a role in constraining water from the north side of the Azores Current to retroflect and flow west. Ollitrault (1995) has shown that trajectories of SOFAR floats advected by the Azores Current are strongly influenced by the seamounts along 28°W (see Fig. 1). A detailed explanation is, however, beyond the scope of the present paper. For the moment, the question of whether westward flow of the Azores Current is a seasonal feature or more permanent remains open.

Acknowledgements

The authors thank ESA and John Lillibridge (NOAA) for providing the altimeter data. David Cotton manages these data locally (at SOC). Helen Snaith provided some of the altimeter processing software. Discussions with colleagues at SOC and with the SEMAPHORE group were stimulating and informative.

References

Challenor, P.G., J.F. Read, R.T. Pollard, and R.T. Tokmakian. Measuring surface currents in the Drake Passage from altimetry and hydrography. Submitted to Journal of Physical Oceanography, 1996.

Cromwell, D., P.G. Challenor, A.L. New, and R.D. Pingree. Persistent westward flow in the Azores Current as seen from altimetry and hydrography. J. Geophys. Res., accepted, 1996.

King, B.A., and E.B. Cooper, 1993: Comparison of ship's heading determined from an array of GPS antennas with heading from conventional gyrocompass measurements. Deep-Sea Res., 40, 2207–2216.

King, B.A., S.G. Alderson, and D. Cromwell, Enhancement of shipboard ADCP data using DGPS position and GPS heading measurements. Deep-Sea Res., accepted, 1996.

Ollitrault, M., 1995: The general circulation of the Subtropical North Atlantic, near 700 m depth, revealed by the TOPOGULF SOFAR floats. International WOCE Newsletter No. 20 (September 1995),15-18.

Pingree, R.D. Long buoy (drogued at ~200 m depth) tracks, hydrography, circulation and subduction in the eastern subtropical North Atlantic. Deep-Sea Res., submitted, 1996.

Plymouth Marine Laboratory, 1992: RRS Charles Darwin cruise 66/92, 4 March–6 April, PML cruise report, 85pp.

Mass and Heat Fluxes at 36°N in the Atlantic: Comparison of 1993, 1981 and 1959 Hydrographic Surveys

Sergey Dobroliubov, Department of Oceanology, Moscow State University, 119899 Moscow, Russia;
Bob Tereschenkov and Alexey Sokov, P.P. Shirshov Institute of Oceanology, Russian Academy of Sciences, 23 Krasikova st., 117851 Moscow, Russia

In the International WOCE Newsletter No. 18 Tereschenkov *et al.* (1995) have reported changes in the thermohaline structure at 36°N in the Atlantic, based on the data collected during three occupations of the ocean-wide hydrographic section by RV Chain in 1959, RV Atlantis-II in 1981 and RV Professor Multanovskiy in 1993. Considerable changes in the water mass properties at intermediate and deep layers were reported. In the present study we deal with the estimates of integral properties such as the zonally averaged temperature and salinity and the mass and heat fluxes across the section's plane. Previous to evaluation, all the data have been interpolated to fixed pressure levels. It must be noted that nothing has been done to uniform the horizontal resolution of the data from different cruises. In case of 1993 and 1981 surveys it seems to be unimportant because the station spacing and the cruise tracks were almost similar, but the track of 1959 cruise differed from the others in eastern most and western most parts of the section and the station spacing in the mid-ocean part of the section was almost two times greater than in the later cruises. So, all the estimates derived from the RV Chain data must be considered with respect to this fact.

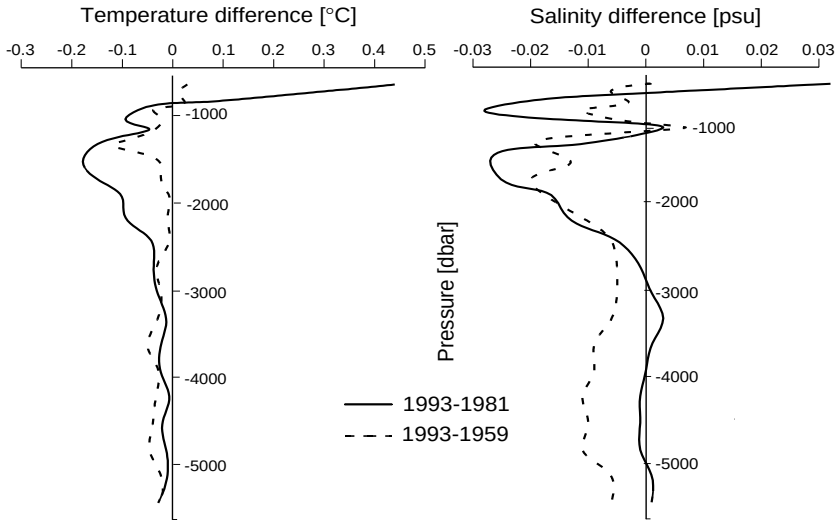

Figure 1. Zonal mean temperature (a) and salinity (b) differences between 1993–1981 and 1993–1959

Zonal mean temperature and salinity differences

Fig. 1 presents zonally-averaged temperature and salinity differences at 36°N below 500 m. The surface layers are subjected to strong annual forcing and therefore are characterized by significant annual changes. The most significant changes of both temperature and salinity differences are observed in a 800–2200 dbar layer, which corresponds to the distribution of the intermediate waters, specifically to AAIW primarily responsible for the changes in 700–1000 dbar layer and LSW responsible for the changes in 1200–2200 dbar layer. If compared to 1981 a freshening of 0.02–0.03 psu and cooling of 0.1–0.2°C took place. Some smaller negative differences are registered between 1993 and 1959. The cooling up to 0.03–0.05°C is observed also in a deeper layers, but the salinity differences here are not so pronounced if compared to 1981. The significant negative salinity anomaly (about 0.01 psu) between 1993 and 1959 is probably due to the salinity problem with the IGY data reported by Mantyla, 1994.

In general the water mass characteristics of the deep waters experienced slight cooling and freshening through the whole period of observations. The intermediate waters became warmer and saltier during 1959-1981 and then cooled and freshened in 1993. It is noticeable that the cooling and freshening in 1993 were more pronounced than preceding warming. Hence, integrally, cooling and freshening took place at the intermediate depth over entire 34-year period.

Mass fluxes

To estimate the total transport through a plane of a zonal section the technique proposed by Bryan (1962) was used. Total meridional velocity is assumed to be a sum of barotropic velocity Vo, shear or geostrophic velocity Vg and Ekman drift velocity Ve. It was assumed that each of three components of the flow is compensated, so that an integral over the plane of the section equals zero. It means, that barotropic flux, determined from a Svedrup's relation for the eastern and mid-ocean parts of the section, is compensated by barotropic counter flux in the western boundary region. Similarly, Ekman flux in a surface layer is compensated by an equal flux uniformly distributed over the rest of the section area. The balance of the geostrophic flux is achieved by a proper selection of the "no-motion" level. It was considered that this level must lie in the density interval separating AAIW and LSW, that move in the opposite directions. To match the transports above and below the "no-motion" level, the value of σ_2 surface was varied until the divergence of the geostrophic flux equalled to the flow through the Bering Strait (-0.8 Sv). The surfaces defined this way differed between cruises rather essentially: from 36.70 in 1993 to 36.76 in 1959 and 36.86 in 1981. The computations of the barotropic and Ekman components were based on the mean climatic values of the wind stress (Hellerman and Rosenstein, 1983). The Ekman transport at 36°N was estimated to be 2 Sv to the south. Barotropic transport according to Sverdrup relation at 36°N was about 20 Sv. The offshore boundary of the Gulf Stream was set at the station, at which the total geostrophic transport in the upper 2000 m was directed to the north (Leaman *et al.*, 1989).

Fig. 2 presents zonally-averaged meridional velocity at 36°N for the three surveys. The depth of the "zero"

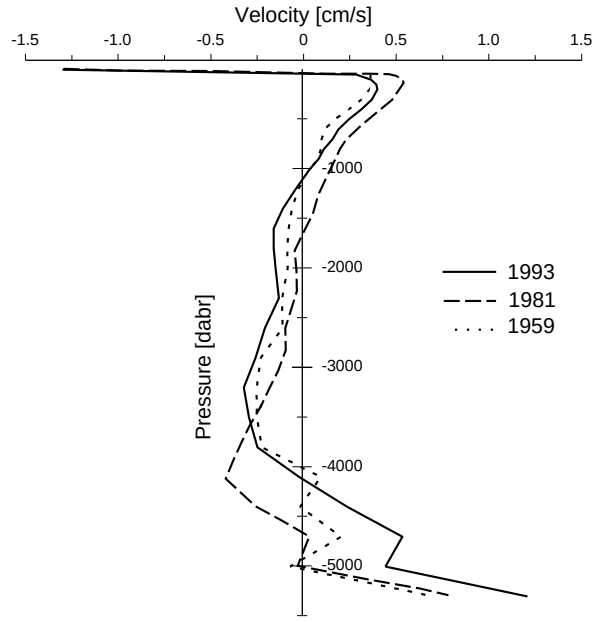

Figure 2. Zonally averaged velocity in 1993, 1981, 1959

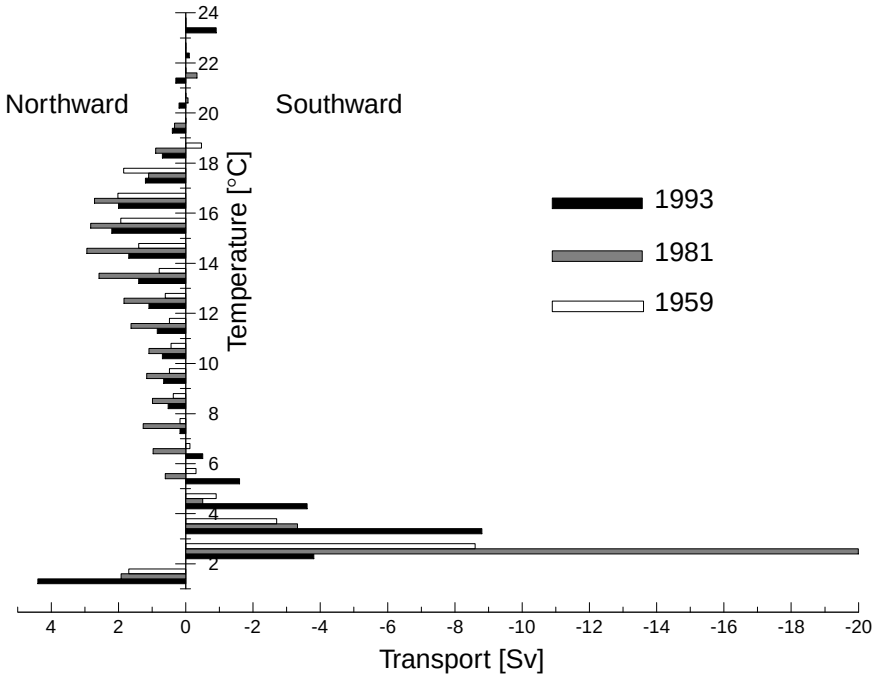

Figure 3. Scheme of volume transport (Sv) distribution across 36°N. Geographically the section plane is divided into Western Boundary area, Western Basin and Eastern Basin. The section is divided into "upper" and "lower" parts by "no-motion" surface. The columns at the right present the integrated values of the volume flux

zonally averaged velocity changes from 1100 m in 1959 and 1993 to 1700 m in 1981. Besides the depth of "zero" velocity separating south flowing NADW and heading north AABW also deepened by about 800 m. The transport of AABW to the north has increased in average by 0.5 cm/s. Because of the intensive northward transport in a bottom layer the total flux to the south below the "no-motion" level was smaller in 1993 than in 1981 by 40%: 14 Sv against 22 Sv. The year 1959 was characterized by even more reduced vertical circulation – less than 11 Sv in a deep layer.

In terms of the "conveyor belt" circulation, the maximum of meridional overturning cell intensification took place in 1981 (Fig. 3). The magnitude of the Gulf Stream transport variations didn't exceed 4 Sv (64–68 Sv). In contrary the DWBC transport varied very significantly: from 25 Sv in 1959 up to 13 Sv in 1981 and then to 31 Sv in 1993. The most striking peculiarity observed on Fig. 3 is reversal flux of deep water in Western basin. Possibly part of this variability was compensated by the barotropic transport (Johns *et al*., 1995).

Meridional transport into temperature classes and heat flux

The information about the changes of the water mass transport as a function of temperature is presented in Fig. 4. 1993 is characterized by the maximum southward transport in temperature class from 5 up to 2.4°C (Upper NADW), accompanied by the increased AABW transport to the north (4.5 Sv instead of 2 Sv in 1981 and 1959). 1981 is characterized by a tremendous volume transport in temperature class from 2.0 to 2.3°C to the south and by the intensification of northward flow of the warm thermocline waters. 1959 is characterized by a intermediate conditions. In order to evaluate the components of the meridional heat transport (MHT) the method described by Bryan (1962) and Bennett (1978) was used. Barotropic heat transport was computed as the Sverdrup's mass flux times the mean potential temperature difference between the Gulf Stream region and mid-ocean part of the section. Ekman component was determined using temperature differ-ence between upper 25-metre layer and the sectional mean value. Baro-clinic (geostrophic) transport was divided into zonal mean, associated with the longit-udinally averaged overturning flux (Bennett, 1978) and horizontal gyre circulation. Values of MHT components across 36°N are presented in Table 1.

Oscillations of barotropic and Ekman fluxes between the surveys are formed by temperature differences because the appropriate volume fluxes are set to be the same. Area-weighted temperature differences between western boundary region and mid-ocean part were obtained to be relatively small: -0.2–0.6°C. Due to this fact errors in barotropic transport estimation couldn't influence the total MHT. Even if the value obtained from the Sverdrup relation is three times less then the real one (Johns *et al*., 1995), barotropic MHT would be only of order 0.1 PWt.

Evaluated differences between overturning cell volume fluxes (Fig. 3) cause the extremely high changes of baroclinic zonal mean heat transport and consequent increase of total MHT from 0.6 PWt in 1959 to 1.2 PWt in 1981. Similar results were presented by Roemmich and Wunsch (1985). Reduction of total MHT in 1993 is also induced primarily by weakening of vertical overturning cell. It is interesting to note that horizontal gyre flux reflects the simultaneous variations as the zonal mean component.

Table 1. Meridional heat flux components (10^{15}W or PWt) across 36°N for 1959, 1981 and 1993

Year	Barotropic heat flux	Ekman heat flux	Baroclinic heat flux zonal mean	gyre	Total heat flux
1959	-0.03	-0.10	0.51	0.20	0.58
1981	-0.05	-0.12	1.01	0.37	1.21
1993	-0.02	-0.14	0.57	0.25	0.66

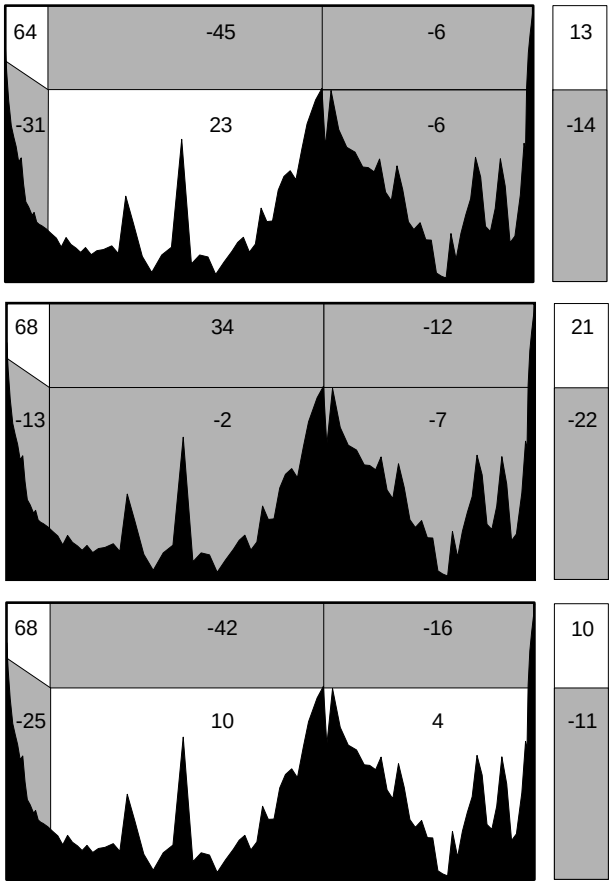

Figure 4. Transport (Sv) across 36°N section as a function of potential temperature for the three surveys

References

Bryan, K., 1962: Measurements of meridional heat transport by ocean currents. J. Geophys. Res., 67, 3403–3414.

Bennett, A.F., 1978: Poleward Heat Fluxes in Southern Hemisphere Oceans. J. Phys. Oceanogr., 8, N9, 785–798.

Dobroliubov, S.A., V.P. Tereschenkov, and A.V. Sokov, 1995: Water mass distribution on 36°N in the Atlantic Ocean in 1993. Oceanology, 35, 6. (In Russian).

Hellerman, S., and M. Rosenstein, 1983: Normal monthly wind stress over the world ocean with error estimates. J. Phys. Oceanogr., 13, 1093–1104.

Helland-Hansen, B., 1934: The Sognefjord Section. Oceanographic observations in the northernmost part of the North Sea and southern part of the Norwegian Sea. In: James Johnstone Memorial Volume, University Press, Liverpool, p.257–274.

Leaman, K.D., E. Johns and T. Rossby, 1989: The average distribution of volume transport and potential vorticity with temperature at three sections across the Gulf Stream. J. Phys. Oceanogr., 19, N1, 36–51.

Mantyla, A.W., 1994: The treatment of inconsistencies in Atlantic deep water salinity data. Deep-Sea Res., 41, N9, 1387–1405.

Johns, W.E., T.J. Shay, J.M. Bane and D.R. Watts, 1995: Gulf Stream structure, transport and recirculation near 68°W. J. Geophys. Res., 100, C1, 817–838.

Roemmich, D., and C. Wunsch, 1985: Two transatlantic sections: meridional circulation and heat flux in the subtropical North Atlantic Ocean. Deep-Sea Res., 32, 619–664.

Tereschenkov, V.P., and A.O. Andreev, 1993: Meridional heat transport across 36°N in the Atlantic. Meteorology and Hydrology, No. 8, 63–73.

Tereschenkov, V.P., A.V. Sokov, and S.A. Dobroliubov, 1995: WHP section A3 across 36° N aboard RV Professor Multanovskiy. I. WOCE Newslett., No. 19, 25–27.

Meetings With a North Atlantic Theme

The ICES Annual Science Conference will be held in Reykjavik, Iceland, 27 September–4 October 1996.

One theme session will be "The North Atlantic Components of Global Programmes: Lessons to ICES-GLOBEC from WOCE/JGOFS", Co-Convenors Prof. B. Zeitzschel (Germany) and Dr W.J. Gould (UK).

Papers and posters are invited on physical and biogeochemical processes and variability and particularly those based on results from the WOCE and JGOFS programmes. Presentations that relate to the synoptic view of marine processes relevant to climate change and/or are of relevance to the GLOBEC programme are particularly welcome.

Titles and abstracts of papers should be submitted to the convenors in time for them to be forwarded to ICES by 30 April 1996.

Copenhagen is the Cultural Capital of Europe 1996 and as part of the celebration there will be a conference 18–20 November 1996 on **The North Atlantic** (Ocean currents, climate, weather and environment).

Sub-themes will be

- Decadal variability in meteorology and oceanography
- Ocean currents, climate, weather, food and environment
- Heat fluxes
- Process studies
- Exchange with Nordic seas
- Ocean modelling results
- Climate impact on fish stocks
- The North Atlantic component of a Global Ocean Observing System.

Send registration form and abstracts toDr Erik Buch, Oceanography Department, Royal Danish Admin. of Navy and Hydrography, Overgaden o Vandet 62B, 1023 Copenhagen K, Denmark, before 1 July 1996.

Surface Currents in the Area of Indo-Pacific Throughflow and Tropical Indian Ocean Observed with Surface Drifters

Yutaka Michida and Hiroyuki Yoritaka, Hydrographic Department, Maritime Safety Agency of Japan, 5-3-1 Tsukiji, Chuo-ku, Tokyo 104, Japan*
**current affiliation: Japan Marine Science and Technology Center, 2-15 Natsushima, Yokosuka 237, Japan*

Water circulation in the eastern Indian Ocean and the seas adjacent to Indonesia has been an interesting issue for oceanographers from the following viewpoints:

- mass/heat/salt exchange between the Pacific Ocean and Indian Ocean through the Indonesian Waters,
- seasonal change of the surface circulation of the Indian Ocean caused by the strong monsoon signal in the wind field over the Indian Ocean.

Maps of the surface currents in the Indian Ocean have been produced by previous studies: *e.g.* Wyrtki (1971) shows that the southwest monsoon current (the dominant eastward flow in the Equatorial area in boreal summer) is replaced by the North Equatorial Current which flows westward in boreal winter. It has also been pointed out by Wyrtki (1973) that an Equatorial Jet, a strong eastward current along the equator, is observed twice a year during the transition periods of the monsoon. A schematic view of Indian Ocean currents including seasonal changes has been proposed by Molinari *et al*. (1990), who have prepared a monthly climatology of surface currents there by analysing surface buoy trajectories.

Several numerical experiments have been conducted to assess the transport and variability of the Indo-Pacific throughflow (*e.g*. Semtner and Chervin, 1988; Masumoto and Yamagata, 1993).

Thirty-one surface drifters were deployed by 1993 in the Indian Ocean within the Japanese EXperiment on Asian Monsoon (JEXAM) to illustrate the surface current system of the tropical Indian Ocean and the seas adjacent to Indonesia.

In this study, we describe some of the trajectories of the drifters which reveal interesting flows in the monsoon currents and Indo-Pacific throughflow. Then we compare the trajectories and current field with previous images and results of numerical models.

We have also calculated grid-averaged (2° square) seasonal currents, which are discussed in Michida and Yoritaka, 1996.

Surface drifter experiments

We have been deploying 6–10 drifters every year since 1990, mainly in the tropical Indian Ocean and the adjacent seas of Indonesia, where several research activities have been attempted recently from the viewpoint of the Indo-Pacific throughflow.

We have used drifters designed according to the specification recommended by the Surface Velocity Programme of WOCE, with a holey-sock drogue at 15 m depth. The locations of the drifters are fixed usually 3–10 times a day by the ARGOS system. Ten drifters were deployed in the tropical area south of the Indian Peninsula in February 1990 in cooperation with the Ocean Research Institute, University of Tokyo. As for the other 21 drifters, 6 south of Java in May 1991, 9 southwest of Sumatra in November 1992, 5 south of Java and one in Makassar Strait in December 1993, were deployed in cooperation with the Faculty of Fisheries of Kagoshima University.

The drifter data have been screened to remove erroneous positions. Then daily averaged drift velocities were calculated from the first fixed locations of the day for each drifter. All trajectories of the drifters deployed within JEXAM are shown in Fig. 1 (page 24), as a 'spaghetti' diagram. They show zonal flows near the equator and at 10–20°S and a clockwise gyre, though it is a composite map of different seasons and years.

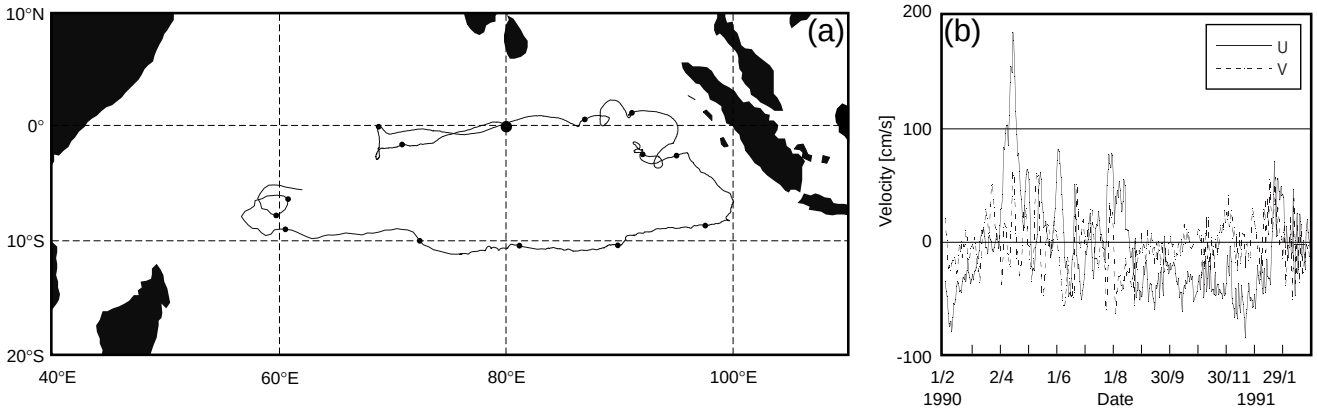

Figure 2. (a) Trajectories, and (b) time series of daily drifting velocity for drifter #11216. (Large dots mark the release point, small dots mark one month)

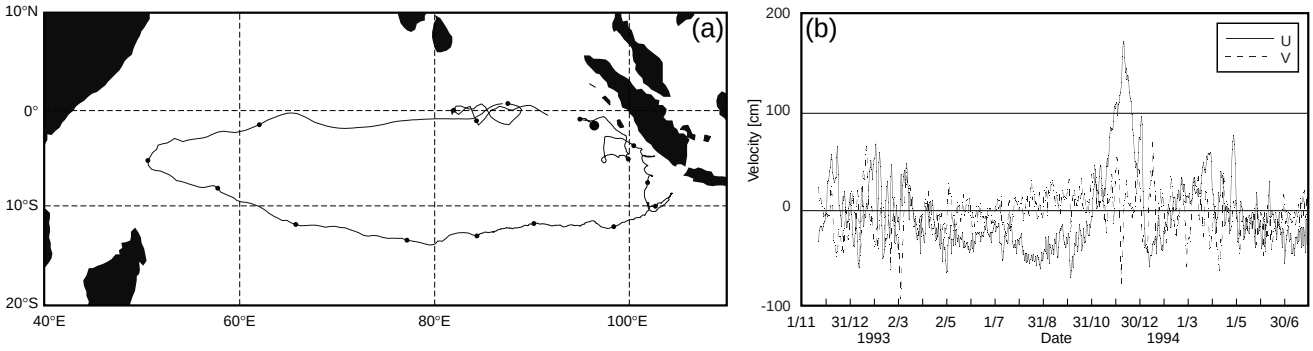

Figure 3. Same as Fig. 2, except for drifter #17260.

Drifter tracks in the Equatorial Jet

In 1990, 10 drifters were deployed south of the Indian Peninsula, two were released at the same time at each point. Seven of them drifted ashore on the coasts or reefs of the Maldive Islands about two weeks after deployment. Three survived for one year or longer. The trajectories and the time series of drift velocity for drifter #11216 which survived until March 1991 are shown in Fig. 2. It drifted westward for about two months after deployment in early February 1990, and turned eastward in April 1990. It is suggested that a strong eastward flow of the Equatorial Jet appeared in boreal spring, a transition period of the monsoon. The maximum eastward component of the drift velocity was larger than 180 cm/s as shown in Fig. 2b.

The trajectories and the time series of drift velocity for drifter #17260, which was deployed southwest of Sumatra in November 1992, are shown in Fig. 3. A clockwise gyre south of the equator was tracked by the drifter. It reached the north of Madagascar and then turned eastward in November 1993. Then it drifted eastward along the equator for two months with eastward velocity components greater than 150 cm/s, following the Equatorial Jet which appeared in boreal autumn.

Flow in Indo-Pacific throughflow region

Drifter deployments were made south of Java in May 1991 (boreal spring) and in November 1993 (boreal winter), to display the seasonal differences in surface currents in the area of the Indo-Pacific throughflow. The drifter tracks for the two experiments are shown in Fig. 4. All the drifters deployed in boreal spring in 1991 stayed in the area between Java and Australia until September 1991 and one of them stayed until December 1991. Then they drifted consistently westward, except for one which landed on Java in December 1991. On the other hand, those deployed in boreal winter in 1993 generally drifted north or northeast toward the Indonesian Seas, except for one which also landed on Java in December 1993.

Drifter #17274 drifted eastward along the south coast of Java, in the South Java Current, then into Flores Sea through Lombok Strait in mid-December, as a drifter reported by Quadfasel and Cresswell (1992). It drifted further east and reached Banda Sea in February 1994. Three drifters (#17276, #17277 and #17278) drifted along the south coast of the Indonesian Islands and reached the Savu Sea; one of them drifted further to Arafura Sea through the narrow channel between Timor and Solor, while two of them stopped transmission near Timor.

The drifters deployed in boreal spring to summer typically went westward towards the central area of Indian Ocean, but those deployed in boreal autumn to winter, went in the opposite direction toward Banda or Arafura Sea. This observational fact allows us to note that currents at least in the surface layer south of the Indonesian archipelago show a remarkable seasonal change. The waters in the surface layer there flow from the Indian Ocean to the Indonesian Seas in boreal winter.

Masumoto and Yamagata (1993) have simulated seasonal circulation in the Indonesian Seas by use of a numerical model. As a part of the results, they have presented numerically simulated surface (at 5 m level) circulation for the area where we have drifter data mentioned above. By comparing the drifter tracks and modelled currents, we point out that the drifter motions can be well explained by the simulated current field. They have displayed the surface currents for February, May, August and November that

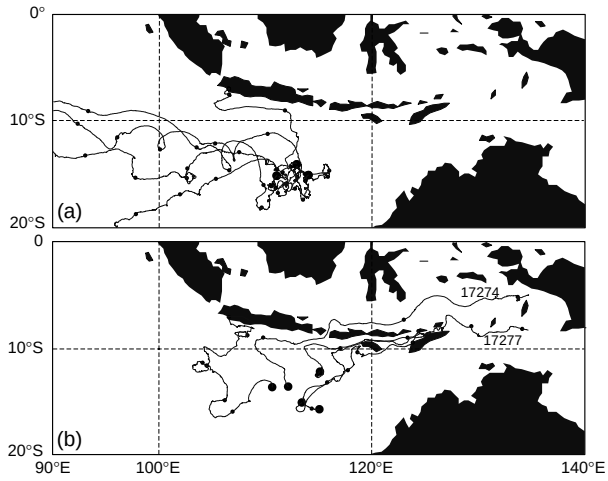

Figure 4. Trajectories of the drifters deployed (a) in May 1991, and (b) in November 1993

represent the seasons. The modelled currents in the area south of the Indonesian archipelago and the Indonesian Seas (Flores, Banda and Arafura Sea) for February are quite different from other months, *i.e*. (1) the current direction in the Lombok Strait is northward in February and southward in other months, (2) north to northeast flows are dominant south of Java and Lesser Sunda in February and east to southeast flows in other months, and (3) strong eastward flows can be seen in Flores Sea and Banda Sea in February and mostly westward flows in other months.

These features are all consistent with the drifter tracks, and the results of our drifter experiments have supported the reliability of the model in respect of the surface circulation. These surface currents which flow from the Indian Ocean toward the Pacific, with opposite direction to the Indo-Pacific throughflow, may be an important influence on the seasonal variation of total mass and heat transport between the Pacific and Indian Ocean, by reducing the transport toward the Indian Ocean across the Lombok Strait in boreal winter, as numerically predicted by Masumoto and Yamagata (1993).

Fig. 5 shows the daily mean velocity of drifters that drifted into the Banda Sea (#17274) and Arafura Sea (#17277). The meridional velocity component for #17274 had its maximum v>100 cm/s in mid-December when it passed Lombok Strait northward to Flores Sea. In the Flores Sea, the zonal velocity component of the drifter was typically about 50 cm/s or greater, unless it was mostly smaller than 20 cm/s when drifted into the Banda Sea in mid-January 1994 (Fig. 5a). Meridional and zonal velocity components for #17277, which drifted in the Indian Ocean along the south coast of Indonesia, were both generally smaller than those for #17274, though they reached sometimes greater than 50 cm/s (Fig. 5b).

In attempting to make quantitative comparisons, we see the velocities in the Flores Sea where the maximum model velocity of the surface current is approximately 50 cm/s in February (Masumoto and Yamagata, 1993). The mean velocity of drifter #17274 while drifting in Flores Sea is also about 50 cm/s that is agreeable with the model, although the daily velocity sometimes exceeds 100 cm/s (Fig. 5). This suggests that the numerical model has well simulated at least the surface currents in a quantitative sense, too.

Summary

The surface current field in the tropical Indian Ocean observed with surface drifters is consistent with the previous studies, including the features of seasonal changes and appearances of the Equatorial Jet in the transition period of the monsoon. The zonal components (eastward) of drifting velocities in the Equatorial Jet derived from the movements of drifters are mostly greater than 150 cm/s, and greater than 100 cm/s even for the grid averaged velocities (Michida and Yoritaka, 1995). They are a little larger than the estimation by Molinari *et al*. (1990).

Surface currents in the area south of Indonesian archipelago and Indonesian Seas (Flores, Banda and Arafura) visualized with the drifters deployed there in different seasons show an obvious seasonal change. Surface currents flow from the Indonesian Seas to the Indian Ocean in boreal spring to summer, and showing a clear contrast, from the Indian Ocean to Indonesian Seas in boreal winter. Trajectories of a drifter which drifted from the Indian Ocean to Flores Sea through Lombok Strait and then into Banda Sea give us observational evidence of the surface current reversal in Lombok Strait and Indonesian Seas in boreal winter, which has been demonstrated by the numerical experiments of Masumoto and Yamagata (1993), as well as by previous climatologies or observations.

Acknowledgements

We acknowledge financial support for drifter experiments from JEXAM, promoted by the Science and Technology Agency. We thank training vessel Kagoshima-Maru of Kagoshima University and research vessel Hakuho-Maru of Ocean Research Institute of the University of Tokyo, for cooperation in deploying the drifters. We also thank Y. Masumoto, T. Yamagata, T. Awaji and H. Ishii for their discussion and helpful comments, H. Nishida and M. Hishida for continuous encouragement, and F. Suguro for assistance in maintaining the drifter data base.

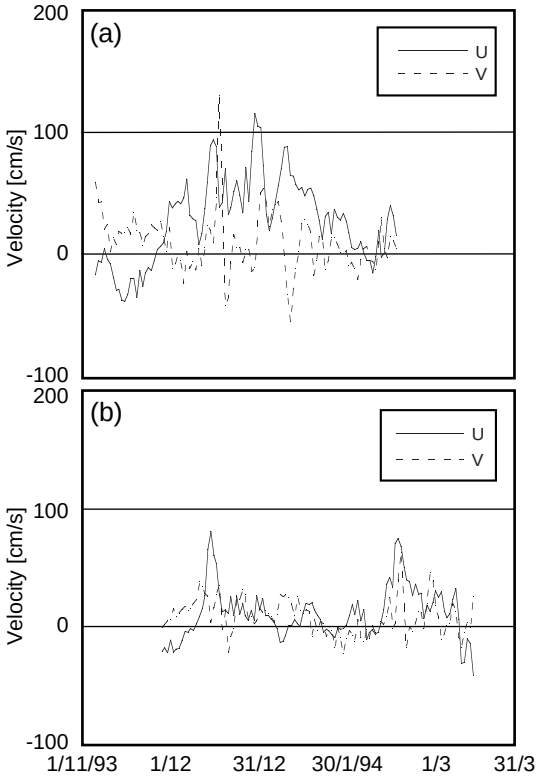

Figure 5. Time series of velocity (a) for drifter #17274 that drifted into Banda Sea, and (b) for #17277 that drifted into Arafura Sea (positive: eastward).

References

Masumoto, Y., and T. Yamagata, 1993: Simulated seasonal circulation in the Indonesian Seas. J. Geophys. Res., 98, 12501–12509.

Michida, Y., and H. Yoritaka, 1996: Surface currents in the area of the Indo-Pacific throughflow and in the tropical Indian Ocean observed with surface drifters. J. Geophys. Res. (submitted).

Molinari, R.L., D. Olson and G. Reverdin, 1990: Surface current distributions in the tropical Indian Ocean derived from compilations of surface buoy trajectories. J. Geophys. Res., 95, 7217–7238.

Semtner, A.J., and R.M. Chervin, 1988: A simulation of the global ocean circulation with resolved eddies. J. Geophys. Res., 93, 15502–15522.

Wyrtki, K., 1971: Oceanographic atlas of the International Indian Ocean Expedition. National Science Foundation, Washington, DC.

Wyrtki, K., 1973: An equatorial jet in the Indian Ocean. Science, 181, 262–264.

WCRP PROGRAMMES: The Global Energy and Water Cycle Experiment

Pierre Morel, International GEWEX Project Office, Washington, DC 20024, USA

Climate is the integrated result of weather, *i.e*. the summation of highly variable, essentially random manifestations of the chaotic nature of global atmospheric circulation dynamics. Yet we believe that, for all this meteorological variability, climate statistics are stable enough that we can legitimately ask what would be the change in the prevalent climate regime caused by a small but persistent shift in climate-forming factors such as the concentration of "greenhouse gases" in the atmosphere, the aerosol loading or solar irradiance.

Global climate change

The response or "sensitivity" of climate to a small perturbation, that would not materially disturb the slow components of the climate system (the oceans and ice-sheets), is determined to first order by the planetary radiation balance and various feedback processes involving adjustments in atmospheric water vapour and the distribution and optical properties of clouds. Now, many scientists, especially climate modellers, may believe that we have learned all there was to know about atmospheric processes in the 1970's, in the course of the Global Atmospheric Research Programme (GARP). The truth of the matter is that, while GARP led to major advances in global atmospheric circulation modelling, observing capabilities were inadequate at the time to allow quantitative studies of global thermodynamic and hydrological processes.

GEWEX is the programme launched by the World Climate Research Programme (WCRP) to foster the international cooperation (especially, that of the world space agencies) and interdisciplinary linkages needed to address these "fast climate processes", especially the factors that determine atmospheric radiation transfer and radiative heating within an air column. The on-going effort includes the first global climatology of monthly-mean cloud amount and optical depth from geostationary satellites (International Satellite Cloud Climatology Project), an accurate determination of the planetary radiation balance and contribution of clouds to this balance (Earth Radiation Budget Experiment) in 1985–87, a global climatology of total precipitable water vapour combining *in situ* measurements with satellite observations (GVap), and many field studies of physical cloud/radiation processes, complemented by the GEWEX Cloud System Study, a major interpretative effort using the most recent cloud-resolving microphysical process models.

All this is still insufficient, however, and GEWEX is now looking into still more capable satellite observing techniques to probe into the moist atmosphere from space: considerably improved atmospheric temperature and moisture sounders, active lidar and millimetre-wave radars to observe the 3-dimensional distribution of clouds, differential absorption or Raman laser techniques to determine the fine vertical structure of water vapour, etc.

The response of the atmosphere to changes in sea surface temperature

The atmospheric response to changes in sea-surface temperature involves, in a crucial way, the release of latent heat associated with precipitation and changes in the rainfall regime are themselves an essential aspect of climatic variability. Thus a major thrust of GEWEX is characterizing and understanding the components of the global hydrological cycle, the transport and precipitation of atmospheric water vapour, the storage of ground water and evaporation from vegetation and soil, the runoff from rainfall and river flow.

A central task of GEWEX has been to engage the cooperation of hydrological scientists and engineers and foster interdisciplinary studies of climate-related hydrological phenomena in collaboration with the atmospheric and space research communities. One approach toward this objective has been large-scale joint meteorological-hydrological field studies for different terrain and climate conditions, from moist Western Europe and the Mississippi river basin to the arid landscape of the African Sahel, from the Arctic forest (BOREAS and the Mackenzie GEWEX Study) to the Brazilian rain forest.

In order to foster advances in climate modelling, GEWEX has assembled and validated the first global record of monthly mean rainfall over oceans as well as continents (Global Precipitation Climatology Project), combining raingauge data with remote-sensing estimates

from geostationary and polar orbiting satellites. Likewise GEWEX organized comparisons of possible model formulations of ground heat and moisture budgets under standard forcing conditions (Programme for Intercomparison of Parameterizations of Land Surfaces) and is currently producing the first global climatology of "soil wetness" (International Satellite Land Surface Climatology Project).

Coupled ocean-atmosphere dynamics and climate variability

We know that the non-linear nature of ocean circulation dynamics and vertical mixing can generate significant variations on climatic time-scales, decades to centuries, even under perfectly constant atmospheric boundary conditions and fluxes. We also know that one mode of climate fluctuation is a result of the coupled dynamics of the tropical Pacific Ocean circulation and the Southern Oscillation of the atmosphere. Studying the possibility of other coupled modes of natural climate variability is, of course, one principal objective of CLIVAR. Because these transient variations can span several decades or even longer periods of time, research must remain largely theoretical and rely on numerical experiments with coupled atmosphere-ocean-ice models. Result will remain unreliable, however, as long as computed interface fluxes do not balance in the atmosphere and ocean.

GEWEX is working on improving the formulation of energy and fresh water transport and exchanges in atmospheric circulation models to the point where no substantial systematic error remains in boundary fluxes and no *ad-hoc* "flux correction" is needed. Of particular relevance is the Surface Radiation Budget climatology project, aiming to produce and refine estimates of the net radiation flux at the Earth surface, based on satellite observations of cloud, meteorological analyses of temperature and moisture, and precision measurements from the GEWEX Baseline Surface Radiation Network. Basic studies of the global hydrological cycle will hopefully lead to adequate models of water transport and net fresh water fluxes at the air-sea interface.

Altogether, GEWEX is currently the largest international climate research endeavour mounted by WCRP. Its success is a prerequisite for quantitative investigations of the domain of intrinsic variability of the Earth climate system and science-based assessments of possible future climate changes.

For more information contact:
International GEWEX Project Office
Suite 203, 409 Third Street SW
Washington, DC 20024
USA.
Tel: 1-202-863-1435/0012
Fax: 1-202-488-5364
e-mail: gewex@cais.com

Meeting Timetable 1996

WOCE Meetings

May 14–17	SVP-8	Toulouse
April 30–May 2	SMWG-2	Southampton
October 7–9	WHP-15	Woods Hole, MA
October 15–17	WOCE-23	Southampton

Science and other Meetings

May 6–10	XXI Assembly of the European Geophysical Society, Den Haag
May 20–24	AGU Spring Meeting, Baltimore, MD
July 8–11	TOS Meeting on Marine Environment and Global Change Programmes, Amsterdam
July 23–27	AGU Western Pacific Geophysics Meeting, Brisbane
August 13–16	Pacific Ocean Remote Sensing Conference, Victoria, CA
August 19–23	WOCE Pacific Workshop, Newport Beach, CA
September 27–October 1	ICES Annual Science Conference, Special WOCE/JGOFS/CLIVAR Session, Reyjkavik
October 7–11	First International Conference on EuroGOOS, Den Haag
November 18–23	The North Atlantic: Ocean Currents, Climate, Weather and Environment, Copenhagen

For more information on the above meetings contact the IPO. If you are aware of any conferences or workshops which are suitable for the presentation of WOCE results and are not mentioned in the above list please let the IPO know.

Dear Colleagues:

We have completed and make available to the community Power OceanAtlas 1.0 for Macintosh computers, an enhanced version of the OceanAtlas for Macintosh application. Separate versions – all with the same features – are available for PowerPC Macintosh models, 680x0 models with floating point math co-processor (*e.g.* IIci's and Quadras), and 680x0 models without the floating point math co-processor (*e.g.* most 680x0 Performas). Thanks to the National Science Foundation Power OceanAtlas 1.0 is available free of charge.

Power OceanAtlas data plots include offset profiles, property-property plots, contour plots, and 3D plots, using color as a third (or fourth) plotted variable to aid interpretation. We also provide station position maps and a comprehensive data display window. All plots are linked and may be "browsed" by sample and/or by station. Plots can be re-scaled, re-sized, or have their colored variable changed. Selected areas of most plots can be made into new plots. Standard levels, scales, contours, and colors can be changed via user interfaces similar to those used in commercial Macintosh applications. OceanAtlas provides data filtering, exporting, and editing, plus allows data import. Many different types of calculations can be performed.

Power OceanAtlas runs "native" on PowerPC-based Macintoshes. It is easier now to create ratios and scaled variables. Data import options are greatly expanded: Power OceanAtlas can directly import WOCE and NODC SD2 format files. In addition, many bugs have been fixed in importing spreadsheet format files. Power OceanAtlas adds animated 3D property-property plots and 3D profile plots, and an additional criterion to station filters allows filtering by reported parameters.

Principal distribution of Power OceanAtlas 1.0 will be carried out by the EOSDIS PODAAC at JPL. Because Power OceanAtlas uses the same data format and data files used by earlier versions, and because the manuals from the earlier versions are essentially correct, we provide only a "User Guide" which reviews features new to Power OceanAtlas plus the new ancillary files listed below. Therefore, users new to OceanAtlas should state that they also need the original data files and OceanAtlas version 2.0 and 2.5 manuals. Contact information:

User Services
EOSDIS PODAAC
Jet Propulsion Laboratory
MS 300-320
4800 Oak Grove Dr.
Pasadena, CA 91109 USA
(818) 354-9890
podaac@podaac.jpl.nasa.gov

(Be sure to specify which version of Power OceanAtlas you want.)

A 3.14 Mbyte file named poa.pkg.sit.hqx, containing all versions of Power OceanAtlas 1.0, ancillary applications (OceanAtlas Tools and a working version of OceanAtlas Convert), update documentation, and sample import data files, has been placed on the anonymous ftp site in the directory /pub/OceanAtlas on the odf.ucsd.edu computer. The data files are not yet on the ftp site, but will soon be posted. Also we will soon have a Home Page with ftp information at http://odf.ucsd.edu/oceanatlas.

Happy data exploring!

John ("Oz") Osborne ocean@wolfenet.com
Jim Swift jswift@ucsd.edu

PS: Watch for release in late 1996 of Power OceanAtlas 1.5 on CD-ROM. This will contain all versions of Power OceanAtlas, all ancillary applications and files we have available, a significant enlargement of the OceanAtlas collection of sections (these will be provided in multiple formats and will also contain some multi-tracer sections with CFCs, helium/tritium, and 14C data) and a new, complete manual (presently one must have the OceanAtlas 2.0 manual, the OceanAtlas 2.5 manual addendum, and the Power OceanAtlas 1.0 User Guide to have a complete documentation set).

Note on Copyright

WOCE is a component of the World Climate Research Programme (WCRP), which was established by WMO and ICSU, and is carried out in association with IOC and SCOR. The scientific planning and development of WOCE is under the guidance of the Scientific Steering Group for WOCE, assisted by the WOCE International Project Office.

The WOCE Newsletter is edited at the WOCE IPO at the Southampton Oceanography Centre, Empress Dock, Southampton SO14 3ZH (Tel: 44-1703-596789, Fax: 44-1703-596204, e-mail: woceipo@soc.soton.ac.uk).

We hope that colleagues will see this Newsletter as a means of reporting work in progress related to the Goals of WOCE as described in the Scientific Plan. The SSG will use it also to report progress of working groups, experiment design and models.

The editor will be pleased to send copies of the Newsletter to institutes and research scientists with an interest in WOCE or related research.

Printed by the Design and Print Centre of the University of Southampton